CHEMICAL ENGINEERING SCIENCE
GENIE CHIMIQUE

VOL. 6 APRIL/MAY 1957 Nos. 4/5

Studies on gas-solid reactions—I

The oxidation rate of zinc sulphide

K. J. CANNON* and K. G. DENBIGH†
The Chemical Engineering Department, Cambridge

(*Received* 18 *December* 1956)

Abstract—The rate of oxidation of the 110 faces of zinc sulphide has been studied by the use of a thermobalance. Experiments were carried out at temperatures between 680°C and 940°C and with oxygen partial pressures between 0·014 and 0·50 atm.

Below 830°C the oxidation rate varies as an exponential function of the temperature and is largely independent of the thickness of the zinc oxide layer; it is thus "chemically controlled." Above 830°C there is evidence of the onset of a diffusion resistance. At temperatures above 900°C, the thickness of the oxide layer becomes very uneven, due, it is believed, to a phenomenon of thermal instability. At still higher temperatures an entirely different mechanism sets in, namely the dissociative vaporisation of zinc sulphide, followed by its oxidation in the vapour phase.

Résumé—Les auteurs étudient à l'aide d'une balance thermique, les vitesses d'oxydation des faces 110 du sulfure de zinc. Ces essais ont été faits entre 680 et 940°C avec une pression partielle d'oxygène de 0,014 et 0,50 atm.

Au-dessous de 830°C la vitesse d'oxydation est une fonction exponentielle de la température et elle est indépendante de l'épaisseur de la couche d'oxyde de zinc; elle est alors chimiquement contrôlée. A des températures supérieures à 830°C il se produit une résistance due à la diffusion. Au-dessus de 900°C la couche d'oxyde de zinc devient irrégulière : ceci est dû à un phénomène d'instabilité thermique. Enfin à des températures plus élevées, un mécanisme entièrement différent entre en jeu : la vaporisation et la dissociation du sulfure de zinc suivies d'une oxydation en phase vapeur.

1. INTRODUCTION

REACTIONS between solids and gases are an important class which includes the combustion of solid fuels, together with many examples from the metallurgical industry, such as the roasting and smelting of ores. The study of such processes falls within the field of the chemical engineer, especially in so far as they involve mass and heat transfer taking place simultaneously with the chemical reaction. However, there is a lack of knowledge concerning the rate limiting factors, and at present the engineer could not hope to carry out a successful design for such a process in the same *a priori* manner as he would use for a distillation column or a vessel for a homogeneous reaction.

In this paper we shall describe some work on a reaction of the above type, the oxidation of zinc sulphide, which is of technical importance in zinc production. The work is confined to a study of the reaction rate, the diffusion of the gases through the layer of reaction product, and the

* Present address : Division of Industrial Chemistry, C.S.I.R.O., Fisherman's Bend, Melbourne.
† Present address : The Department of Chemical Technology, King's Buildings, West Mains Road, Edinburgh.

conditions of thermal stability. For the purposes of a fundamental study, the reaction in question has the merit of simplicity, for over a considerable range of temperature it proceeds in accordance with the equation

$$ZnS + \frac{3}{2}O_2 = ZnO + SO_2,$$

to the exclusion of other reactions, such as the formation of zinc sulphate. The high exothermicity of the reaction, on the other hand, gives rise to some difficulty in the control of temperature. Earlier studies on the same reaction have been described by OGAWA [1] and by ONG, WADSWORTH and FASSELL [2].

2. EXPERIMENTAL

(a) *Method.* The experimental method consisted in following the weight change of a single crystal, a few millimetres in size, suspended in a furnace from a sensitive balance. The crystal was surrounded by a stream of air, or other oxygen-nitrogen mixture, and conditions were chosen to avoid mass transfer limitation within the gaseous phase. On the other hand, as reaction proceeded, the core of zinc sulphide progressively diminished and was replaced by an adhering layer of zinc oxide, more porous than the sulphide. There was, therefore, the possibility of a mass transfer limitation due to the need for oxygen to pass inwards, and for sulphur dioxide to pass outwards, through this layer.

(b) *Preparation of specimens.* It was considered impractical to grow artificial crystals of zinc sulphide of a sufficient size and use has therefore been made of the best available natural sphalerite, as obtained from the Picos de Europa mine at Santander, through the good offices of the University of Madrid. This material had a yellowish colour, but was transparent in small thicknesses. The main impurities were 0·1–0·3 % of Fe, 0·1–0·3 % of Cd and about 1 % of silica.*

A disadvantage in the use of the naturally occurring crystal is that it tends to decrepitate when placed in the furnace, probably due to small inclusions of water or of free sulphur. To obviate this difficulty, we have used for our rate measurements only those crystals which had successfully undergone a previous heat treatment.

The crystals, a few millimetres in size, as obtained from this treatment, usually manifested two or three of the natural cleavage planes (110 faces), but were otherwise irregular in shape. Before using for the rate measurements, these crystals were therefore brought to a regular shape by grinding and polishing on a suitable machine having a double dividing head with horizontal and vertical rotating axes. By using any two of the pre-existing 110 faces on the specimen for purposes of orientation, it was thus possible to reduce the whole surface to a set of known faces (usually chosen as all 110) to within an accuracy of about $\pm 1°$.

(c) *The thermobalance.* A large vertical tube furnace was mounted on slides and provided with counterweights so that it could be moved up and down to allow loading of the crystal without upsetting the balance. The latter – an Oertling Model 52M with optical projection scale – was supported on a strong shelf, two feet above the furnace.

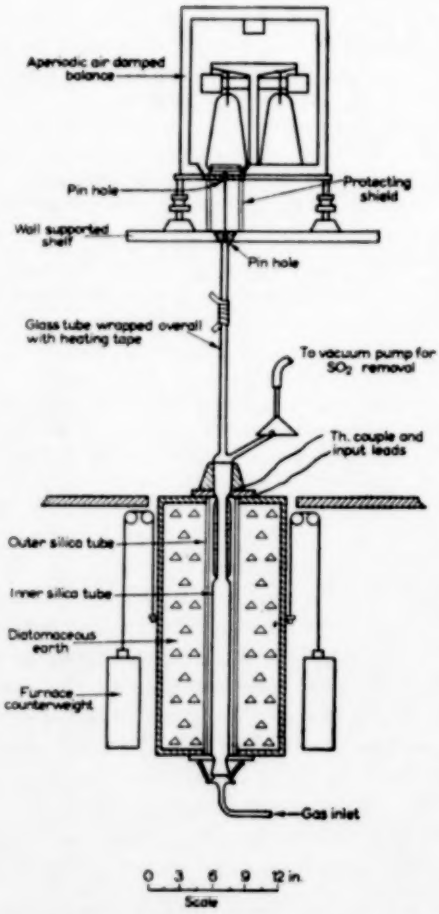

FIG. 1. Schematic layout of thermo-balance.

* Independent experiments carried out by Mr. J. F. PEARSON at these laboratories have shown that a very impure black zinc sulphide oxidises at the same rate as a fairly pure yellow variety. It appears, therefore, that the presence of the commonly occurring impurities in varying amounts does not significantly affect the observed reaction rate.

A silica thread hung vertically downwards from one of the balance pans, through a hole in the shelf, and supported at its lower end, within the furnace, a small platinum tray for carrying the crystal, which was supported on a platinum wire frame above the tray to allow O_2 to reach its underside. Details of the arrangement are shown in Figs. 1 and 2.

The furnace contained two concentric silica tubes, and the current through the primary winding on the outer tube was permanently "on." The secondary winding on the upper part of the inner tube, in the vicinity of the crystal, was used for control purposes and was activated by a thermo-junction within the furnace, together with a Cambridge Direct Deflectional Indicating Controller. In the reaction zone the temperature remained steady to within $\pm$ 0·5°C and the vertical variation of temperature was no more than 5°C per inch; since specimens were of the order $\frac{1}{8}$ in. in size, and thermo-junctions could be suspended as close as $\frac{1}{16}$ in. to the specimen, the errors due to temperature gradients were probably small.

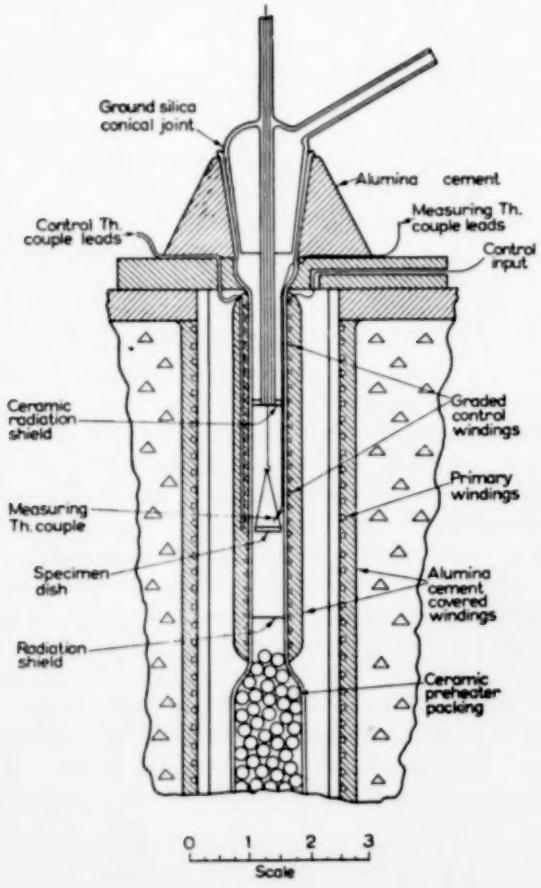

FIG. 2. Detail of reaction zone.

Radiation shields were provided and thermo-couples were periodically recalibrated.

(d) *Control of the gas flow.* A prepared nitrogen-oxygen mixture, contained in a gas holder, was passed through drying tubes, and a flow meter, and thence into the lower part of the inner tube of the furnace, where it was heated by the ceramic packing shown in Fig. 2. The flow of gas (maintained constant at 400 c.c./min) gave rise to a certain amount of "lift" on the thermo-balance, but this was allowed for in its calibration.

(e) *Experimental procedure.* The various dimensions of the crystal were first determined by use of a travelling microscope and its weight was measured on an ordinary balance. Meanwhile the furnace had been adjusted to the required temperature with an approximate oxygen-nitrogen mixture passing through. The crystal was mounted above the thermobalance pan and, at $t = 0$ for the rate measurement, the furnace was lifted on its counterweights until it surrounded the crystal. Thereafter the reaction rate was followed over a period of hours on the optical scale of the thermobalance.

At the completion of the run, the total weight change, as measured on the thermobalance, was checked by transferring the crystal, now at least partly zinc oxide, to an analytical balance. The crystal was finally cut across in order to check the equality of the oxide layer on all faces. This was necessary as several specimens were found to have contained undetected cracks, which were penetrated by the oxygen, thus invalidating the particular experiment; it served also to confirm the equal ease of diffusion of oxygen up to the various crystal faces.

(f) *Temperature correction.* Due to the exothermic nature of the reaction, the temperature of the crystal was usually somewhat higher than was measured by the thermo-junction in its vicinity. The magnitude of this effect was investigated by placing a thermo-junction between a pair of crystals, the leads from the junction being wound several times round the pair and the whole assembly being hung in the furnace in the position normally occupied by the platinum tray. It was found that the temperature within the pair of crystals exceeded the external temperature by as much as 10° at 800°C and 20° at 900°C, in fair agreement with values calculated theoretically (Part II). The temperatures used in connection with equations (1) and (2) below are the actual temperatures within the crystal, as estimated by means of this correction.

3. Experimental Results

(a) *Chemical control.* For the rate measurements of Tables 1 and 2 below, the crystal faces were all 110 and thus had known angles between them. From a knowledge of the original dimensions of each individual crystal, it was therefore

possible to calculate what would be its weight change for a progressively increasing inward movement, assumed equal on each face, of the ZnO–ZnS interface. This calculated weight

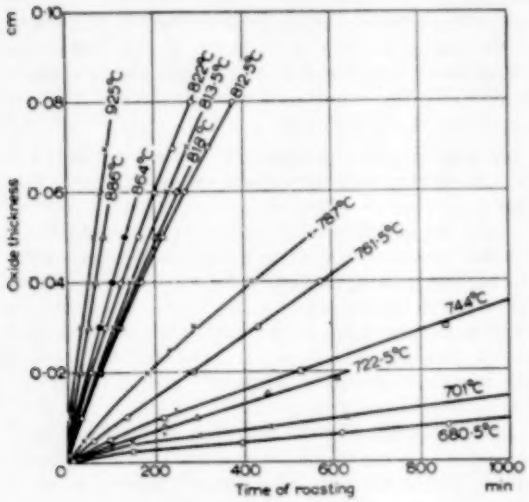

FIG. 3. The effect of temperature on the rate of film growth in air.

change could then be plotted against the movement of the interface, or " penetration " as it will be called. From the thermo-balance readings

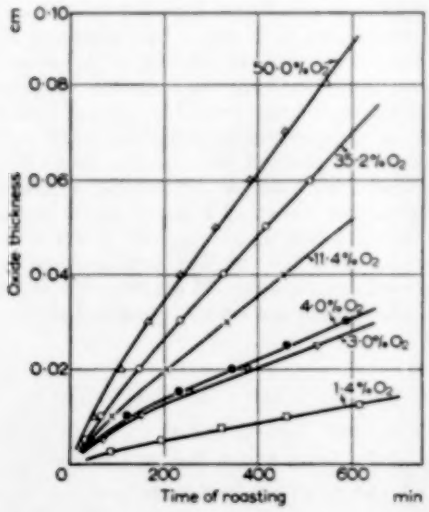

FIG. 4. The effect of oxygen concentration on the rate of film growth at 780°C.

each run also gave a plot of the observed weight change against time. Thus, from a comparison of the two plots, the penetration was obtained as a function of the time.

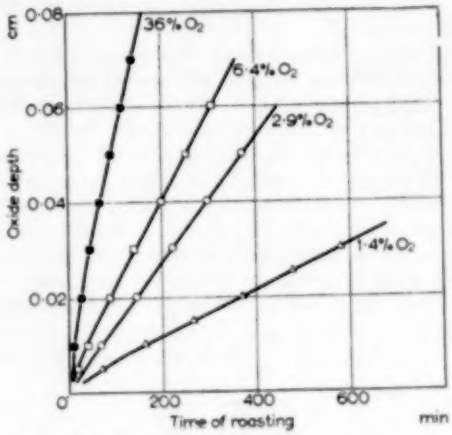

FIG. 5. The effect of oxygen concentration on the rate of film growth at 850°C.

These results are shown in Figs. 3, 4 and 5. It will be seen that in almost all runs the rate of penetration diminished somewhat during the early stages of reaction, but subsequently approached an almost constant rate, the thickness of the oxide layer increasing linearly with the time.* The cause of the initial decrease of rate is not known, but it appears to be a fairly common feature of such processes and a number of possible causes have been put forward by GULBRANSEN and ANDREW [3]. On the other hand, the linearity which follows the initial period is consistent with the assumption that the observed rate is " chemically controlled," i.e. the rate of movement of the ZnO–ZnS interface depends on the processes taking place at this interface and not on the diffusion through the overlying layer of zinc oxide.

What will be called the " steady reaction rate," as measured in centimetres penetration per second, has been calculated from the linear portion of these curves and the results are shown in Tables 1

* ONG, WADSWORTH and FASSELL [2] report linearity over the entire range. However, an inspection of their Fig. 3 indicates an initial fall-off in rate in their runs at 771°C and 799°C.

and 2. The first of these refers to variable temperature at constant gas composition (air) and the other refers to variable oxygen partial pressure at two approximately constant temperature levels.

Table 1. *Oxidation in air at atmospheric pressure*

Furnace temperature °C	*Corrected reaction temperature* °C	*Steady reaction rate* (cm/sec) × 10^6	*Calculated reaction rate* (cm/sec) × 10^6
680	680	0·15	0·14
700	701	0·24	0·23
720	722	0·45	0·41
740	744	0·54	0·69
757	761	1·13	1·05
780	787	1·54	1·88
802	812	3·3	3·3
803	813	4·0	3·4
807	818	3·6	3·7
810	822	4·2	4·0
816	829	4·6	4·6
845	864	6·0	(9·3)
865	886	8·8	(14·2)
903	925	11·8	(29)
903	925	10·0*	(29)
925	946	11·3*	(41)
937	957	12·5*	(49)

* These results were not obtained by use of the thermobalance, but by direct measurement of the oxide thickness.

Table 2. *Oxidation in oxygen-nitrogen mixtures*

Furnace temp. °C	*Corrected reaction temperature* °C	*Oxygen partial pressure atm.*	*Steady reaction rate* (cm/sec) × 10^6	*Calculated reaction rate* (cm/sec) × 10^6
778	779	0·014	0·33	0·41
776	779	0·030	0·66	0·60
778	781	0·040	0·71	0·73
776	782	0·114	1·37	1·25
780	786	0·21	1·54	1·88
780	787	0·35	1·8	2·4
779	788	0·50	2·1	3·0
841	845	0·014	0·81	(1·7)
843	851	0·029	1·87	(2·7)
844	854	0·064	3·1	(4·2)
845	864	0·21	6·0	(9·7)
846	865	0·36	7·2	(12·5)

Using the data of Table 1, the logarithm of the steady reaction rate is shown in Fig. 6 plotted against the reciprocal of the absolute temperature. Over the range 680°C to 830°C, the relationship is a linear one and the rate can thus be represented by the relation :

$$\text{rate} = \text{const} \times e^{-E/RT}, \qquad (1)$$

with $E = 50$ kcal/g mole. However, at temperatures above 830°C the measured rate is seen from Fig. 6 to become less than corresponds to this equation and this is believed to be due to the onset of an appreciable rate limitation arising from diffusion through the oxide layer.

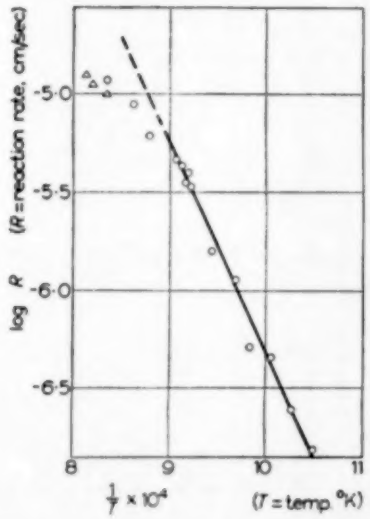

Fig. 6. The effect of temperature on the oxidation rate of sphalerite in air. ○ Thermobalance results ; △ Microscope measurements.

Turning now to the effect of the oxygen partial pressure, it will be seen that the two parts of Table 2 do not refer to temperatures which are quite constant. Equation (1) above has been used to reduce the rates to temperatures of 780°C and 850°C and these were then found to be roughly proportional to the square root of the oxygen partial pressure (Figs. 7 and 8). The combined effect of temperature and partial pressure may

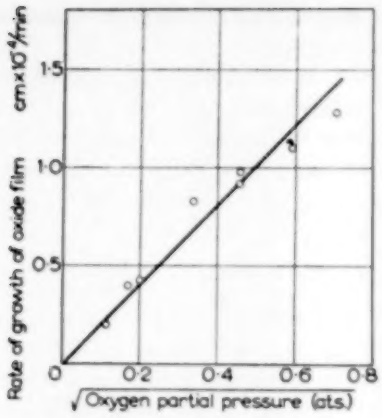

FIG. 7. The effect of oxygen concentration on the oxidation rate of zinc sulphide at 780°C.

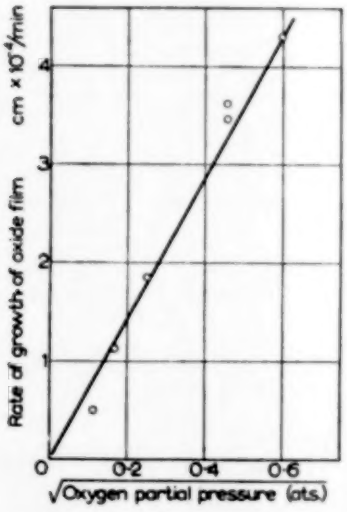

FIG. 8. The effect of oxygen concentration on the oxidation rate of zinc sulphide at 850°C.

thus be represented approximately by the relation*

$$\text{rate} = Ae^{-E/RT}p^{\frac{1}{2}} \qquad (2)$$

where p is the partial pressure in atmospheres. E has the value 50 kcal/g mole; A has the value $8{\cdot}0 \times 10^4$ when the rate is expressed as centimetres penetration per second, or has the value $3{\cdot}2 \times 10^3$ when the rate is expressed as gm. moles of ZnS per cm^2 per second. The rate as calculated by the use of equation (2) is shown in the last column of Tables 1 and 2; the figures enclosed in brackets refer to temperatures above 830°C where equation (2) is no longer applicable due to the onset of diffusion control.

The above results apply to zinc sulphide crystals having entirely 110 faces. In order to investigate the possibility of anisotropy in the roasting rate, a series of additional faces were ground on to the crystal at 5° intervals between the 110 faces, which met at an external angle of 60°. Thus the most oblique of the new planes was at 30° to the 110 faces. After roasting for one hour at 780°C, the crystal was cut through a plane normal to the previously established faces; the thickness of the oxide layer was found to be greater the larger the angle to the 110 face, reaching a maximum of 35% greater for the face at 30°.

Similar results were obtained for more prolonged periods of heating and it appears therefore that there is a significant variation in roasting rate from face to face, the cleavage planes (110) reacting the most slowly. A 100 plane was cut on another crystal and was found to develop an oxide layer 10% thicker than on a 110 plane.

(b) *Onset of diffusion control.* At all temperatures below 830°C, the penetration was very uniform over the faces, the ZnO–ZnS interface was sharply defined and the corners of the sulphide core remained sharp, as shown by the full lines in Fig. 9. On the other hand, at temperatures above 830°C, the corners began to show a rounding as indicated by the dotted line in Fig. 9. This is clearly what would be expected if the diffusion of oxygen or sulphur dioxide through the oxide layer was becoming significant as a rate controlling factor. The fact that diffusion becomes intrinsically slower than reaction *above*

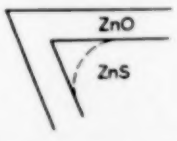

FIG. 9. Showing the sharp corners resulting from oxidation below 830°C, and the rounded corners obtained at higher temperatures (dotted line).

* An alternative expression for the dependence of the rate on the oxygen partial pressure will be considered in the discussion.

a certain temperature is due, of coures, to its smaller temperature coefficient and this effect has previously been demonstrated very clearly in the case of carbon combustion by Tu, Davis and Hottel [4].

(c) *Uneven penetration.* At temperatures over 900°C the penetration became very uneven over different parts of the crystal. By making sectional examinations at various stages of roasting, it became clear that, whereas the reaction was initially uniform, small deviations soon developed and magnified themselves during the progress of reaction. The characteristic appearance of a section, showing also the laminar structure of the oxide layer, is shown in Fig. 10.

Fig. 10. Non-uniform growth pattern of oxide films on ZnS above 900°C.

The uneven penetration was at first thought to be due to cracks or other faults in the crystal, but this does not explain why the effects become marked only above 900°C. It seems more probable that it is due to thermal instability : the thickness of the oxide layer impedes the escape of the heat of reaction which thereby causes a local rise in temperature and therefore a still further increase in reaction rate. This theory will be discussed in more detail in Part II.

The occurrence of uneven penetration made it impossible to obtain a satisfactory measure of the reaction rate at temperatures much above 900°C, by use of the thermobalance. Accordingly the last three results recorded in Table 1 were obtained by direct microscopic measurement of the thickness of the oxide layer, over those parts of the crystal where penetration was uniform, at early stages in roasting.

(*d*) *Vaporization.* When crystals were roasted at temperatures above 950°C there was a considerable deposition of woolly zinc oxide on the platinum and silica supports of the roasting tray. At these temperatures it is known (5) that zinc sulphide has an appreciable dissociation pressure, whilst zinc oxide itself is still almost involatile. It seemed therefore that an evaporation of zinc sulphide was taking place, followed by a vapour phase oxidation and a deposition of zinc oxide on available surfaces.

The structure of the oxide layer surrounding the crystal was also entirely different to that which was obtained at lower temperatures. Below 900°C the oxide layer was laminar, fragile and porous (the zinc oxide having a smaller molar volume than the zinc sulphide). Above 950°C the layer was dense, nonlaminar and quite hard, and under electron diffraction was found to have a completely random orientation of its microcrystalline structure.* These observations suggested that the porous structure which would otherwise have been formed was being filled in by the deposition of oxide by the vapour phase reaction.

As noted above, penetration was far from uniform at higher temperatures and, over parts of the crystal, the thickness of oxide layer was sometimes *less* than at lower temperatures, in the same time. This was probably due to its impervious structure preventing the inflow of oxygen. Such layers commonly showed blisters and eruptions, due to the dissociation pressure of the zinc sulphide causing them to be lifted off the underlying solid sulphide.

4. Diffusion and Reaction on a Plane Surface

We shall put forward an approximate theory of simultaneous reaction at the ZnO–ZnS interface and of diffusion of oxygen through the overlying layer of zinc sulphide. The theory will be based on a number of approximations, the main purpose being to illustrate the transition from chemical control at low temperature to diffusion control at higher temperature, with an intervening region where both processes are significant.

For simplicity we shall consider the case of plane surfaces and neglect the edge effects. The treatment will thus apply approximately to the

* At lower temperatures the oxide formed on zinc sulphide shows preferred orientation [9], [10] and [11].

roasting of a crystal when the penetration is still comparatively small. A comparable theory can be readily developed for the case of a spherical particle, allowing for the progressive diminution of the interfacial area.

Again for simplicity we shall apply FICK's law to the inwards diffusion of oxygen through the porous zinc oxide, despite the existence of a flow of sulphur dioxide in the reverse direction.* The concentration gradient will also be assumed to be linear;† the number of moles of oxygen diffusing in unit time up to unit area of the interface is therefore

$$D(c_0 - c)/x, \tag{3}$$

where D is the diffusion coefficient and x is the oxide layer thickness at time t, c and c_0 are the oxygen concentrations at the ZnO–ZnS interface and at the outer surface of the crystal respectively (the latter being equal to the concentration in the bulk gas phase, in the absence of any appreciable mass transfer resistance in this phase).

The reaction rate at the interface will be taken as being approximately proportional to the square root of c, as indicated by the experimental results.

Thus the number of moles of oxygen reacting in unit time at unit area of the interface is

$$kc^{\frac{1}{2}}, \tag{4}$$

where k is a velocity constant. Equating (4) and (5) at the steady state,

$$kc^{\frac{1}{2}} = D(c_0 - c)/x$$

and hence

$$c = c_0(1 + r - r\sqrt{1 + 2/r}), \tag{5}$$

where r is the dimensionless quantity

$$r = x^2k^2/2D^2c_0 \tag{6}$$

The penetration rate, dx/dt, is obtained by multiplying (4) by V, the molar volume of zinc sulphide and by a factor $\frac{2}{3}$, from the stoichiometry of the reaction. Thus, from (4) and (5), together with these factors,

$$\frac{dx}{dt} = \tfrac{2}{3}kVc_0^{\frac{1}{2}}(1 + r - r\sqrt{1 + 2/r})^{\frac{1}{2}} \tag{7}$$

This expression reduces to simpler forms under two limiting conditions:

(1) If $r \ll 1$, which occurs at temperatures at which k is small,

$$\frac{dx}{dt} \doteq \tfrac{2}{3}kVc_0^{\frac{1}{2}} \tag{8}$$

This corresponds to "chemical control" since the rate is independent of the thickness, or of the value of the diffusion coefficient.

(2) If $r \gg 1$, which occurs at higher temperatures where k is relatively large,

$$\frac{dx}{dt} \doteq \tfrac{2}{3}\frac{DVc_0}{x}, \tag{9}$$

which corresponds to "diffusion control." Integrating (9)

$$x^2 = \frac{4}{3}DVc_0t, \tag{10}$$

and the thickness is thus proportional to the square root of the time.

Below 830°C, the limiting case represented by eq. (8) is in satisfactory accord with the present results. On the other hand, the "parabolic" law (10) has not been encountered, probably because a high enough temperature could not be reached before the onset of the phenomena of uneven penetration and vaporisation. For the same reason we have not made any detailed application of the more general equation (7), which is applicable in the intermediate range of temperature where chemical reaction and diffusion are both significant as controlling factors.

5. DISCUSSION

As mentioned previously, earlier studies on the oxidation rate of naturally occurring crystals of zinc sulphide have been made by OGAWA [1] and by ONG, WADSWORTH and FASSELL [2]. At 800°C OGAWA obtained a penetration rate in air of $4{\cdot}2 \times 10^{-6}$ cm^{-1} sec^{-1} as compared to $2{\cdot}6 \times 10^{-6}$ cm sec^{-1} by interpolation from Fig. 6 of the present work.

* For a more elaborate treatment of such cases, see JOST [6].

† For a discussion on this point, see BOOTH [7] and DANCKWERTS [8].

Much more extensive results were obtained by ONG, WADSWORTH and FASSELL [2]. Under similar conditions the rates described by these workers are between 25% and 50% of those obtained in the present work, and thus lie in the opposite direction to the figure quoted from OGAWA [1].

As described above, we have expressed the dependence of the " chemically controlled " rate on the oxygen partial pressure in terms of a half power. However an inspection of the calculated results in the upper part of Table 2 shows that the representation of the experimental data by means of this relationship is by no means good, especially at the extremes of partial pressure. The results of ONG, WADSWORTH and FASSELL [2] – published since our own work was completed – cover a much wider range of partial pressures. The general characteristic of their results at temperatures below 846°C is that the rate increases more and more slowly with increasing partial pressure and eventually becomes independent of it. This behaviour they interpret as due to the rate limiting step being dependent on the concentration of adsorbed oxygen molecules on the zinc sulphide surface, this adsorption being determined by a LANGMUIR type isotherm :

$$\theta = \frac{K_1 [O_2]}{1 + K_1 [O_2]} \qquad (11)$$

where θ is the fraction of the surface covered and $[O_2]$ is the concentration of oxygen in the gas phase. This function accounts for their measured rates very satisfactorily, and it can also be used to express our own results quite as well, if not better than the half power relationship.* Nevertheless the latter is an adequate approximation in the region of oxygen partial pressures which are of interest in the technical process of zinc production and is a simpler relationship for practical use.

As discussed above, it is believed that the diffusion of oxygen through the bulk oxide become significant as a rate limiting factor at temperatures in excess of 830°C. At still higher temperatures, however, it seems that an entirely different mechanism of reaction sets in, and it may eventually become faster than the mechanism discussed above. This is the dissociative evaporation of zinc sulphide, followed by its oxidation in the vapour phase. The rate of this process may be expected to depend on temperature according to an exponential factor $e^{-E_v/RT}$, where the activation energy E_v is at least equal to the latent heat of evaporation. According to VESELOVSKI [5] and the unpublished work of Dr. RICHARDS†, this latent heat is considerably larger* than the value, 50 kcal/mole, obtained in Section 3 above for the activation energy in the low temperature region of " chemical control." This evaporation mechanism may therefore be expected to overtake the mechanism discussed above at a sufficiently high temperature ; at even higher temperatures this evaporative process itself may run into a second region of diffusion control, connected with the mixing of the reactants in the gaseous phase. It is these processes which are probably the most significant in the hottest regions of the bed, as used in the industrial roasting method. In particular, the deposition of zinc oxide from a vapour phase reaction may contribute to the mechanism of sintering.

Financial assistance, which enabled this work to be done, was given by C.S.I.R.O. and the Imperial Smelting Corporation, and is gratefully acknowledged.

* However, at an oxygen concentration at which the rates measured by the American workers have become independent of the concentration, our own rates are still increasing. This indicates a different value of K_1.

† Dr. A. W. RICHARDS of the Imperial Smelting Corporation, Avonmouth.

* VESELOVSKI's figure is 65 kcal per mole.

REFERENCES

[1] OGAWA Y. *Tech. Rep. Tohuku Imp. Univ.* 1929 **9** 175.

[2] ONG WADSWORTH, and FASSELL *J. Metals* 1956 257 (*Transactions A.I.M.E.* Vol. 206).

[3] GULBRANSEN E. A. and ANDREW K. F. *J. Electrochem. Soc.* 1951 **98** 241.

[4] TU C. M. DAVIS H. and HOTTEL H. C. *Ind. Eng. Chem.* 1934 **26** 749.

[5] VESELOVSKI B. K. *J. Appl. Chem.* (U.S.S.R.) 1942 **15** 422.

[6] JOST W. *Chem. Eng. Sci.* 1953 **2** 199.

[7] BOOTH F. *Trans. Faraday Soc.* 1948 **44** 796.

[8] DANCKWERTS P. V. *Trans. Faraday Soc.* 1950 **46** 701.

[9] YAMAGUTI T. *Proc. Phys.-Math. Soc. Japan* 1935 **17** 443.

[10] AMINOFF G. and BROOMÉ B. *Nature* 1936 **137** 995; *Kungl. Svenka. Vetensk Handl.* 1938 **16** 3.

[11] PINSKER *Electron Diffraction.* p. 264 Butterworths, London.

Chemical Engineering Science, 1957, Vol. 6, pp. 155 to 159. Pergamon Press Ltd.

Studies on gas-solid reactions—II

Causes of thermal instability

K. J. CANNON* and K. G. DENBIGH†
The Chemical Engineering Department, Cambridge

(*Received* 18 *December* 1956)

Abstract—The paper describes two distinctive forms of thermal instability which can make their appearance in gas-solid reactions. The first is due to an unstable type of crossing of the curves which represent the rate of heat generation by reaction within the solid and the rate of heat loss from its surface. In this connection the significance of the concept of ignition temperature is discussed. The second type of instability is one which affects localised regions of the reacting solid ; under conditions where the temperature of the reaction interface becomes higher the larger the thickness of the layer of reaction product, any small initial variations in the thickness of this layer will rapidly augment themselves. A theory of this effect is put forward.

Résumé—Les auteurs décrivent deux formes différentes d'instabilité thermique susceptibles de se produire dans des réactions gaz-solides.

La première serait dûe à un type instable d'intersection des courbes : vitesse de génération de chaleur à l'intérieur du solide et vitesse de diperdition de chaleur par sa surface. Les auteurs discutent, à ce sujet, du concept de la température d'ignition.

La seconde forme d'instabilité affecterait des régions bien localisées du solide en réaction ; si la température de l'interface de réaction s'élève, l'épaisseur de la couche du produit de réaction devient plus grande ; de petites différences initiales dans l'épaisseur de cette couche s'amplifient rapidement d'elles-mêmes. Les auteurs approfondissent cette dernière théorie.

1. INTRODUCTION

IN PART I [1] we have described experimental work on the oxidation rate of zinc sulphide and during the course of this work it was noticed that there are interesting phenomena of thermal instability. Since these phenomena may be met with throughout the field of gas-solid reactions, including combustion, it has seemed worth while presenting our conclusions in a separate paper.

It appears that thermal instability may occur in two distinctive forms according to whether it is due to (1) an unstable crossing of the curves of heat generation and heat loss, (2) the effect of solid reaction product in impeding the loss of heat. The former affects the solid particle as a whole ; the latter results in uneven growth of the layer of reaction product on different parts of the surface.

2. UNSTABLE CROSSINGS

Phenomena of this kind have been described in the literature, notably by VAN HEERDEN [2] and VAN LOON [3], but are not yet well known. Consider a reaction of the type

$$ZnS + \frac{3}{2}O_2 = ZnO + SO_2$$

As discussed in Section 4 of Part I, there is a transition from chemical control to diffusion control with rising temperature. Thus at low enough temperatures the overall rate is determined by the chemical kinetics and increases rapidly and exponentially with temperature ; at higher temperatures the rate limiting factor becomes the diffusion of the gases through the solid reaction product and this process has a relatively low temperature coefficient. The

* Present address : Division of Industrial Chemistry, C.S.I.R.O., Fisherman's Bend, Melbourne.
† Present address : The Department of Chemical Technology, King's Buildings, West Mains Road, Edinburgh.

overall rate, as a function of temperature, is thus as shown by the sigmoid curve of Fig. 1 (which has been drawn from equation (7) of Part I, using the known temperature dependence of k and D). In so far as the heat of reaction is approximately independent of temperature, the rate of heat generation in the reacting solid will be of the same form and the sigmoid curve will be taken henceforth to refer to the heat generation.

Consider now the rate of heat loss from the solid. If convective transfer to a gas stream is the most significant mechanism, the heat loss will be approximately proportional to $T - T_g$, where T and T_g are the temperatures of solid and gas respectively. On Fig. 1, the heat loss will thus be represented by straight lines* AB, $A'B'$, etc.,

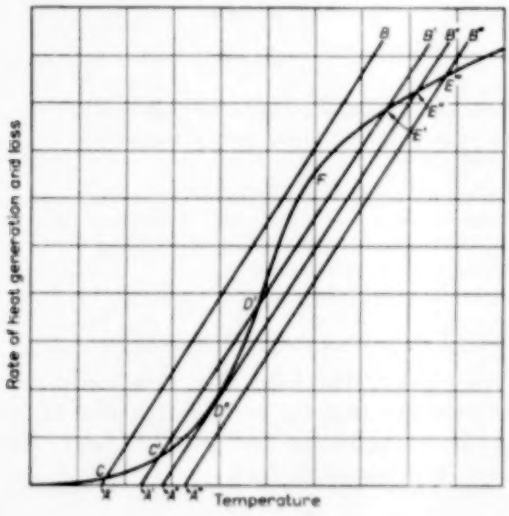

Fig. 1. Rate of heat generation and loss from a reacting particle.

whose gradient is determined by the heat transfer coefficient and whose intercepts A, A', etc. on the horizontal axis represent the particular values of T_g in the system in question.

The points C and C' clearly represent stable states of low reaction rate in the chemically controlled region; they are stable in the sense that any momentary rise or fall of temperature will cause the heat loss to become greater or less respectively than the heat generation and will thus cause the system to return to the points C or C'. Similarly points E', E'' and E''' represent stable states of high reaction rate in the diffusion controlled region.

Point D', on the other hand, is an *unstable crossing point*; although heat loss is equal to heat generation, any small downward variation of temperature will cause the system to fall to point C' and any small upward variation will cause the system to rise to point E'. Thus the region C' to E' cannot be realized under the prevailing conditions.

Consider the introduction of the solid into the gas when the latter is at a temperature A'; if the solid is initially *cold* its temperature will rise to the lowest point at which there is a stable crossing, namely C'. On the other hand, if the solid is initially *hot* and at a temperature exceeding the value corresponding to D', the temperature will rise to E', where there is a high reaction rate in the diffusion controlled region. Thus D' may be referred to as an *ignition temperature*. (The use of this terminology implies that the solid is not regarded as being "ignited" in the region of points C and C' where the reaction rate is very low.)

The introduction of the cold solid into the gas when the latter is at a slightly higher temperature A''' will result in the solid reaching the high temperature corresponding to E'''. It is evident that the line $A''B''$, which is tangential to the heat generation curve at D'', represents a critical condition; D'' is the *minimum ignition temperature* of the solid and the gas temperature A'' is the *minimum gas temperature* for ignition of the cold solid.

The tangent, (which is not shown), at point F also represents a critical condition of a different type; the temperature at F is the lowest temperature, under the prevailing conditions, at which there is rapid reaction and is referred to by van Loon [3], in his discussion of carbon combustion, as the *minimum combustion temperature*.

The actual values of these critical temperatures are determined not only by the nature of the

* If loss of heat by radiation is also a significant factor, the straight lines will be replaced by curves which are convex towards the temperature axis.

particular reactants but also by the partial pressure of the reactive gas and by the value of the heat transfer coefficient under the prevailing conditions, since it is these which determine the relative positions and slopes of the curves. The notion of ignition temperature is thus by no means absolute, but is relative to a particular set of conditions.

It may be noted also that if the heat transfer coefficient is large, or if the reaction is such that the rate of heat release is always low, the unstable crossings may not be obtained.

3. The Effect of the Layer of Reaction Product

As described in Part I, at temperatures above 900°C small initial variations in the thickness of the oxide layer tend to magnify themselves, giving rise to a sort of autocatalytic growth of the layer on different parts of the surface. This type of instability evidently occurs when the local reaction rate at the interface is greater the thicker is the overlying layer of reaction product. For when this condition is satisfied, any regions of the particle where the layer is accidentally slightly thicker than elsewhere will tend to develop relatively still thicker layers. It is therefore of interest to examine the conditions under which the reaction rate at the interface increases with increasing penetration.

Consider a partially oxidized spherical particle of zinc sulphide whose radius is r_0. Let r_i be the radius up to the sulphide-oxide interface, i.e. $r_0 - r_i$ is the thickness of the oxide layer. Let T_0 and T_i be the temperatures at the outer surface and at the interface respectively and let Q be the rate of heat generation per unit area of the interface due to reaction.

The total rate of heat generation is $4\pi r_i^2 Q$; at the stationary state at which the temperatures are time independent, this is equal to the rate at which heat passes outwards through any spherical shell within the zinc oxide layer. Thus

$$4\pi r_i^2 Q = -K\, 4\pi r^2 \frac{dT}{dr},$$

where T is the temperature at a radius r and K is the thermal conductivity of the layer. Integrating between the limits

$$r = r_i \quad , \quad T = T_i,$$

$$r = r_0 \quad , \quad T = T_0,$$

we obtain

$$T_i - T_0 = \frac{r_i^2 Q}{K}\left(\frac{1}{r_i} - \frac{1}{r_0}\right) \qquad (1)$$

The spherical particle will be assumed to be suspended in a moving gas stream at a temperature T_g and to be "seeing" furnace walls at a temperature T_f. If the particle may be regarded as being "grey," the rate of heat loss will be

$$4\pi r_0^2 \{\sigma\epsilon (T_0^4 - T_f^4) + h (T_0 - T_g)\},$$

where σ and ϵ are the Stefan-Boltzmann constant and the emissivity respectively and h is the heat transfer coefficient. At the stationary state this expression must equal $4\pi r_i^2 Q$, the rate of heat generation at the interface. Thus

$$\frac{r_i^2 Q}{r_0^2} = \sigma\epsilon (T_0^4 - T_f^4) + h (T_0 - T_g) \qquad (2)$$

If $T_f > T_0 - T_f$ and $T_g \doteq T_f$ (as under the experimental conditions described in Part I), equation (2) may be approximated by

$$\frac{r_i^2 Q}{r_0^2} = (4\sigma\epsilon\, T_f^3 + h)(T_0 - T_f) \qquad (3)$$

Eliminating T_0 between (1) and (3) we obtain

$$T_i - T_f = \frac{r_i^2 Q}{r_0^2}\left\{\frac{r_0 (r_0 - r_i)}{K r_i} + \frac{1}{4\sigma\epsilon\, T_f^3 + h}\right\} \qquad (4)$$

which gives the value of $T_i - T_f$, the amount by which the temperature at the reacting interface exceeds the controlled temperature of the environment of the particle.

In this equation the rate of heat generation, Q, is itself a function of T_i. It will be assumed for simplicity that the chemical kinetics at the interface remain the controlling factor over the whole

temperature range.* (In a more elaborate treatment it would be preferable to use the equation for a spherical particle, analogous to equation (7) of Part I, which allows for both reaction and diffusion.) With this assumption Q may be written

$$Q = Be^{-E/RT_i}, \tag{5}$$

where B is a constant which includes the heat of reaction. Substituting (5) in (4) we obtain

$$T_i - T_f = Be^{-E/RT_i}\left\{\frac{r_0 p}{K}(1-p) + a(1-p)^2\right\}, \tag{6}$$

where p, the fractional penetration, is defined by

$$p = (r_0 - r_i)/r_0, \tag{7}$$

and

$$a = 1/(4\sigma\epsilon T_f^3 + h). \tag{8}$$

By differentiation of (6),

$$\frac{dT_i}{dp} = \frac{Be^{-E/RT_i}\left\{\frac{r_0}{K}(1-2p) - 2a(1-p)\right\}}{1 - \frac{E}{RT_i^2}(T_i - T_f)} \tag{9}$$

An instability of the type under discussion will occur if dT_i/dp is positive : for in this case the temperature at the interface is higher the greater is the penetration. Areas of the solid where the oxide layer is already slightly thicker than elsewhere will have a higher interface temperature and a higher reaction rate, and any initial disparities in thickness will thus tend to magnify themselves.

The denominator of (9) is normally positive : the condition of instability is therefore

$$\frac{r_0}{Ka} > \frac{2(1-p)}{1-2p} \tag{10}$$

This condition is the more readily satisfied (a) the smaller is the degree of penetration, (b) the smaller is the thermal conductivity K, (c) the larger is the radius r_0 of the particle, (d) the larger is the furnace temperature, the emissivity and the heat transfer coefficient, which determine the value of the quantity a, defined by equation (8).

The physical situation may perhaps be understood most clearly by considering the two opposing factors :

(1) with increasing penetration of a spherical particle r_i diminishes and this tends to cause a reduction in the total heat generation $4\pi r_i^2 Q$, within the crystal ;

(2) with increasing penetration the thickness of the oxide layer, $r_0 - r_i$, increases and this tends to reduce the loss of heat from the interface by thermal conduction.

If the second factor more than offsets the first, the interface temperature will increase with increasing penetration and thus cause instability.

The effect of greater heat loss from the *surface* of the particle in favouring instability (item (d) above) appears paradoxical, but is due to the fact that T_0, the surface temperature, tends to diminish with increasing penetration, as may be seen from equation (3) ; however the larger is the surface heat loss the smaller is the relative magnitude of this decrease and therefore the more readily does T_i increase with increasing penetration.

Equation (6) cannot be solved directly for $T - T_f$, as a function of T_f and p, since T_i also occurs in the exponential term. However, by trial and error solution, a set of values of $T_i - T_f$ have been obtained which satisfy the equation. For this purpose it was necessary to use estimated values of the emissivity and thermal conductivity of the porous layer of zinc oxide, and also of the heat transfer coefficient h.* It was found that a reasonable choice of these quantities leads to values of $T_i - T_f$ which are of the same order of magnitude as the experimentally measured "self-heating," as described in Section 2 (f) of Part I.

* In the experimental work described in Part I, diffusion through the zinc oxide layer began to have an appreciable influence at temperatures above 830°C. Nevertheless, the chemical reaction remained the main controlling factor to above 900°C. It may be noted that under conditions where diffusion becomes the controlling factor the instability described in this section cannot occur, as may be seen by replacing equation (5) above by an equation analogous to (9) in Part I. Diffusion control causes the reaction rate to diminish with increasing penetration.

* The values of the parameters E and B, which also appear in equation (6), have been taken from the results of Part I, together with the known heat of reaction.

The family of curves obtained in this way is shown in Fig. 2. which pertain to a particle of radius $r_0 = 0{\cdot}25$ cm. Due to the uncertainty in the assumed values of the emissivity etc., these curves have actually been drawn using a value for a, as defined by equation (8), which brings the calculated self-heating effect into exact agreement with the experimentally observed values, i.e. about 10° at 800° and upwards of 20° at 900°C. It is a useful check on the theory that the same value of a, viz. $3{\cdot}7 \times 10^{-6}$, when applied in the expression (10), predicts an onset of instability at about 900°, as observed experimentally. This point of instability is also made apparent in Fig. 2 as the temperature at which there commences an upward slope of the $T_i - T_f$ curves at low degrees of penetration.

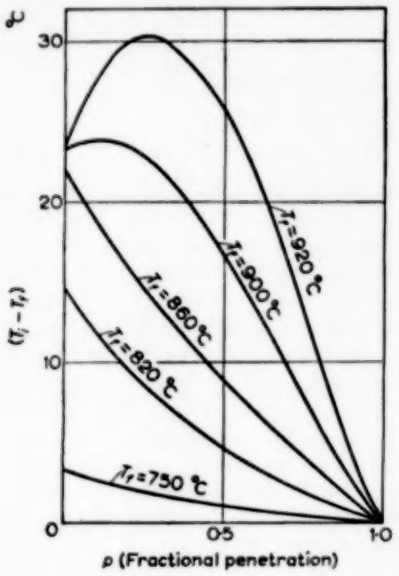

FIG. 2. Variation of reaction interface temperature with penetration.

It may be remarked that a self-heating effect (or self-cooling, if the process is endothermic) in gas-solid reactions has been observed previously [4], [5], [6], but the theory of instability to which it may give rise seems not to have been described hitherto.

Financial assistance by C.S.I.R.O. and the Imperial Smelting Corporation, which enabled this work to be done, is gratefully acknowledged.

REFERENCES

[1] CANNON K. J. and DENBIGH K. G. *Chem. Eng. Sci.* 1957.

[2] VAN HEERDEN C. *Ind. Eng. Chem.* 1953 **45** 1242.

[3] VAN LOON W. Thesis, Delft 1952.

[4] ANOUS M. M. T., BRADLEY R. S. and COLVIN J. *J. Chem. Soc.* 1951 3348.

[5] PILLING N. B. and BEDWORTH R. E. *J. Inst. Metals* 1923 **29** 579.

[6] LEVESQUE P. and CUBICCIOTTI D. *J. Amer. Chem. Soc.* 1951 **73** 2028.

Chemical Engineering Science, 1957, Vol. 6, pp. 160 to 169. Pergamon Press Ltd.

Einige neue Verfahrensprinzipien mit Wirbelschichten*

E. WICKE

Institut für Physikalische Chemie der Universität Hamburg

(*Received* 30 *October* 1956)

Abstract—Quantities of heat locally supplied to or produced in fluid beds are very rapidly dissipated. Likewise, gases introduced at a given spot or formed inside the fluid bed by a chemical reaction are thoroughly mixed with the fluidized material. Hence, it is an obvious step to utilize these properties of the fluid bed for stopping rapid chemical reactions and to examine whether unstable intermediate products can thus be isolated. This may be achieved by two methods :

(1) The reaction starts outside the fluid bed, which acts as quenching medium ;
(2) The reaction proceeds inside the fluid bed with direct participation of the fluidized material.

These two principles are explained by means of three practical examples.

Résumé—Les quantités de chaleur fournies en des points isolés d'un lit fluidisé ou dégagées à l'intérieur du lit sont trés rapidement dissipées. De même, des gaz introduits en un point donné ou formés à l'intérieur du lit fluidisé par réaction chimique sont intimement mêlés au matériau fluidisé. Par suite, il est logique d'utiliser ces propriétés du lit pour arrêter les réactions chimiques rapides et pour tenter d'isoler s'il y a lieu les produits intermédiaires instables.

L'auteur propose deux méthodes :

(1°) Amorces de réaction extérieures au lit fluidisé, lorsque celui-ci se comporte comme un inhibiteur.

(2°) Développement de processus réactionnels à l'intérieur du lit fluidisé avec participation directe du matériau fluidisé.

Ces deux principes sont illustrés par 3 exemples pratiques.

1. EINLEITUNG

DEN Begriff der "Wirbelschicht" gibt es seit dem Jahre 1921, als FRITZ WINKLER erstmalig die "kochende" Bewegung einer glühenden Feinkohlefüllung beobachtete, die von Luft aufwärts durchströmt wurde. Seine Erfahrungen mit diesem neuartigen hydrodynamischen Zustand legte er in den Patenten zur Vergasung von feinkörniger Kohle oder Koks nieder, die zu der bekannten Entwicklung des Winkler-Generators führten, aber auch schon die Anwendung auf Röstprozesse u. dergl. erwähnten. Bereits 1926 wurde auch für katalytische Crackverfahren dieses Prinzip der früheren I. G. Farben-Industrie A. G. patentiert. Der eigentliche grosse Ausbau des Wirbelschicht-Crackens begann jedoch erst etwa 12 Jahre später in den Vereinigten Staaten, als dort die Wirbelschicht unter der Bezeichnung "fluidized bed" neu entdeckt wurde. Entscheidend war die kurz darauf gemachte Feststellung, dass feinkörnige Stoffe im Wirbelzustand ähnlich wie Flüssigkeiten durch Rohrleitungen gefördert werden und mit Hilfe von Standrohren auch Druckdifferenzen gehalten werden können [1]. Aus dieser Feststellung, die auf den ersten Blick vielleicht etwas unbedeutend erscheinen mag, entwickelten sich in USA die grossen fluidized Crackverfahren mit Kreislauf des Katalysators zwischen Reaktor und Regenerator, wie sie unter den modernen Einrichtungen der Erdölraffinerien auch in Europa errichtet wurden. Inzwischen ist die "Fluidization" – die Wirbelschichttechnik mitt Feststoff-Kreislauf oder mit einmaligem Feststoff-Durchsatz – auch für andere chemische Prozesse von Bedeutung geworden; ihre Entwicklung ist noch keineswegs abgeschlossen.

* Vortrag anlässlich des Jahrestreffens 1956 der Verfahrensingenieure in Hamburg am 2.10.1956.

Neben der hohen hydrodynamischen Beweglichkeit – dem "Fliessvermögen" – des Wirbelzustandes liegen seine besonderen Vorteile in der grossen Grenzfläche zwischen dem feinkörnigen Wirbelgut und der Gasströmung sowie in der hohen Intensität der Wärmedurchmischung innerhalb der Wirbelschicht. Diese starke Wärmedurchmischung beruht ebenso wie der hohe Wärmeübergang an Heiz- und Kühlelementen auf dem Wärmetransport durch die wirbelnden Partikeln, der die Wärmekonvektion der Gasströmung um Grössenordnungen übersteigt und für sehr schnellen Ausgleich örtlicher Temperaturunterschiede sorgt. Auch die Einmischung eines etwa seitlich oder von oben eingeführten Gasstrahls in das Wirbelgut erfolgt verhältnismässig schnell, doch fehlt hier ein analoger Transporteffekt der wirbelnden Partikeln, sodass diese stoffliche Durchmischung langsamer vor sich geht als z.B. bei turbulenter Strömung im leeren Rohr.

Immerhin legen diese Eigenschaften der Gaswirbelschichten nahe zu versuchen, ob man mit ihnen schnell verlaufende mehrstufige chemische Reaktionen abbrechen und dabei instabile Zwischenprodukte erfassen kann. Von drei Versuchen dieser Art, die sich durch das Arbeitsprinzip und die apparative Anordnung voneinander unterscheiden, soll im folgenden die Rede sein: vom Wirbelschicht-Tauchbrenner, von der Wirbelschicht-Funkenentladung und von der heiss-kalten Wirbelschicht.

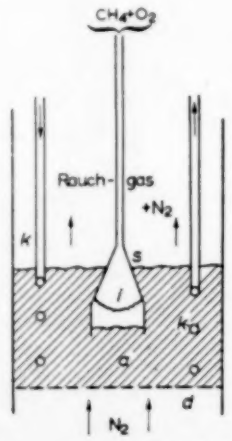

Abb. 1. Tauchbrenner in der Wirbelschicht, Prinzip der Anordnung.

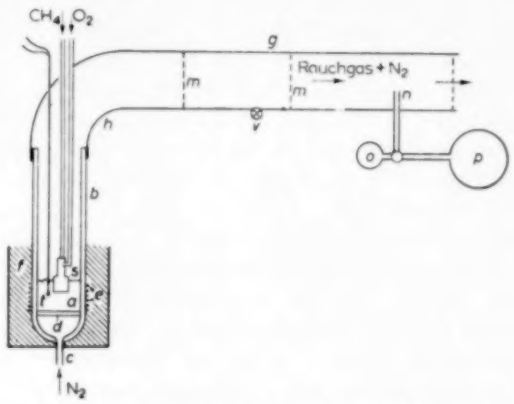

Abb. 2. Gesamte Versuchseinrichtung mit Wirbelschicht-Tauchbrenner.

2. Wirbelschicht-Tauchbrenner (gemeins. mit F. Fetting) [2]

Der Wirbelschicht-Tauchbrenner arbeitet nach dem Prinzip, die schnelle chemische Reaktion als Flamme vorgemischter Gase ausserhalb der Wirbelschicht anlaufen zu lassen und die heissen Flammengase durch die Wirbelschicht schnell abzukühlen bzw. abzuschrecken. Als *Modellreaktion* wurde die *unvollständige Verbrennung von Methan mit Sauerstoff* gewählt, die in dem bekannten Verfahren von Sachsse und Bartholomé durch Abschreckung der Flammengase mit eingespritztem Wasser das instabile Zwischenprodukt *Acetylen* liefert. Als Wirbelgut bewährte sich Siliciumcarbid von 50 bis 70 μ Korngrösse, als Wirbelgas wurde Stickstoff verwendet. Abb. 1 zeigt schematisch die Anordnung des in die Wirbelschicht eingehängten Tauchbrenners (*s*), der hier als Kelchbrenner gezeichnet ist, mit der angedeuteten Flammenfront (i). Die Temperatur der Wirbelschicht wurde in der Regel durch eine Kühlschlange (*k*) niedrig gehalten; sie musste aber natürlich genügend oberhalb des Taupunktes der Rauchgase liegen, um Kondensationen zu vermeiden.

Die gesamte apparative Anordnung ist in Abb. 2 dargestellt. Die Wirbelschicht (*a*) von 8 cm Ruheschichthöhe befand sich in einem Rotosiltiegel (*b*) von 12 cm Innendurchmesser. Als

Anströmboden war eine keramische Filterplatte (*d*) eingekittet. Die Kühlschlange zur Temperaturhaltung der Wirbelschicht auf ca. 100°C ist hier nicht eingezeichnet. Für eine Reihe von Versuchen mit höheren Abschrecktemperaturen konnte der Wirbelschichtbereich von aussen beheizt (*e*) und auch der von unten zuströmende Stickstoff vorgeheizt werden. Ein Thermoelement (*t*) diente zur Messung der mittleren Wirbelschichttemperatur. Als Tauchbrenner (*s*) ist hier der Typ eines Bunsenbrenners mit zylindrischer Misch- und Brennkammer eingezeichnet. Die Siliciumcarbid-Schicht wurde mit 350 bis 400 cm^3 NTP Stickstoff je Sekunde homogen aufgewirbelt, das entspricht einer Lineargeschwindigkeit von 8,5 bis 4 cm/sec unter Normalbedingungen im leeren Rohr. 1/6 bis 1/3 dieser Menge wurde an Brenngasgemisch dem Tauchbrenner zugeführt. Der Brennerrand tauchte 3 bis 5 cm unter die Wirbelschichtoberfläche. Dies genügte zur Abschreckung der Flammengase, brachte aber noch keine völlig gleichmässige Verteilung der Konzentrationen über den Schichtquerschnitt. Daher wurden in den Abzugskanal (*g*) zwei Turbulenzsiebe (*m*) eingebaut, die sicherstellten, dass durch den Saugstutzen (*n*) zuverlässige Analysenproben in die Glaskolben (*o*) und (*p*) gezogen werden konnten.

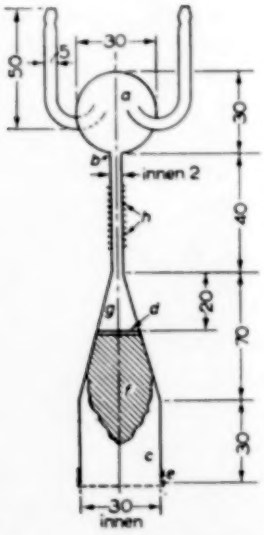

ABB. 3. Kelchbrenner aus Quarzglas (Maße in mm).

Von verschiedenen untersuchten Brennerarten bewährten sich am besten die Typen des Kelchbrenners und des Bunsenbrenners. Abb. 3 zeigt einen ganz aus Quarzglas gefertigten *Kelchbrenner*. Die getrennt zugeführten Gase Methan und Sauerstoff mischten sich in der Kugel (*a*) und der turbulent durchströmten Kapillare (*b*). Der Flammenraum war als Diffusor ausgebildet; ein eingeschmolzener Quartzstab (*d*) diente zur Stabilisierung des Flammensitzes. Die Brenngase durchströmten die Flammenzone in 0,02 bis 0,03 sec; unmittelbar unterhalb der Flammenfront setzte die Kühlwirkung der Wirbelschicht mit Temperaturgradienten von etwa 400 grd/cm ein. Nach einer Abkühlzeit von etwa 0,05 sec, d.h. ungefähr 2 mm vor der Brennermündung, hatten die Rauchgase bereits die mittlere Wirbelschichttemperatur angenommen. Bei einer Reihe von Versuchen wurde die Brennermündung mit einem Nickeldrahtnetz (*e*) (Maschenweite 0,8 mm) abgedeckt, um die Flamme vor stossenden Partikelwolken bei heftiger Bewegung der Wirbelschicht zu schützen. Dadurch wurde die Abkühlzone aus der Brennkammer heraus in die Brennermündung verlegt, doch blieb dies auf die Abgaszusammensetzung ohne Einfluss.

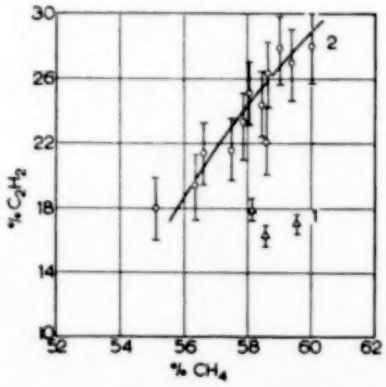

ABB. 4. Mit dem Kelchbrenner nach Abb. 3 erhaltene Acetylenausbeute,n abhängig vom Methangehalt im Brenngas-Gemisch (O_2–CH_4–Gemisch).

Die *Acetylenausbeuten* dieses Kelchbrenners bei einer Wirbelschichttemperatur von ca. 100°C sind in Abb. 4 dargestellt, als Funktion des Methangehaltes im Brenngasgemisch. Ausbeute bedeutet

hier Anteil des Kohlenstoffes, der aus dem umgesetzten Methan in Acetylen übergegangen ist. Die eingezeichneten Unsicherheitsspannen geben die Fehlerstreubreite der Acetylenanalysen an. Die Punktgruppe 1 wurde mit frei im Rohr hängendem Kelchbrenner, 10 cm oberhalb der Wirbelschicht, erhalten. Auch dabei treten schon erhebliche Acetylenausbeuten auf; durch Eintauchen des Brenners in die Wirbelschicht werden sie etwa verdoppelt (Punktgruppe 2). Mit steigendem Methangehalt im Brenngas steigen die Acetylenausbeuten etwa linear an, wie man es zu erwarten hat, solange die Flammentemperaturen noch nicht unter den günstigen Bereich von etwa 1300°C absinken. Ausser dem Acetylen enthalten die Abgase neben Stickstoff und Wasserdampf erhebliche Mengen Wasserstoff und Kohlenoxyd sowie geringe Anteile an Kohlendioxyd und nicht umgesetztem Sauerstoff und Methan. Die höchsten Ausbeuten von 26 bis 30% liegen in dem Bereich der Werte, die für den Acetylenbrenner von SACHSSE und BARTHOLOMÉ angegeben werden.

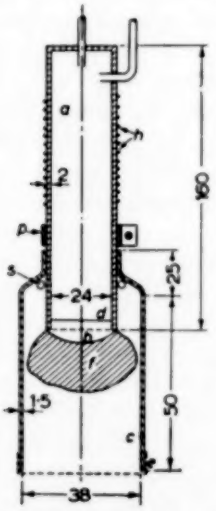

ABB. 5. Bunsenbrenner aus Stahlrohr mit Quarzglasglocke (Maße in mm).

Über einen Methangehalt von 60% hinaus konnte in dem Kelchbrenner keine stabile Flamme aufrechterhalten werden. Dies gelang jedoch mit dem in Abb. 5 skizzierten *Bunsenbrenner*. In einem Stahlrohrstutzen (*a*) wurden die Brenngase gemischt und konnten von aussen (*h*) vorgeheizt werden. Den Abschluss zur Brennkammer bildete eine Quarzwolleschicht (*d*) mit einem Drahtnetz (*b*), auf dem die Flamme aufsass. Die Brennkammer selbst bestand aus einer übergeschobenen Quarzglasglocke, deren Mündung wieder ein Nickeldrahtnetz (*e*) abdeckte. Die Flammentemperatur von etwa 1300°C reichte bis dicht an dieses Netz heran, darauf folgte ein sehr steiler Temperaturabfall von etwa 1800 grd/cm. Bereits 4 mm jenseits der Brennermündung hatten die Rauchgase nach nur etwa 0,01 sec Abkühlzeit die mittlere Wirbelschichttemperatur angenommen.

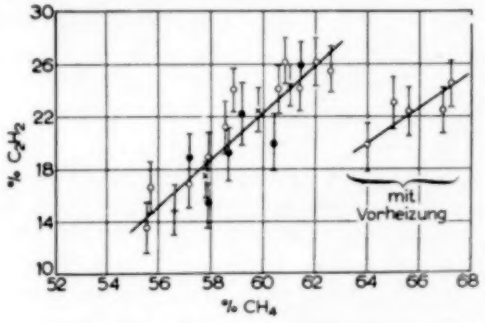

ABB. 6. Mit dem Bunsenbrenner nach Abb. 5 erhaltene Acetylenausbeuten, abhängigvom Methangehalt im Brenngas-Gemisch.

Die mit diesem Brenner erzielten *Acetylenausbeuten* bei 100°C Wirbelschichttemperatur zeigt Abb. 6. Die Werte des Kelchbrenners wurden nicht ganz erreicht, obwohl hier der Methangehalt im Brenngas bis auf 62,5% gesteigert werden

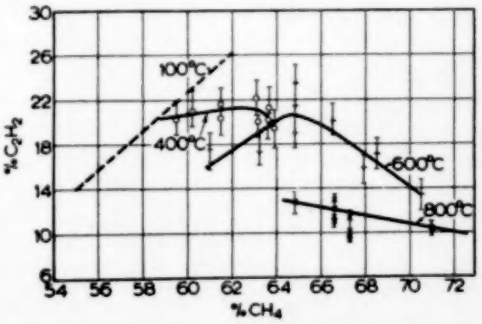

ABB. 7. Acetylenausbeuten des Bunsenbrenners bei höheren Wirbelschichttemperaturen.

konnte. Bei Vorheizung auf 650°C brannten sogar Gemische mit bis zu 67% Methan noch mit stabiler Flamme, doch ergaben auch diese keine höheren Acetylenausbeuten.

Mit dem Bunsenbrenner wurde auch bei erhöhter Wirbelschichttemperatur gearbeitet. Abb. 7 zeigt die Ergebnisse bei Abschrecktemperaturen von 400, 600 und 800°C. Die Acetylenausbeuten blieben auch hier noch erstaunlich hoch; erst bei 800°C fielen sie erheblich ab. Das bei 400°C und insbesondere bei 600°C auftretende Maximum ist offenbar darauf zurückzuführen, dass bei höheren Methangehalten die Flammentemperaturen unter den optimalen Bereich absinken. In den Versuchen mit 100° Wirbelschichttemperatur wurde keine Andeutung eines solchen Maximums gefunden; durch günstige Flammenstabilisierung sollte man daher die Acetylenausbeute dort eventuell noch steigern können.

Die Untersuchungen ergaben somit, dass Wirbelschichten durchaus geeignet sind, schnelle Reaktionen abzubrechen und instabile Zwischenprodukte zu fassen. Für die zu diesem Nachweis benutzte Modellreaktion, die Acetylenbildung aus Methan durch Teilverbrennung mit Sauerstoff, ist dieses Verfahren technisch allerdings kaum von Bedeutung. Dazu sind die Anteile des Acetylens im Abgas zu gering (0,3 bis 2,2 Vol.-%) und die Durchsätze im Brennerquerschnitt zu klein (einige Prozente der Durchsätze im Acetylenbrenner nach Sachsse und Bartholomé). Man könnte zwar beide Nachteile dadurch vermindern, dass man unter erhöhtem Gasdruck arbeitet und anstatt Stickstoff als Wirbelgas Wasserdampf benutzt. Dieser könnte bei der Temperaturhaltung der Wirbelschicht selbst erzeugt und aus dem Abgas unter Wärmerückgewinnung wieder herauskondensiert werden. Doch sollte ja kein neues Acetylenverfahren entwickelt sondern vielmehr gezeigt werden, dass bei Abschreckvorgängen Wirbelschichten mit gutem Erfolg und in breiten Temperaturbereichen Verwendung finden können.

8. Die Wirbelschicht-Funkenentladung (gemeinsam mit H. Schmidt u. M. Buschmann)

Eine zweite Arbeitsweise besteht darin, die zu unterbrechende Reaktion innerhalb der Wirbelschicht ablaufen zu lassen, wobei dann auch das Wirbelgut selbst an der Umsetzung beteiligt sein kann. In diesem Falle sind Temperaturgradienten in der Wirbelschicht erforderlich, die bekanntlich nur schwer aufrecht erhalten werden können. Bei elektrisch leitendem Wirbelgut sind jedoch durch Funkenentladung örtlich und zeitlich schnell wechselnde Temperaturgradienten leicht zu erzeugen. Die *eine* Elektrode kann z.B. als Drahtnetz oder Drahtspirale auf den Anströmboden gelegt, die andere als Spitzen- oder Büschelelektrode in Rohrmitte in geeignetem Abstand oberhalb des Anströmbodens angebracht werden. Befindet sie sich etwa 1 cm oberhalb der Schichtoberfläche, so geschieht bei ruhender Schicht auch nach Anlegen einer Wechselspannung von einigen KV zunächst noch nichts. Erst wenn die Partikeln nach Aufwirbelung und Schichtexpansion in die Nähe der Spitzenelektrode aufsteigen, setzt ein Funkenregen ein, indem zahlreiche Teilentladungen, von Korn zu Korn springend, die Wirbelschicht durchsetzen. Besonders feinteilig und gleichmässig aufgespalten ist dieser Funkenregen bei feinkörniger, graphitischer Kohle bzw. bei Kokspartikeln als Wirbelgut. Bei aufgewirbelten Metallpulvern teilt sich die Entladung weniger stark auf; die einzelnen Funken werden kräftiger und härter und durchsetzen nur einen Teil des Wirbelschichtraumes in der Umgebung des nächsten Abstandes zwischen den Elektroden. In jedem Fall glühen jedoch die von den Funken auf ihrem Zickzackweg getroffenen Partikeln momentan hell auf. In dieser Weise entstehen die erwähnten steilen Temperaturgradienten in den örtlich und zeitlich schnell wechselnden Einzelentladungen, insbesondere an den Brennflecken auf den Partikeloberflächen. Dort können chemische Umsetzungen thermisch gezündet werden, die anschliessend durch Abkühlung sehr schnell wieder abbrechen.

Mit feinkörniger Aktivkohle als Wirbelgut wurden einige *Vorversuche* zur Umsetzung mit verschiedenen Wirbelgasen in der Funkenentladung durchgeführt. Die Gase strömten mit Zimmertemperatur an, die mittlere Temperatur der Wirbelschicht lag infolge der Wärmeentwicklung durch den Stromfluss von 50 bis 100 mA

zwischen 100 und 200°C. Mit Wasserstoff als Wirbelgas wurde Acetylen gebildet, mit Stickstoff Dicyan, mit Ammoniak Cyanwaserstoff, Kohlendioxyd setzte sich zu Kohlenoxyd um. Die Ausbeuten dieser endothermen Reaktionen, gerechnet als Verhältnis der chemisch gebundenen Energie zur elektrisch aufgewandten, waren natürlich gering; im besten Falle, bei der Reduktion des Kohlendioxyds, kamen sie an 10% heran.

Grössere stoffliche Umsätze liessen sich erwarten, wenn die endothermen Prozesse – ähnlich wie bei der Teilverbrennung des Methans – mit exothermen gekoppelt sind. Als *Modellreaktion* für einen solchen Fall wurde die *Vergasung von Kohle* mit Wasserdampf und Sauerstoff gewählt [3]. Mit steigendem Sauerstoffgehalt im Wirbelgas sollte man hier den Bereich von der elektrothermischen Arbeitsweise – mit reinem Wasserdampf sowie geringem Sauerstoffzusatz – bis zum autothermischen Verhalten überstreichen können, bei dem die chemische Wärmeerzeugung durch die exotherme Verbrennung überwiegt und sich die Temperatur der Wirbelschicht daher selbständig einstellt.

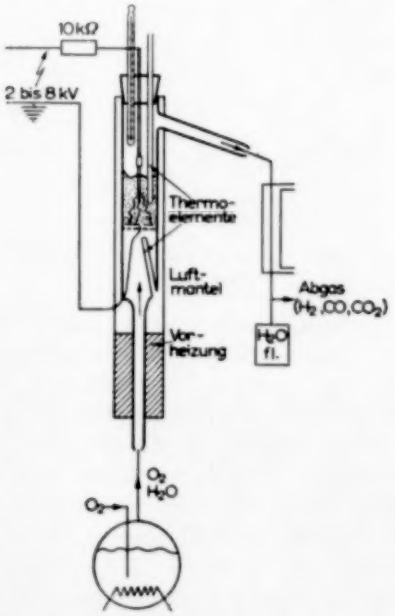

Abb. 8. Wirbelschichtreaktor aus Quarzglas mit Hochspannungs-Funkenentladung.

Die für diese Untersuchungen benutzte *Apparatur* ist in Abb. 8 skizziert. Das Wirbelschichtrohr aus Quarzglas von 40 mm Durchmesser besass eine eingeschmolzene Quarzfilterfritte als Anströmboden; die beschriebene Elektrodenanordnung wurde mit 2 bis 8 kV Wechselspannung betrieben. Als Wirbelgut wurde durchweg Aktivkohle Supersorbon von 0.1 bis 0.4 mm Korngrösse verwendet und zu 1 bis 3 cm Schichthöhe eingefüllt. Mit Wasserdampf sowie Wasserdampf-Sauerstoff-Gemischen wurden die Schichten aufgewirbelt und auf 3 bis 7 cm expandiert. Es wurde mit Elektrodenabständen zwischen 1,5 und 5 cm, mit Entladungsströmen zwischen 50 und 150 mA gearbeitet. Um störende Kondensationen zu vermeiden, wurden die Wirbelgase auf 250 bis 350°C vorgeheizt. Zur Wärmeisolierung war das Reaktionsrohr lediglich von einem etwas weiteren, der Länge nach in zwei Hälften geteilten Glaszylinder umgeben, sodass man die Vorgänge in der Wirbelschicht gut beobachten konnte. Thermoelemente und Thermometer dienten zur Temperaturkontrolle. Nach Kondensation des umgesetzten Wasserdampfes wurde das Abgas, das im wesentlichen aus Wasserstoff, Kohlenoxyd und Kohlendioxyd bestand, analysiert bzw. in einer kleinen Flamme laufend verbrannt.

Massgebend für das Verhalten der Wirbelschicht und die Gasproduktion war erwartungsgemäss der Sauerstoffgehalt im Frischgas. Mit wachsendem Sauerstoffgehalt stieg die mittlere Temperatur der Wirbelschicht stetig an bis schliesslich zur sich selbst unterhaltenden Verbrennung der Kohlefüllung. Eine Übersicht über den ganzen Bereich der verschiedenen Zustände

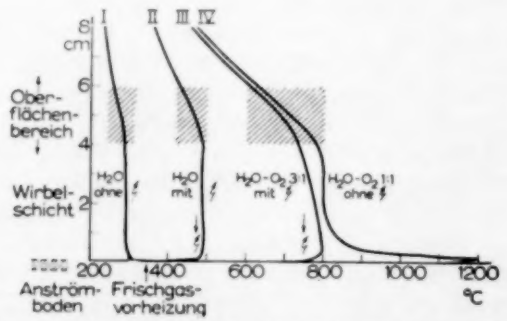

Abb. 9. Temperaturverlauf in Aktivkohle-Wirbelschichten.

gaben Messungen der *Temperaturverteilung* längs der Schichthöhe. Sie wurden mit einem verschiebbaren Thermoelement durchgeführt, das in einem an der Spitze besonders dünnwandigen Quarzröhrchen steckte. Die Ergebnisse sind in Abb. 9 zusammengestellt. Bei Aufwirbelung mit reinem Wasserdampf ohne angelegte Hochspannung (Kurve I) lag die Temperatur an der Oberseite des Anströmbodens bereits etwa 50° unter derjenigen des Frischgases, blieb längs der Wirbelschicht konstant und begann erst im Oberflächenbereich der Schicht abzusinken. Bei Zufuhr elektrischer Energie durch Funkenentladung (Kurve II) lag die Temperatur der Schicht über der des Frischgases, die Temperaturverteilung blieb jedoch gleichförmig. Wurden nun steigende Anteile des Wasserdampfes durch Sauerstoff ersetzt, so verschob sich das Temperaturprofil bei zunächst noch gleicher Gestalt weiter zu höheren Temperaturen hin. Von etwa 15 bis 20% Sauerstoff ab bildete sich jedoch ein Temperaturgefälle von unten nach oben aus, das bei 25% schon recht ausgeprägt war (Kurve III). Gleichzeitig begann die Wirbelschicht, sich durch die chemische Wärmeerzeugung selbständig glühend zu erhalten und von der elektrischen Energiezufuhr unabhängig zu werden. Oberhalb 30% Sauerstoff war dieser autothermische Zustand erreicht, mit einer mehr oder weniger ausgeprägten *Oxydationszone* am Fusse der Schicht. Das höchstliegende Temperaturprofil in Abb. 9, Kurve IV, stellt dieses Verhalten etwas überspitzt dar. Wegen des schnellen Abbrandes bei 50% Sauerstoff musste hier eine gröbere Kohlekörnung bis 2 mm verwendet werden, bei der die grösseren Partikeln sich in der Nähe des Anströmbodens anreicherten; daher dort die stark ausgeprägte Temperaturspitze der Oxydationszone. Hier war somit der Zustand eines *thermischen Wassergas-Generators* erreicht, allerdings eines schlechten Generators, da wegen des kleinen Schichtquerschnittes und der mangelnden Wärmeisolierung hohe Sauerstoffgehalte im Frischgas erforderlich waren und die Temperatur unmittelbar oberhalb der Oxydationszone steil absank, so dass sich keine wirksame Reduktionszone ausbilden konnte.

Für den gesamten Bereich von reinem Wasserdampf bis zu 60% Sauerstoffgehalt wurden die *Abgase* nach Menge und Zusammensetzung bestimmt. Die Gasproduktion, welche ohne Sauerstoff nur einige cm^3/sec, d.h. wenige Prozente des durchgesetzten Wasserdampfs, betrug, stieg mit wachsnedem Sauerstoffzusatz stärker als linear bis auf etwa 35 cm^3/sec an. Einen Überblick über die Zusammensetzung der (trockenen) Abgase gibt Abb. 10. Mit *reinem Wasserdampf* entstanden bei mittleren Temperaturen der Wirbelschicht um 500°C etwa 52% H_2, 36% CO, 9% CO_2, 2% CH_4 sowie 1% O_2 und Spuren von C_2H_2. Ausserdem bildeten sich höhermolekulare Verbindungen, die sich im Kondenswasser lösten, insbesondere Ameisensäure. Der Methananteil konnte durch Verwendung sehr feinteiliger Kohle (mittlerer Korndurchmesser 60 μ) und Zusatz von Nickeloxyd oder Raney-Nickel als Katalysatoren zur Wirbelschicht bis auf 5% erhöht werden. Die gesamte Energieausbeute dieser elektrothermischen Wasserdampfvergasung bei niedrigen Wirbelschichttemperaturen betrug 5 bis 10%.

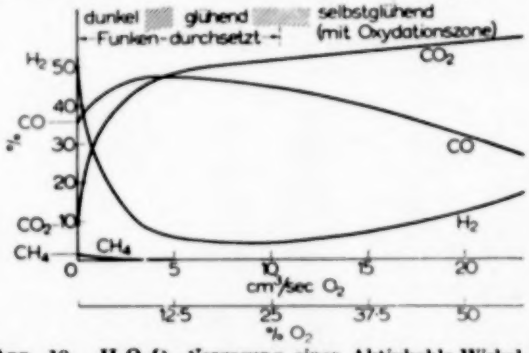

Abb. 10. H_2O–O_2–Vergasung einer Aktivkohle-Wirbelschicht.

Bei *Sauerstoffzusatz* zum Frischgas stieg die gesamte Gasproduktion durch verstärkte Bildung von Kohlenoxyd und Kohlendioxyd erheblich an. Primär erzeugt der Sauerstoff durch Angriff an den heissen Brennflecken der Funkenentladung Kohlenoxyd; dieses verbrennt jedoch, beschleunigt durch die katalytische Wirkung der anwesenden Wasserstoffverbindungen, zu einem erheblichen Teil zu Kohlendioxyd nach; daher die steile Zunahme dieser Komponente in Abb. 10 bei steigendem Sauerstoffzusatz. Die Wasserdampfzersetzung wird durch die lokale Wärmeer-

zeugung beim Angriff des Sauerstoffs auf die Kohle verstärkt; doch verbrennt ein erheblicher Teil des Wasserstoffs wieder zu Wasserdampf. Diese Nachverbrennung des Wasserstoffs, zusammen mit dem starken Anstieg der gesamten Abgasmenge, verursacht das steile Absinken des Wasserstoffgehaltes (wie auch des Methangehaltes) im Abgas. Mit weiter steigender Sauerstoffzufuhr und auf 600 bis 800°C wachsenden Wirbelschichttemperaturen verbrennen immer grössere Anteile des Kohlenoxyds zu Kohlendioxyd; ausserdem greift hier der Sauerstoff, unabhängig von der Funkenentladung, die gesamte Oberfläche der Kohlepartikeln an und erzeugt dabei im Primärprozess bereits erhebliche Mengen CO_2 neben CO. Daher fällt der Kohlenoxydanteil im Abgas gegenüber dem Kohlendioxyd immer stärker ab. Erst bei verhältnismässig hohen Saurestoffzusätzen und selbstglühender Wirbelschicht deutet der Wiederanstieg der Wasserstoffausbeute einen Übergang zu andersartigem Verhalten an. Dies hängt jedoch, wie schon an den Temperaturkurven in Abb. 9 erläutert, mit dem vollständigen Verbrauch des Sauerstoffs in einer verhältnismässig schmalen Oxydationszone und der Ausbildung einer darüberliegenden Reduktionszone, also den üblichen Verhältnissen rein thermischer Gaserzeugung, zusammen.

Die aus diesen Ergebnissen zu ziehenden Schlüsse können kurz folgendermassen formuliert werden: Die Abschreckwirkung einer Kohlewirbelschicht reicht aus, um Verbindungen, die sich in der beschriebenen Funkenentladung mit geeigneten Wirbelgasen bilden, wie z.B. Methan, Ameisensäure, Acetylen, Cyanverbindungen usw, zum Teil zu niedrigen Temperaturen herunter zu retten, bevor sie thermisch wieder zerfallen. Sie reicht jedoch nicht aus, um bei Sauerstoff-haltigem Wirbelgas die Nachverbrennung von Wasserstoff und von Kohlenoxyd in wasserstoffhaltiger Atmosphäre in stärkerem Ausmass zu verhindern.

4. Heiss-kalte Wirbelschicht (gemeinsam mit M. Buschmann)

Parallel mit den Versuchen an der Funkendurchsetzten Wirbelschicht wurde geprüft, ob es nicht doch möglich sei, in einer Wirbelschicht auch ein *stationäres* Temperaturgefälle zu erzeugen und aufrechtzuerhalten. Hierzu wurde das Wirbelgas vor Eintritt in die Schicht stark vorgeheizt – auf 800 bis 1100°C – und in den Oberflächenbereich der Wirbelschicht eine Kühlschlange eingehängt. Abb. 11 zeigt die *apparative Anordnung*. Das Wirbelschichtgefäss mit Frischgaszufuhr war wieder aus Quarzglas hergestellt.

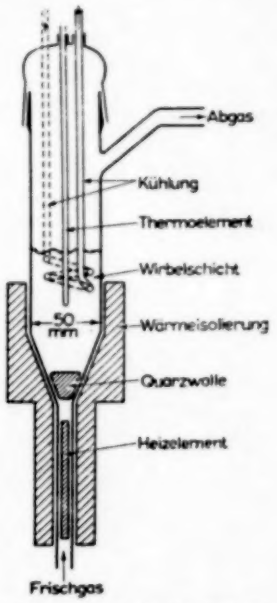

Abb. 11. Heiss-kalte Wirbelschicht.

In den Frischgasstutzen wurde ein Pythagorasstab mit aufgewickelten Heizdrahtwendeln eingebaut. Oberhalb dieses Heizelementes erweiterte sich das Rohr diffusorartig zum Wirbelschichtraum. Am Grunde dieser Erweiterung sass ein Quarzwollepfropfen als Anströmboden, 5 bis 8 cm oberhalb tauchte die Kupferkühlschlange in den Oberflächenbereich der brodelnden Wirbelschicht ein. Zu-und Ablauf des Kühlmittels waren durch eine Schliffkappe am Kopf des Apparates geführt; ebenso ein Thermoelement, das längs der Rohrachse verschoben werden konnte, um die Temperaturverteilung über die Schichthöhe zu messen. Solche *Temperaturprofile* zeigt Abb. 12. Sie wurden erhalten mit feinkörnigem Calciumnitrid (Ca_3N_2) als Wirbelgut und Stickstoff als Wirbelgas, der auf 800 bzw. 1000°C vorgeheizt worden

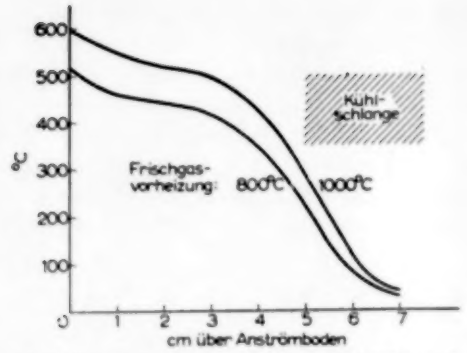

ABB. 12. Temperaturverlauf in heiss-kalter Wirbelschicht.

war. Quarzsand als Wirbelgut zeigte ähnliche Ergebnisse. Bei geringerer Gasströmung und ruhender Schicht ergaben die Messungen im stationären Zustand bis einige cm vor der Kühlschlange die Vorheiztemperatur des Gases, dann folgte ein sehr steiler Temperaturabfall. Mit beginnender Aufwirbelung der Schicht brach dieses steile Temperaturgefälle zusammen; unmittelbar oberhalb des Quarzwollepfropfens wurden im Wirbelzustand Temperaturen gemessen, die bereits erheblich unter der Gasvorheizung lagen. Trotzdem verblieb in der Wirbelschicht, wie Abb. 12 zeigt, noch ein Temperaturabfall von mehreren Hundert Graden. Wir haben diesen Zustand daher eine " heiss-kalte " Wirbelschicht genannt. Sie erscheint geeignet für Umsetzungen, in denen das Wirbelgut in verschiedenen Temperaturbereichen für eine Reaktion genutzt und wieder regeneriert wird und eventuell gleichzeitig gasförmige Zwischenprodukte im Strom der Wirbelgase abgeschreckt werden sollen.

Als *Modellreaktion* für einen solchen Fall wurde die Umsetzung von Calciumnitrid mit Wasserstoff gewählt, in der ein Teil des Nitrids in Calciumhydrid umgewandelt wird:

$$Ca_3N_2 + 3H_2 \rightleftarrows 3CaH_2 + N_2$$

Bei etwas höheren Temperaturen lässt sich das Hydrid durch Stickstoff wieder in das Nitrid zurückverwandeln. Bei der Hydrierungsreaktion tritt intermediär Ammoniak auf, d.h. sie verläuft zum Teil über die beiden Stufen:

$$Ca_3N_2 + 6H_2 \rightarrow 3CaH_2 + 2NH_3$$
$$\rightarrow 3CaH_2 + N_2 + 3H_2$$

Diese Verhältnisse wurden bereits im Jahre 1905 von Haber aufgeklärt [4], bei seinen ersten Versuchen zur Ammoniakgewinnung aus den Elementen. Beim Überleiten von Wasserstoff über Calciumnitrid in einem Porzellanschiffchen stellte er oberhalb 600°C Ammoniak im abziehenden Gasstrom fest, doch waren die Prozentsätze so gering – entsprechend der ungünstigen Lage des Ammoniakgleichgewichtes bei diesen Temperaturen – dass er diesen Weg nicht weiter verfolgte.

Es wurde nun frisch hergestelltes Calciumnitrid in der beschriebenen heiss-kalten Wirbelschicht mit einem Stickstoff-Wasserstoff-Gemisch aufgewirbelt, das auf etwa 1000°C vorgeheizt war, und das Abgas nach Staubabscheidung auf Ammoniak analysiert. Abb. 13 zeigt die Ergebnisse. Die Ammoniakgehalte lagen zwischen 5 und 10%, mit steigendem Gasdurchsatz erwartungsgemäss abnehmend. Damit war das Ziel dieser Modell-

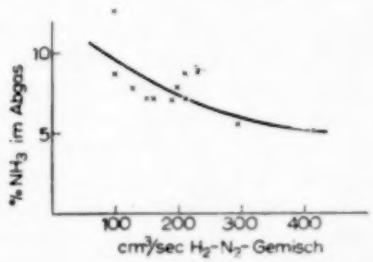

ABB. 13. Ammoniakausbeuten in einer heiss-kalten Wirbelschicht mit Calciumnitrid als Wirbelgut.

versuche erreicht: mit der Arbeitsweise der heiss-kalten Wirbelschicht lassen sich Zwischenprodukte, die bei höheren Temperaturen durch Reaktion mit dem Wirbelgut intermediär auftreten – wie im vorliegenden Falle das Ammoniak – durch schnelle Abkühlung zu einem Teil vor dem thermischen Zerfall bewahren und auf normale Temperaturen herunterretten.

Auch diese Art der Ammoniakdarstellung geht jedoch über den Charakter einer Modellreaktion nicht hinaus und hat insbesondere keine Bedeutung für eine technische Ammoniakgewinnung. Abgesehen von dem Wärmeaufwand für die Gasvorheizung hält die Wirksamkeit des Calciumnitrids nicht lange genug an. Die wechselseitigen Umwandlungen in Hybrid und Nitrid führen zusammen mit

der heftigen Wirbelbewegung der Partikeln zu starkem Abrieb; es bildet sich viel Flugstaub, der ausgetragen wird. Ausserdem nimmt das Ausmass der Nitrid-Hydrid-Umwandlung allmählich ab. Wie Abb. 14 zeigt, tritt bei der erstmaligen Hydrierung einer frisch hergestellten Calciumnitrid-Probe oberhalb 300°C ein kräftiger Wasserstoffverbrauch ein. Es ist hier der Gasdruck in einer Kreislaufapparatur aufgetragen, in

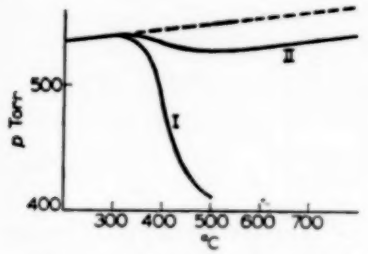

Abb. 14. Wasserstoff-Umsatz mit Calciumnitrid.

Kurve I: erste H_2-Behandlung,

Kurve II: Druckabfall in H_2-Atmosphäre nach mehrmaliger H_2- und N_2-Behanfdlung.

der das Calciumnitrid unter Wasserstoff langsam auf die längs der Abszisse angegebenen Temperaturen aufgeheizt wurde. Nach Rückbildung des Nitrids durch eine analoge Stickstoffbehandlung wurde bei der nachfolgenden Hydrierung weniger Wasserstoff umgesetzt, und nach mehrmaligem Wechsel zwischen Hydrierung und Nitrierung sank der Wasserstoffumsatz auf den durch Kurve II in Abb 14 dargestellten geringen Wert. Das Calciumnitrid hat daher für die Ammoniakgewinnung keine genügende Dauerwirkung.

Die voranstehend beschriebenen Untersuchungen haben somit zu keinem direkt anwendbaren technischen Verfahren geführt. Sie haben jedoch gezeigt, dass Reaktionsgemische mit Wirbelschichten nach verschiedenen Methoden wirksam abgeschreckt und dabei instabile Zwischenprodukte gefasst werden können.

Die Arbeiten wurden apparativ und finanziell unterstützt durch die *Deutsche Forschungsgemeinschaft* und den *Fonds der Chemischen Industrie*, denen ich an dieser Stelle meinen besonderen Dank zum Ausdruck bringen möchte.

Literatur

[1] Gohr E. J. in *Fluidization* (herausgegeben von D. F. Othmer) 1956, S.102 ff.Reinhold Publ. Corp. New York.

[2] Fetting F. und Wicke E. *Chem.-Ing.-Techn.* 1956 **28** 88.

[3] Schmidt H. Diplomarbeit Göttingen 1955.

[4] Haber F. und van Oordt G. Z. *Anorg. Chemie* 1905 **44** 341.

Chemical Engineering Science, 1957, Vol. 6, pp. 170 to 182. Pergamon Press Ltd.

Mass transfer between co-current fluid streams and boundary layer solutions

OWEN E. POTTER

Chemical Engineering Laboratory, Manchester College of Science and Technology and University of Manchester,

(*First received* 9 *December* 1955; *in final form* 3) *November* 1956)

Abstract—Approximate laminar boundary layer solutions for mass transfer across the plane interface between two co-current parallel fluid streams are derived in the form

$$\frac{k_1 x}{D_1} = \left(\frac{\mu_1}{\rho_1 D_1}\right)^p \cdot \left(\frac{U_1 x}{\nu_1}\right)^{\frac{1}{2}} \cdot \phi\left[\frac{U_2}{U_1}, \frac{\mu_2\rho_2}{\mu_1\rho_1}\right]$$

$$\frac{k_2 x}{D_2} = \left(\frac{\mu_2}{\rho_2 D_2}\right)^q \cdot \left(\frac{U_1 x}{\nu_2}\right)^{\frac{1}{2}} \cdot \psi\left[\frac{U_2}{U_1}, \frac{\mu_2\rho_2}{\mu_1\rho_1}\right]$$

where p and q are not constants but are functions of U_2/U_1 and $\mu_2\rho_2/\mu_1\rho_1$.

It is suggested that the boundary layer theory provides a more realistic physical picture than either the LEWIS and WHITMAN stagnant film theory or the HIGBIE Penetration Theory.

Résumé—L'auteur présente des équations approchées basées sur la théorie des couches limites à écoulement laminaire exprimant l'échange massique à travers l'interface plane de deux co-courants fluides, sous la forme

$$\frac{k_1 x}{D_1} = \left(\frac{\mu_1}{\rho_1 D_1}\right)^p \cdot \left(\frac{U_1 x}{\nu_1}\right)^{\frac{1}{2}} \cdot \phi\left[\frac{U_2}{U_1}, \frac{\mu_2\rho_2}{\mu_1\rho_1}\right]$$

$$\frac{k_1 x}{D_2} = \left(\frac{\mu_2}{\rho_2 D_2}\right)^q \cdot \left(\frac{U_1 x}{\nu_2}\right)^{\frac{1}{2}} \cdot \psi\left[\frac{U_2}{U_1}, \frac{\mu_2\rho_2}{\mu_1\rho_1}\right[$$

où p et q ne sont pas C^{te} = mais fonctions de U_2/U_1 et $\mu_2\rho_2/\mu_1\rho_1$.

Cette théorie donne une image physique plus fidèle que les théories de LEWIS et WHITMAN du film stagnant ou théorie de la pénétration de HIGBIE.

1.1. INTRODUCTION

IN 1912 LANGMUIR [1] suggested that the resistance to heat transfer between a solid body and neighbouring air could be taken to be that of a thin layer of stagnant air in contact with the hot body, so that the heat lost was *conducted* through the thin stagnant layer of air. This model for convective heat transfer was taken up by LEWIS and WHITMAN [2], [3], [4], [5] and applied to convective mass transfer.

1.2. LEWIS AND WHITMAN THEORY

In considering the heat transfer between a drop of water and a hot gas, WHITMAN wrote [3], " It is well known that the layer of gas against any solid or liquid surface is almost at rest compared to the mass of gas outside, and it is this so-called *film* through which heat must pass by the slow process of diffusion . . . Similarly, a liquid film exists on the surface of the water-drop, and the combination of gas and liquid films in series gives a *two-film* resistance . . . The rate of absorption of matter from gas to liquid . . . is a process paralleling that of heat transfer." (This analysis into two resistances in series could easily be modified to incorporate an interfacial resistance if this should prove necessary.) The concept of the stagnant film, while valuable in its day, has now been replaced in heat transfer studies by the concept of the boundary layer. It is the object of this paper to show how the boundary layer concept can be applied to mass transfer between fluid phases.

1.3. Higbie Penetration Theory

The model of unsteady state diffusion into a stagnant fluid was proposed by Higbie [6] for the prediction of mass-transfer coefficients for falling liquid films. The theory predicts that at time t, the mass transfer coefficient k is given by the following equation

$$k = \left(\frac{D}{\pi t}\right)^{\frac{1}{2}} \tag{1}$$

Also, if two fluids are in contact and a solute diffusing from one to the other then

$$k_1 = \left(\frac{D_1}{\pi t}\right)^{\frac{1}{2}}, k_2 = \left(\frac{D_2}{\pi t}\right)^{\frac{1}{2}} \tag{2}$$

It follows from the fact that k_1/k_2 is independent of time that the interfacial concentrations $(a_1)_0$ and $(a_2)_0$ are also independent of time and therefore constant throughout the period of diffusion.

1.4. Danckwerts' Modification of the Penetration Theory

The Higbie Penetration Theory was revived in 1951 by Danckwerts [7] but in a modified form. In a liquid maintained in turbulent motion by stirring at a steady rate, Danckwerts supposed that the motion of the liquid would continually replace with fresh surface those parts of the surface which have been exposed for a finite length of time. Then, if the mean rate of production of fresh surface (per unit area of surface) is constant and equal to f, and the chance of an element of surface being replaced within a given time is assumed to be independent of its age, and if the rate of absorption into fresh surface is given by the Higbie relationship, then

$$k = \sqrt{(Df)} \tag{3}$$

The fact that k is proportional to the square root of the diffusion coefficient is not significant since it is in essence assumed in the derivation. Furthermore, the theory is valueless if no method for predicting f can be found. However f could not be predicted without a detailed knowledge of the fluid dynamics of the system, and if a detailed knowledge of the fluid dynamics of the system were available then the Danckwerts' theory would not be needed.

1.5. Gas-Film–Boundary Layer Theory

Due to the similarity of heat and mass transfer [8] it is always possible to write down a mass-transfer relationship if the corresponding heat transfer relation is available and if the mass transfer is small, i.e. at low concentrations. The heat transfer between fluid and a flat plate has been studied both theoretically [9], [10] and experimentally [11], [12], the agreement between theory and experiment being satisfactory.

For laminar flow in the boundary layer

$$\mathrm{Nu} = 0{\cdot}331\ Pr^{\frac{1}{3}}\ Re^{\frac{1}{2}} \tag{4}$$

In a corresponding mass transfer problem, say the evaporation of mercury from an amalgamated surface into an air stream,

$$\frac{kx}{D} = 0{\cdot}331 \left(\frac{\mu}{\rho D}\right)^{\frac{1}{3}} \left(\frac{U\rho x}{\mu}\right)^{\frac{1}{2}} \tag{5}$$

The experimental results of Maxwell and Storrow [13] for evaporation of mercury confirm the above equation, which is a convenient approximation for mass transfer when a gas is flowing over a liquid. It can only be an approximation since the liquid will be set in motion under the tangential stress of the gas.

If a liquid is flowing over another then the shear stresses set up by their relative motion will determine a velocity distribution which will in its turn determine the rate of mass transfer. It is this problem which is to be discussed in what follows.

2.1. Boundary Layer Theory

When a fluid flows past a flat plate placed parallel to the direction of flow of the fluid, the influence of the viscosity of the fluid is confined to a thin layer called the *boundary layer* (see Fig. 1). In this thin layer the velocity of the fluid increases from zero at the plate to the full velocity of the fluid. Prandtl [14] therefore suggested that the field of flow could be divided for the purposes of mathematical analysis, into two regions: the

thin boundary layer near the wall in which friction must be taken into account, and the region outside the boundary layer where the forces due to friction are small and may be neglected, and where therefore the classical theory of ideal fluids offers a very good approximation.

With this simplification PRANDTL was able to replace the NAVIER-STOKES differential equations of fluid motion – which are difficult to solve – by the simpler equation (two-dimensional case)

$$\frac{\partial u}{\partial t} + u\frac{\partial u}{\partial x} + v\frac{\partial u}{\partial y} = -\frac{1}{\rho}\frac{\partial p}{\partial x} + \nu\frac{\partial^2 u}{\partial y^2} \qquad (6)$$

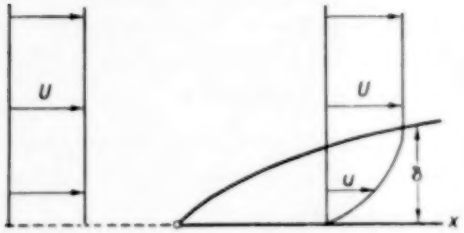

FIG. 1. Boundary layer on a flat plate and velocity distribution curves in the fluid ahead of and at a point on the plate.

combined with the equation of continuity

$$\frac{\partial u}{\partial x} + \frac{\partial v}{\partial y} = 0 \qquad (7)$$

For steady flow, equation (6) simplifies to

$$u\frac{\partial u}{\partial x} + v\frac{\partial u}{\partial y} = -\frac{1}{\rho}\frac{\partial p}{\partial x} + \nu\frac{\partial^2 u}{\partial y^2} \qquad (8)$$

Furthermore, in the case of a fluid flowing past a flat plate the pressure gradient is zero and hence equation [8] may be further simplified to

$$u\frac{\partial u}{\partial x} + v\frac{\partial u}{\partial y} = \nu\frac{\partial^2 u}{\partial y^2} \qquad (9)$$

2.2. SIMILARITY OF VELOCITY PROFILES

An important simplification can be introduced into the equation of motion if a "similarity" solution can be found. "Similar" solutions are those in which two velocity profiles at different co-ordinates differ only by a scale factor in u and y. The velocity is made dimensionless by making the stream velocity U the scale factor, and distance normal to the plate is made dimensionless by making the boundary layer thickness the scale factor. The partial differential equation (9) can then be reduced to an ordinary differential equation. For the case of two liquids in co-current flow, KEULEGAN [15] and LOCK [16] have shown the existence of a similarity solution. A corollary of the similarity of the velocity profiles is that the velocity at the interface is constant.

2.3. VON KARMAN MOMENTUM EQUATION

It is convenient to regard the boundary layer as having a definite thickness δ so that at the plate where $y = 0$, $u = 0$ and at the edge of the boundary layer where $y = \delta$, $u = U$, the velocity of the fluid stream. In actual fact the velocity u will approach U asymptotically but the error introduced is small [17].

If the equation of motion (9) is integrated with respect to y between the limits 0 and δ,

$$\int_0^\delta \left(u\frac{\partial u}{\partial x} + v\frac{\partial u}{\partial y}\right) dy = \int_0^\delta u\frac{\partial u}{\partial x}\,dy + [uv]_0^\delta - \int_0^\delta u\frac{\partial v}{\partial y}\,dy$$

From the equation of continuity (7)

$$\frac{\partial v}{\partial y} = -\frac{\partial u}{\partial x}$$

hence

$$(v)_{y=\delta} = -\int_0^\delta \frac{\partial u}{\partial x}\,dy$$

It follows that

$$\int_0^\delta \left(u\frac{\partial u}{\partial x} + v\frac{\partial u}{\partial y}\right) dy = \int_0^\delta \frac{\partial}{\partial x}(u^2)\,dy - U\int_0^\delta \frac{\partial u}{\partial x}\,dy$$

which is equivalent to

$$\frac{\partial}{\partial x}\int_0^\delta u^2 dy - U\frac{\partial}{\partial x}\int_0^\delta u\,dy$$

Also

$$\int_0^\delta \nu \frac{\partial^2 u}{\partial y^2}\, dy = \nu \left[\frac{\partial u}{\partial y}\right]_0^\delta$$

but

$$\left(\frac{\partial u}{\partial y}\right)_\delta = 0$$

Hence

$$\frac{\partial}{\partial x}\int_0^\delta (U - u)\, u\, dy = \nu \left(\frac{\partial u}{\partial y}\right)_0$$

and if

$$\tau_0 = \mu \left(\frac{\partial u}{\partial y}\right)_0$$

Therefore

$$\tau_0 = \frac{\partial}{\partial x}\int_0^\delta \rho\,(U - u)\, u\, dy \qquad (10)$$

This is the VON KARMAN momentum equation [18].

Approximate solutions for the flow of a fluid over a flat plate can be obtained by inserting into [14] various approximate expressions for the velocity distribution.

3.1. CO-CURRENT PARALLEL FLUID STREAMS – LOCK'S APPROXIMATE SOLUTION

Two parallel co-current streams, the upper of uniform velocity U_1 and the lower of uniform velocity U_2 are brought together at O (see Fig. 2). It is assumed that the interface remains plane. The x-axis is the interface and O is the origin. The y-axis is taken normal to the interface. Let the velocity of either phase parallel to the x-axis be u; μ_1 and μ_2 the viscosities of the upper and lower phases, ρ_1 and ρ_2 their densities. Due to the shear stresses arising from the difference between U_2 and U_1, two laminar boundary layers are formed wherein the velocity changes from the interfacial value u_0 to the stream values U_1 and U_2. Let δ_1 and δ_2 be the thicknesses of the respective layers. The shear stress at the interface is τ_0 and ν_1, ν_2 the kinematic viscosities of the two phases.

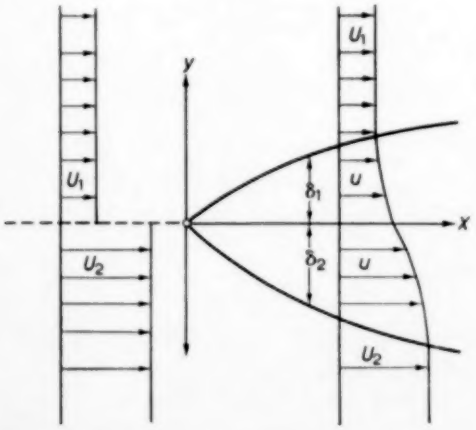

FIG. 2. Hydrodynamic boundary layers at the interface of co-current streams.

The considerations which led to the derivation of equation (10) for the flow of a fluid over a flat plate apply equally in the present case only the boundary conditions are different.

Thus, for the upper and lower streams

$$\frac{\tau_0}{\rho_1} = \nu_1 \left(\frac{\partial u}{\partial y}\right)_{0+} = \frac{\partial}{\partial x}\int_0^{\delta_1} (U_1 - u)\, u\, dy \qquad (11)$$

$$\frac{\tau_0}{\rho_2} = \nu_2 \left(\frac{\partial u}{\partial y}\right)_{0-} = \frac{\partial}{\partial x}\int_0^{-\delta_2} (U_2 - u)\, u\, dy \qquad (12)$$

It then remains to choose suitable velocity distributions to insert in equations (11) and (12). KEULEGAN [15] has utilized quartic and sextic polynomials for the special case of the lower fluid at rest ($U_2 = 0$), LOCK [16] has utilized a quartic polynomial for the general case ($U_2 \neq 0$) and POTTER [19] has investigated the use of a sextic polynomial for the general case. Here the quartic polynomial will be used. Thus for the upper and lower streams respectively

$$\frac{u}{U_1} = r + (1 - r)\left\{2\left(\frac{y}{\delta_1}\right) - 2\left(\frac{y}{\delta_1}\right)^3 + \left(\frac{y}{\delta_1}\right)^4\right\} \qquad (13)$$

$$\frac{u}{U_1} = r + (\lambda - r)\left\{2\left(\frac{y}{-\delta_2}\right) - 2\left(\frac{y}{-\delta_2}\right)^3 + \left(\frac{y}{-\delta_2}\right)^4\right\} \qquad (14)$$

where $r = u_0/U_1$, $\lambda = U_2/U_1$.

3.2. BOUNDARY CONDITIONS

Some of the boundary conditions can now be written down

$$\left.\begin{aligned} &y = \delta_1,\ u = U_1,\ \frac{\partial u}{\partial y} = 0,\ \frac{\partial^2 u}{\partial y^2} = 0 \\ &y = 0+,\ u = u_0 \\ &y = 0-,\ u = u_0 \\ &y = -\delta_2,\ u = U_2,\ \frac{\partial u}{\partial y} = 0,\ \frac{\partial^2 u}{\partial y^2} = 0 \end{aligned}\right\} \quad (15)$$

These boundary conditions merely assert that the velocity must equal u_0 at the interface and U_1 or U_2 at the edge of the respective boundary layer, and that the velocity profile must pass over to the stream velocity without discontinuity at the " edge " of the respective boundary layers.

The shear stress should be continuous at the interface, so that

$$\mu_1 \left(\frac{\partial u}{\partial y}\right)_{0+} = \mu_2 \left(\frac{\partial u}{\partial y}\right)_{0-} \quad (16)$$

If the conditions at the interface are inserted into the equation of motion (9) it reduces to

$$\left(\frac{\partial^2 u}{\partial y^2}\right)_{0+} = 0 = \left(\frac{\partial^2 u}{\partial y^2}\right)_{0-} \quad (17)$$

since $\frac{\partial u}{\partial x} = 0$ and $v = 0$ at $y = 0$. It should be noted that if mass transfer is occurring, the latter statement $v = 0$ at $y = 0$ will only be approximately true, but the more true as the solutions are more dilute and the rate of mass transfer correspondingly less.

These boundary conditions are met by the assumed velocity distributions (13) and (14).

3.3. Solution in Terms of Assumed Velocity Profiles

If u from equations (13) and (14) is substituted in the momentum equations (11) and (12) and integration performed with respect to y

$$\nu_1 \left(\frac{\partial u}{\partial y}\right)_{0+} = \frac{\partial}{\partial x}\left[U_1^2 \delta_1 (1-r)(74+115r)/630\right] \quad (18)$$

$$\nu_2 \left(\frac{\partial u}{\partial y}\right)_{0-} = \frac{\partial}{\partial x}\left[U_1^2(-\delta_2)(\lambda-r)(74\lambda+115r)/630\right] \quad (19)$$

But,

$$\left(\frac{\partial u}{\partial y}\right)_{0+} = U_1 (1-r)\, 2/\delta_1 \quad (20)$$

$$\left(\frac{\partial u}{\partial y}\right)_{0-} = U_1 (\lambda - r)\, 2/(-\delta_2) \quad (21)$$

therefore on integrating equations (18) and (19) with respect to x, and rearranging,

$$\delta_1^2 = (4\nu_1 x/U_1)\{630/(74 + 115r)\} \quad (22)$$

$$\delta^2 = (4\nu_2 x/U_1)\{630/(74\lambda + 115r)\} \quad (23)$$

Hence

$$\frac{\delta_2^2}{\delta_1^2} = \frac{74 + 115r}{74\lambda + 115r} \cdot \frac{\nu_2}{\nu_1} \quad (24)$$

From equation (16), utilising (20) and (21)

$$r = \frac{\delta_2/\delta_1 + \lambda\, \mu_2/\mu_1}{\delta_2/\delta_1 + \mu_2/\mu_1} \quad (25)$$

Equation (24) becomes

$$\left[\left(\frac{\delta_2}{\delta_1}\right)\Big/\left(\frac{\mu_2}{\mu_1}\right)\right]^2 = \frac{189\left[\left(\frac{\delta_2}{\delta_1}\right)\Big/\left(\frac{\mu_2}{\mu_1}\right)\right] + 74 + 115\lambda}{\left[\left(\frac{\delta_2}{\delta_1}\right)\Big/\left(\frac{\mu_2}{\mu_1}\right)\right](74\lambda + 115) + 189\lambda} \cdot \frac{\mu_1\rho_1}{\mu_2\rho_2} \quad (26)$$

Equation (26) can be solved by successive approximation for any λ and $\mu_2\,\rho_2/\mu_1\rho_1$. Then

$$\tau_0 = \mu_1 \left(\frac{\partial u}{\partial y}\right)_{0+} = \mu_1\, U_1 (1-r)\, 2/\delta_1$$

whence

$$\frac{\tau_0}{\rho_1 U_1^2} = (1-r)\left(\frac{74 + 115r}{630}\right)^{\frac{1}{2}} \left(\frac{U_1 x}{\nu_1}\right)^{-\frac{1}{2}} \quad (27)$$

$$= c \left(\frac{U_1 x}{\nu_1}\right)^{-\frac{1}{2}} \quad (28)$$

where c is the shear stress coefficient defined by equations (27) and (28).

Note that when the interface is at rest, i.e. $r = 0$, then $c = 0{\cdot}343$. This compares well with the exact solution for flow over a flat plate where $c = 0{\cdot}331$ [20].

In Fig. 3 values of c for $\lambda = 0$ and $\lambda = 0{\cdot}1$ are plotted against $\mu_2\rho_2/\mu_1\rho_1$ and in Fig. 4 the velocity profiles for $\lambda = 10$ at various values of $\mu_2\rho_2/\mu_1\rho_1$ are presented in terms of the dimensionless parameters u/U_1 and η, where

$$\eta_1 = (U_1/2\nu_1 x)^{\frac{1}{2}} y, \quad \eta_2 = (U_1/2\nu_2 x)^{\frac{1}{2}} y$$

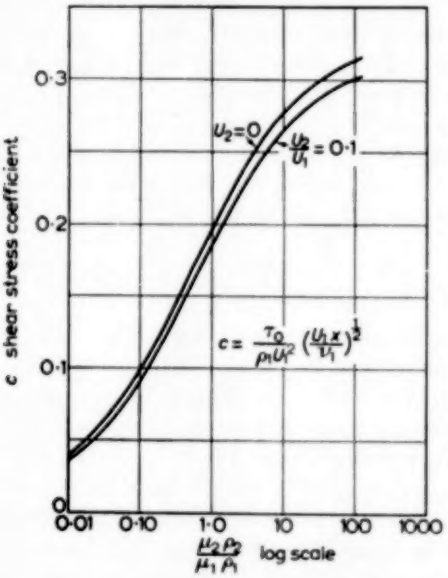

FIG. 3. Shear stress coefficients vs. $\mu_2\rho_2/\mu_1\rho_1$ for $U_2/U_1 = 0{\cdot}1$ and $U_2 = 0$.

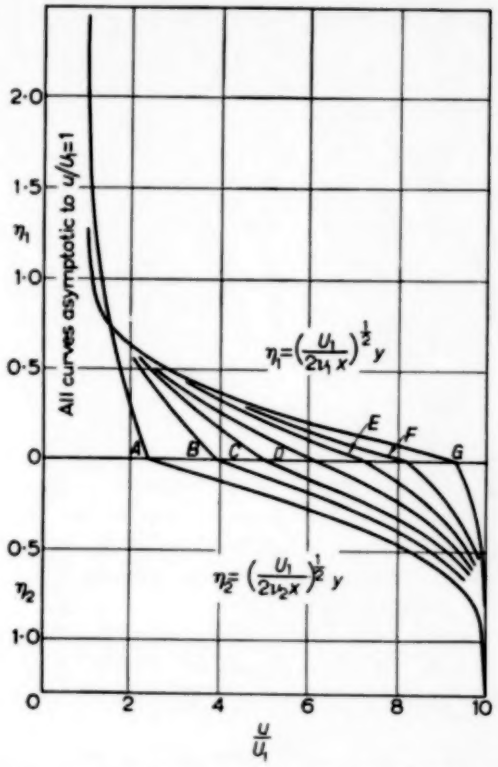

FIG. 4. Dimensionless velocity profiles for $U_2/U_1 = 10$, and values of $\mu_2\rho_2/\mu_1\rho_1$ from 0·01 to 100·0.

Symbol $\mu_2\rho_2/\mu_1\rho_1$.
A – 0·01 ; B – 0·10 ; C – 0·316 ; D – 1·00 ;
E – 3·16 ; F – 10·00 ; G – 100·0.

The values shown in Figs. 3 and 4 were actually computed from the sextic polynomial solutions.

4.1 Two-Resistance Theory applied to Momentum Transfer

For mass-transfer between two fluid phases

$$\frac{\text{Mass}}{\text{Area} \times \text{Time}} = k_1\{A_1 - (a_1)_0\} = k_2\{(a_2)_0 - A_2\} = K_1\{A_1 - (A_1)_e\} \quad (29)$$

where k_1 and k_2 are the gas and liquid film coefficients and K_1 is an overall coefficient.

If

$$(A_1)_e = m\,A_2 \quad (30)$$

then

$$\frac{1}{K_1} = \frac{1}{k_1} + \frac{m}{k_2} \quad (31)$$

Similar relations to these can be written down for momentum transfer between two fluid phases in relative motion.

$$\tau_0 = \frac{\text{Momentum}}{\text{Area} \times \text{Time}} = k_1^*(\rho_1 U_1 - \rho_1 u_0) = k_2^*(\rho_2 u_0 \rho_2 U_2) = K_1^*(\rho_1 U_1 - \rho_1 U_2)$$

where k_1^* and k_2^* are the respective momentum transfer film coefficients and K_1^* is an overall momentum transfer coefficient. It will be observed that

$$k_1^* = \frac{\tau_0}{\rho_1 U_1 - \rho_1 u_0}; \quad k_2^* = \frac{\tau_0}{\rho_2 u_0 - \rho_2 U_2}; \quad K_1^* = \frac{\tau_0}{\rho_1 U_1 \rho_1 U_2}$$

Also,

$$\frac{1}{K_1^*} = \frac{1}{k_1^*} + \frac{m^*}{k_2^*}$$

where

$$m^* = \rho_1/\rho_2$$

Substituting for τ_0 from equation (31)

$$k_1^* = U_1 \left(\frac{74 + 115r}{630}\right)^{\frac{1}{2}} \left(\frac{U_1 x}{\nu_1}\right)^{-\frac{1}{2}}$$

$$k_2^* = \frac{\rho_1}{\rho_2} \cdot U_1 \frac{1 - r}{r - \lambda} \left(\frac{74 + 115r}{630}\right)^{\frac{1}{2}} \left(\frac{U_1 x}{\nu_1}\right)^{-\frac{1}{2}}$$

whence

$$\frac{k_1^*}{k_2^*} = \frac{\rho_2}{\rho_1} \cdot \frac{r - \lambda}{1 - r}$$

It will be noted that while a particular solution of the flow problem depends on λ and $\mu_2\rho_2/\mu_1\rho_1$, values of k_2^* must additionally incorporate the term ρ_1/ρ_2 which cancels out however when m^*/k_2^* is evaluated.

From LOCK's solution for air flowing over still water at 10°C, taking $\rho_1/\rho_2 = 0{\cdot}001247$

$$k_1^*/k_2^* = 17{\cdot}29 \quad ; \quad k_1^*/K_1^* = 1{\cdot}0215$$

As m^* is very small, this case in momentum transfer is the analogue of the case of a very soluble gas in gas-absorption and it can be seen that the gas-film momentum transfer coefficient equals the overall momentum transfer coefficient with an error of two per cent.

5.1. BOUNDARY LAYER THEORY FOR MASS-TRANSFER

The differential equation for molecular diffusion in a fluid in two-dimensional motion under steady conditions and with insignificant density changes, is

$$u \frac{\partial a}{\partial x} + v \frac{\partial a}{\partial y} = D \frac{\partial^2 a}{\partial y^2} \qquad (32)$$

where a is concentration and D the diffusion coefficient.

5.2. SIMILARITY OF CONCENTRATION PROFILES

Just as before (Section 2.2) an important simplification can be introduced if the concentration profiles are similar at different co-ordinates x. This will be so if the concentration can be expressed in such a way as to follow the same boundary conditions as the velocity ratio u/U in the viscous boundary layer problem, and this can be done if a/A be taken to represent the concentration. Comparison of equations (9) and (32) establishes that the velocity and concentration distributions will be identical provided that $\nu = D$, i.e. provided that the SCHMIDT number equals unity. It follows that if the velocity distributions are similar at different co-ordinates x then the concentration distributions will be similar. As a corollary the concentrations at the interface will be independent of the co-ordinate x.

5.3. CO-CURRENT FLUID STREAMS, AUTHOR'S APPROXIMATE SOLUTION

Suppose now that two streams are flowing co-currently as in Fig. 2 and that a solute is being transferred from one phase to the other by diffusion. It is assumed that the solutions are dilute and identical in density and viscosity with the pure liquids. If the solutions are dilute then the mass-transfer will be small. Modifications must be made in the theory if the concentrations at the interface and in the stream are widely different. This point will be discussed later.

On each side of the interface there will now be two boundary layers, the viscous boundary layer of thickness δ_1 (or $-\delta_2$) and the diffusion boundary layer of thickness Δ_1 (or $-\Delta_2$). The thickness of the diffusion boundary layer is the distance measured normally from the interface in which the concentration changes from the interfacial value to the stream value.

If equation (32) is integrated with respect to y from $y = 0+$ to $y = h$ where h is a length which is greater than the thickness of either the viscous or diffusion boundary layers

$$\int_0^h \left(u \frac{\partial a_1}{\partial x} + v \frac{\partial a_1}{\partial y}\right) dy = -D_1 \left(\frac{\partial a_1}{\partial y}\right)_{0+} \qquad (33)$$

since $\frac{\partial a_1}{\partial y}$ vanishes for $y = h$. The subscript 1 has been introduced to refer to conditions in the upper fluid.

Now,

$$\int_0^h u \frac{\partial a_1}{\partial x} dy = \int_0^h u \frac{\partial}{\partial x}(a_1 - A_1) dy$$

where A_1 is the concentration outside the boundary layer)

$$= \frac{\partial}{\partial x}\int_0^h u(a_1 - A_1) dy - \int_0^h (a_1 - A_1) \frac{\partial u}{\partial x} dy$$

and

$$\int_0^h v \frac{\partial a_1}{\partial y} dy = \int_0^h v \frac{\partial}{\partial y}(a_1 - A_1) dy$$

$$= \left[v(a_1 - A_1)\right]_0^h - \int_0^h (a_1 - A_1) \frac{\partial v}{\partial y} dy$$

Also v vanishes for $y = 0$ and $a_1 = A_1$ for $y = h$ so that the terms with square brackets is equal to zero.

Hence, substituting in equation (33) and making use of the equation of continuity (7)

$$\frac{\partial}{\partial x}\int_0^h u(a_1 - A_1) dy = -D_1 \left(\frac{\partial a_1}{\partial y}\right)_{0+}$$

The limit h can now be replaced by Δ_1 since outside Δ_1 the term $(a_1 - A_1)$, disappears.

$$\frac{\partial}{\partial x}\int_0^{\Delta_1} u(A_1 - a_1) dy = D_1 \left(\frac{\partial a_1}{\partial y}\right)_{0+} \quad (34)$$

Similarly, for the lower stream

$$\frac{\partial}{\partial x}\int_0^{-\Delta_2} u(A_2 - a_2) dy = D_2 \left(\frac{\partial a_2}{\partial y}\right)_{0-} \quad (35)$$

Equations (34) and (35) correspond to the momentum equations (11) and (12).

5.4. Boundary Conditions for Mass Transfer

The concentrations must equal the interfacial values $(a_1)_0$ and $(a_2)_0$ at the interface, and the stream values A_1 and A_2 at the "edge" of the concentration boundary layer, and pass over without discontinuity from their values inside the boundary layer to the stream concentration. Thus

$$\left.\begin{aligned} &y = 0+, \quad a_1 = (a_1)_0 \\ &y = \Delta_1, \quad a_1 = A_1, \quad \frac{\partial a_1}{\partial y} = 0, \quad \frac{\partial^2 a_1}{\partial y^2} = 0 \\ &y = 0-, \quad a_2 = (a_2)_0 \\ &y = -\Delta_2, \quad a_2 = A_2, \quad \frac{\partial a_2}{\partial y} = 0, \quad \frac{\partial^2 a_2}{\partial y^2} = 0 \end{aligned}\right\} \quad (36)$$

It will be noted that it has been taken that the concentrations remain constant along the length of the interface. This point has been discussed previously.

An additional boundary condition is that the rates of mass transfer immediately on each side of the interface should be equal, i.e.

$$D_1 \left(\frac{\partial a_1}{\partial y}\right)_{0+} = D_2 \left(\frac{\partial a_2}{\partial y}\right)_{0-} \quad (37)$$

At the interface, since $(a_1)_0$ is constant $\frac{\partial a_1}{\partial x} = 0$ at $y = 0$ and also $v = 0$ at $y = 0$. It has already been pointed out that this will be true only if the rate of mass transfer is low, i.e. with dilute solutions. It follows that

$$\left(\frac{\partial^2 a_1}{\partial y^2}\right)_{0+} = 0 = \left(\frac{\partial^2 a_2}{\partial y^2}\right)_{0-}$$

5.5. Concentration Profiles

Quartic polynomials which meet the boundary conditions are

upper stream :

$$\frac{a_1}{A_1} = i_1 + (1 - i_1)\left[2\left(\frac{y}{\Delta_1}\right) - 2\left(\frac{y}{\Delta_1}\right)^3 + \left(\frac{y}{\Delta_1}\right)^4\right] \quad (38)$$

lower stream :

$$\frac{a_2}{A_2} = i_2 + (1 - i_2)\left[2\left(\frac{y}{-\Delta_2}\right) - 2\left(\frac{y}{-\Delta_2}\right)^3 + \left(\frac{y}{-\Delta_2}\right)^4\right] \quad (39)$$

where $i_1 = (a_1)_0/A_2$; $i_2 = (a_2)_0/A_2$.

5.6. Solution in Terms of Assumed Profiles

On substituting the velocity distributions from equations (13) and (14) and the concentration

distributions from equations (38) and (39) in equations (34) and (35) respectively, and integrating with respect to y, assuming $\Delta_1 \leqslant \delta_1$ and $\Delta_2 \leqslant \delta_2$, i.e. SCHMIDT numbers greater than unity as will be the case with liquids.

$$I_1 = \int_0^{\Delta_1} (A_1 - a_1)\, u\, dy = A_1 U_1 (1 - i_1)\, \delta_1 \times$$

$$\left[\frac{3}{10} r \sigma_1 + (1-r)\left\{\frac{2}{15}\sigma_1^2 - \frac{3}{140}\sigma_1^4 + \frac{1}{180}\sigma_1^5\right\}\right] \quad (40)$$

$$I_2 = \int_0^{-\Delta_2} (A_2 - a_2)\, u\, dy = A_2 U_1 (1 - i_2)(-\delta_2) \times$$

$$\left[\frac{3}{10} r \sigma_2 + (\lambda - r)\left\{\frac{2}{15}\sigma_2^2 - \frac{3}{140}\sigma_2^4 + \frac{1}{180}\sigma_2^5\right\}\right] \quad (41)$$

where $\sigma_1 = \Delta_1/\delta_1$; $\sigma_2 = -\Delta_2/-\delta_2$.

For the upper stream it follows that

$$\frac{\partial}{\partial x}(I_1) = D_1 \left(\frac{\partial a_1}{\partial y}\right)_{0+} = D_1\, 2A_1(1-i_1)/\Delta_1$$

$$= 2A_1 (1 - i_1)\, D_1/\sigma_1\, \delta_1 \quad (42)$$

If equation (22) is differentiated with respect to x then

$$\delta_1 \frac{d\delta_1}{dx} = \frac{2 \times 630}{74 + 115\, r} \cdot \frac{\nu_1}{U_1}$$

This is substituted in equation (42) which can then be integrated since σ_1 will be independent of x. Thus,

$$\frac{630\, \sigma_1^2}{74 + 115\, r} \times$$

$$\left\{\frac{3}{10} r + (1-r)\left[\frac{2}{15}\sigma_1 - \frac{3}{140}\sigma_1^3 + \frac{1}{180}\sigma_1^4\right]\right\}$$

$$= \frac{D_1}{\nu_1} = N_{Sc_1}^{-1} \quad (43)$$

Similarly for the lower stream

$$\frac{630\, \sigma_2^2}{74\, \lambda + 115\, r} \times$$

$$\left\{\frac{3}{10} r + (\lambda - r)\left[\frac{2}{15}\sigma_2 - \frac{3}{140}\sigma_2^3 + \frac{1}{180}\sigma_2^4\right]\right\}$$

$$= \frac{D_2}{\nu_2} = N_{Sc_2}^{-1} \quad (44)$$

From these equations it is possible to calculate σ_1 and σ_2 and hence Δ_1 and Δ_2.

5.7. MASS TRANSFER COEFFICIENTS

Local values of the mass transfer coefficient can then be calculated. Thus, for the upper stream

$$k_1 A_1 (1 - i_1) = -D_1 \left(\frac{\partial a_1}{\partial y}\right)_{0+} = \frac{2A_1 (1 - i_1)\, D_1}{\sigma_1\, \delta_1}$$

$$\therefore \qquad k_1 = 2D_1/\sigma_1\delta_1$$

where from equation (22)

$$\delta_1 = \left(\frac{630 \times 4}{74 + 115\, r}\right)^{\frac{1}{2}} \left(\frac{\nu_1 x}{U_1}\right)^{\frac{1}{2}}$$

$$\therefore \qquad \frac{k_1 x}{D_1} = \frac{1}{\sigma_1}\left(\frac{74 + 115\, r}{630}\right)^{\frac{1}{2}} \left(\frac{U_1 x}{\nu_1}\right)^{\frac{1}{2}} \quad (45)$$

Similarly, for the lower stream

$$\frac{k_2 x}{D_2} = \frac{1}{\sigma_2}\left(\frac{74\, \lambda + 115\, r}{630}\right)^{\frac{1}{2}} \left(\frac{U_1 x}{\nu_2}\right)^{\frac{1}{2}} \quad (46)$$

For the case of mass-transfer from a flat plate to a parallel stream, $u_0 = 0$ and $r = 0$. In this case equation (43) reduces to

$$\frac{630\, \sigma_1^2}{74}\left\{\frac{2}{15}\sigma_1 - \frac{3}{140}\sigma_1^3 + \frac{1}{180}\sigma_1^4\right\} = N_{Sc_1}^{-1} \quad (47)$$

A solution for (47) which is accurate to within 5 per cent is [21]

$$\sigma_1 = N_{Sc_1}^{-\frac{1}{3}}$$

Equation (45) then reduces to equation (5) with the difference that the constant is 0·343 and not the exact value of 0·331.

If $r = 1$ then the upper liquid is moving at uniform velocity. On substituting $r = 1$ into equation (43), there remains

$$\frac{630\, \sigma_1^2}{74 + 115} \times \frac{3}{10} = N_{Sc_1}^{-1}$$

or

$$\sigma_1 = N_{Sc_1}^{-\frac{1}{3}}$$

If this value of σ_1 is substituted in (45) and r put equal to 1

$$\frac{k_1 x}{D_1} = N_{Sc_1}^{\frac{1}{3}} \left(\frac{189}{630}\right)^{\frac{1}{2}} \left(\frac{U_1 x}{\nu_1}\right)^{\frac{1}{2}}$$

or

$$k_1 = 0{\cdot}548 \left(\frac{D_1 U_1}{x}\right)^{\frac{1}{2}} \quad (48)$$

Since the time of contact $t = U_1/x$

$$k_1 = 0{\cdot}548 \left(\frac{D_1}{t}\right)^{\frac{1}{2}}$$

This result compares well with the exact result for stagnant diffusion, equation (1)

$$k_1 = \left(\frac{D_1}{\pi t}\right)^{\frac{1}{2}} \doteq 0{\cdot}564 \left(\frac{D_1}{t}\right)^{\frac{1}{2}}$$

(It might at this point be suggested that the approximate method given here would be a useful method for introducing unsteady state heat conduction or diffusion to students deficient in mathematics.)

5.8. Variation in Exponent of the Schmidt Number

It has been shown that for flow where the interfacial velocity and hence r is zero the mass transfer coefficient is proportional to the Schmidt number raised to the power of one-third, and also that for stagnant diffusion where $r = 1$, the mass transfer coefficient is proportional to the Schmidt number raised to the power of one-half. The question arises as to what the exponent should be in those cases where r takes a value, between 0 and 1, or greater than 1.

If suitable values for r are inserted in equation (43) then solutions can be found for the relations between σ_1 and Sc_1. In liquid systems the Schmidt number will be large and the thickness of the concentration boundary a small fraction of the viscous boundary layer. It is then possible to neglect the last two terms on the left hand side of equation (43).

To determine the exponent on the Schmidt number, a solution has been assumed of the form

$$\sigma_1 = Sc_1^{-n}$$

and a solution found for a range of values of r between 0 and 1, assuming $Sc_1 = 100$. These solutions will not of course be exact but only accurate to about 5 per cent over the range of Schmidt numbers. The asymptote when $r > 1$ can be found by assigning a large value to r, say 100,000. Then equation (43) becomes approximately

$$\frac{630\,\sigma_1^2}{115 \times 100{,}000}\left\{\frac{3}{10} \times 100{,}000 - 100{,}000 \times \left[\frac{2}{15}\sigma_1 - \frac{3}{140}\sigma_1^3 + \frac{1}{180}\sigma_1^4\right]\right\} = N_{Sc_1}^{-1}$$

This simplifies to

$$\frac{189}{115}\sigma_1^2 - \frac{630}{115}\sigma_1^2\left[\frac{2}{15}\sigma_1\ \frac{3}{140}\sigma_1^3 + \frac{1}{180}\sigma_1^4\right] = N_{Sc_1}^{-1} \quad (49)$$

If $Sc_1 = 1$, then it is necessary that $\sigma_1 = 1$. This can be seen to be true for equation (43).

If the solution to equation (49) is taken as

$$\sigma_1 = Sc_1^{-n}$$

and a value of n sought for $Sc_1 = 100$, then $n = 0{\cdot}55$.

In Fig. 5 values of the exponent n are plotted against the relative interfacial velocity r.

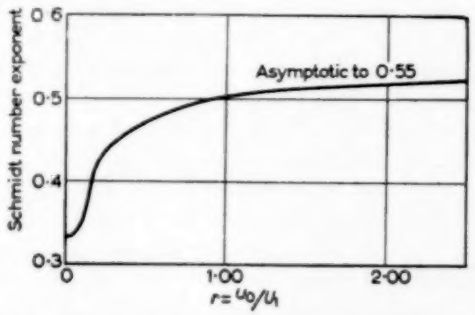

Fig. 5. Exponent on Schmidt number vs. relative interfacial velocity, r.

5.9. Limitation of Solutions to $Sc \gg 1$

The solutions obtained are limited to the case when the diffusion boundary layer is not greater in thickness than the viscous boundary layer. This will be the case with liquids. When the diffusion boundary layer is thicker than the viscous boundary layer the algebra is more complicated because two different expresionss have to be used for the velocity. Squire [21] states that the solution for heat transfer between a fluid and a flat plate is unaltered provided that the Prandtl number is greater than 0·5, so it would therefore

be correct for the present solutions to say that they are accurate to SCHMIDT numbers greater than 0·5.

6.1. LIMITATION TO LOW RATES OF MASS TRANSFER

When a fluid flows past a flat plate it is obvious that the transverse velocity v must be zero at the wall if no mass transfer is occurring. If however there is mass-transfer then the intrusion of this mass into the flowing fluid alters the velocity profile from what it would have been without mass transfer. If the mass transferred is small, then the disturbance is small and can be ignored as in the present theory. If the mass transfer rates are large then a correction must be applied. The appearance or disappearance of mass at the wall makes the flow problem analogous to that of "blowing" or "sucking" boundary layers. In aerodynamics one of the methods [14] proposed for controlling the flow of gas over the foil is to suck the gas through the (porous) foil at a controlled rate. In this case then the transverse velocity v is not zero at the wall, $v_0 \neq 0$. The hydrodynamics solution of SCHLICHTING and BUSSMANN [22] were utilized by MICKLEY *et al.* [23] to provide exact solutions for mass transfer between a fluid and a flat plate. ECKERT and LIEBLEIN [24] have solved the problem for the specific case of water vaporisation. SPALDING [25] has utilized the momentum integral approximate method for the general case. The solutions so obtained show that the rate of mass transfer is an important parameter.

6.2. APPLICABILITY OF PENETRATION THEORY TO CO-CURRENT FLOW

If two liquids are flowing co-currently at different velocities, the interface will move at a constant velocity. In the case of liquids the SCHMIDT numbers are high and so the thickness of concentration boundary layers will only be a fraction of the thickness of the viscous boundary layer and the variation in velocity over the concentration boundary layers small. This leads to the conclusion that unless the viscosities, densities or velocities of the two phases are widely different it will be sufficiently accurate to calculate the mass transfer coefficients on the basis of the Penetration theory, if the time of contact is obtained from the interfacial velocity and the length of the interface. This conclusion would be invalid for countercurrent flow but no solution has yet been obtained for this condition.

7.1. DISCUSSION

Interfacial instability

The question of the stability of the interface has not been raised in the present study but the solutions given are only applicable as long as the interface is in fact stable. Interface (or free surface) stability has been investigated mathematically by LESSEN [26], YIH [27] and CHIARULLI [28]. It has been shown that instability sets in at low Reynolds number. YIH, for a case of vertical flow of a fluid with a free surface, demonstrated mathematically that instability sets in at Reynolds number of 6, a theoretical value which compares well with experimental values of the order 10 to 25. Naturally at such low Reynolds numbers instability means only the onset of waves at the free surface and not the onset of turbulence. It seems clear however that attention must turn to the fundamental study of unstable interfaces including the effect of waves on the rate and mechanism of mass transfer. In this connection the recent study by JACKSON [29] should be noted. He measured the thickness of falling films and concluded that liquids with viscosities greater than that of water give values of the film thickness which are less than for true viscous flow and that the wave motion occurs when the Froude number exceeds unity. A surprising result was obtained by STIRBA and HURT [30] who measured the rates of solution in falling liquid films of slightly soluble solids coated on the wall of a vertical tube. They found the rate of solution in apparently laminar films to be up to two and a half times the theoretical prediction. On the other hand, DAVIDSON and CULLEN [31] have clearly demonstrated that absorption of a pure gas into a ripple-free liquid falling over a spherical surface can be predicted from the laws of flow of a fluid in laminar flow.

7.2. Turbulent Boundary Layers

The present theory cannot be extended easily to deal with the problem of turbulent boundary layers. A more extensive knowledge is first required of the decay of turbulence near liquid/-liquid and gas/liquid interfaces. At one limit, say a gas flowing over a liquid, the situation approximates to a fluid flowing past a solid surface; at an intermediate stage, say a liquid flowing over another liquid nearly identical in density and viscosity, the situation is very complex indeed; finally, at the other limit is a liquid with a free surface.

8.1 Conclusion

In this paper the analogy, first developed by Lewis and Whitman, between heat and mass transfer for a system of two fluid phases is carried a stage further; the simple stagnant film theory is replaced by a boundary layer theory which takes into due account the velocity distribution arising from the relative motion of the two phases. The applicability of the new theory is likely to be reduced considerably by the tendency to instability of a fluid/fluid interface, but the same is true of the stagnant film and Penetration theories.

Acknowledgements—The author wishes to acknowledge his debt to J. A. Storrow for suggesting the problem of extraction across plane interfaces and for his constant stimulus and encouragement; also to Miss R. Rogers for advice in the early stages of this work; also to his colleagues R. W. Maxwell and G. A. Turner for useful discussions. Professor F. Morton kindly criticized the draft when the paper was in process of revision.

Nomenclature

A = concentration in fluid stream outside the boundary layer [ML^{-3}]
a = variable concentration in the diffusion boundary layer [ML^{-3}]
c = shear stress coefficient, dimensionless
D = diffusion coefficient, [$L^2\theta^{-1}$]
f = surface-renewal factor, [θ^{-1}]
i = ratio, concentration at interface to concentration outside the boundary layer, dimensionless
K = overall local mass transfer coefficient, [$L\theta^{-1}$]
K^* = overall local momentum transfer coefficient [$L\theta^{-1}$)
k = local mass transfer film coefficient, [$L\theta^{-1}$]
k^* = local momentum transfer film coefficient, [$L\theta^{-1}$]
m, m^* = Henry's Law coefficients for concentration and momentum, dimensionless
Nu = Nusselt number, dimensionless
p = pressure [$ML^{-1}\theta^{-2}$]
Pr = Prandtl number, dimensionless
r = u_0/U_1, dimensionless
Re = Reynolds number ($U\rho x/\mu$), dimensionless
Sc = Schmidt number ($\mu/\rho D$), dimensionless
t = time, [θ].
U = velocity outside the boundary layer, [$L\theta^{-1}$]
u = variable velocity in x-direction inside the boundary layer, [$L\theta^{-1}$]
v = variable velocity in y-direction, [$L\theta^{-1}$]
x = distance from nose of plate or from point of contact of two fluid streams [L]
y = distance normal to plate or interface [L]
δ = thickness of viscous boundary layer [L]
Δ = thickness of diffusion boundary layer [L]
η_1 = $(U_1/2\nu_1 x)^{\frac{1}{2}}\, y$, dimensionless
η_2 = $(U_1/2\nu_1 x)^{\frac{1}{2}}\, y$, dimensionless
λ = U_2/U_1, dimensionless
μ = viscosity [$ML^{-1}\theta^{-1}$]
ν = kinematic viscosity [$L^2\theta^{-1}$]
ρ = density [ML^{-3}]
σ = Δ/δ, dimensionless
τ = tangential stress [$ML^{-1}\theta^{-2}$]

Subscripts

0 = interface
1 = upper fluid stream
2 = lower fluid stream
e = equilibrium value

References

[1] Langmuir I. *Phys. Rev.* 1912 **34** 401.
[2] Lewis W. K. *Ind. Eng. Chem.* 1916 **8** 825.
[3] Whitman W. G. and Keats J. L. *ibid.* 1922 **14** 185.
[4] Whitman W. G. *Chem. Met. Eng.* 1923 **29** 146.
[5] Lewis W. K. and Whitman W. G. *Ind. Eng. Chem.* 1924 **16** 1215.
[6] Higbie R. *Trans. Amer. Inst. Chem. Eng.* 1935 **31** 365.
[7] Danckwerts P. V. *Ind. Eng. Chem.* 1951 **43** 1460.

[8] HOWARTH L. (Ed.) *Modern Developments in Fluid Dynamics, High Speed Flow* 1953 Vol. II, p. 846. Oxford.

[9] POHLHAUSEN K. *Z. Angew. Math. Mech.* 1921 **1** 115.

[10] KROUJILINE J. *Tech. Phys. U.S.S.R.* 1936 **3** 183.

[11] ELIAS F. *Z. Angew. Math. Mech.* 1929 **9** 434; 1930 **10** 1.

[12] JAKOB M. and DOW W. M. *Trans. Amer. Soc. Mech. Eng.* 1946 **68** 123.

[13] MAXWELL R. W. and STORROW J. A. *Chem. Eng. Sci* to be published.

[14] PRANDTL L. *Proc. III Intern. Math. Congr.*, Heidelberg 1904; translated in *N.A.C.A.* (U.S.A.) TM452 (1928).

[15] KEULEGAN G. H. *J. Res. Nat. Bur. Stds.* (U.S.A.), 1944 **32** 303.

[16] LOCK R. C. *Quart. J. Mech. and Appl. Math.* 1951 **4** 42.

[17] GOLDSTEIN S. (Ed.) *Modern Developments in Fluid Dynamics* 1938 Vol. I, p. 157. Oxford.

[18] *Ibid.* p. 156.

[19] POTTER O. E. *Quart. J. Mech. and Appl. Maths.* (to be published).

[20] SCHLICHTING H. *Boundary Layer Theory* 1955 p. 108. London.

[21] GOLDSTEIN S. (Ed.) *Op. cit.* Vol. II, p. 627.

[22] SCHLICHTING H. and BUSSMANN K. *Schriften d. dt. Ak. d. Luftfahrtforschung* 1943 **7B** No. 2.

[23] MICKLEY H. S. *et al. N.A.C.A.* (U.S.A.) TN 3208, 1954.

[24] ECKERT E. R. and LIEBLEIN V. *Forsch. Arb. Ing. Wes.* 1949 **16** 33.

[25] SPALDING D. B. *Proc. Roy. Soc.* 1954 **A221** 78, 100.

[26] LESSEN M. *N.A.C.A.* (U.S.A.) TN 1929, 1947.

[27] YIH C. S. *Proc. 2nd. U.S. Nat. Cong. Appl. Mech.* 1954, p. 623.

[28] CHIARULLI P. Brown University (U.S.A.) Thesis, 1949.

[29] JACKSON M. L. *A.I.Ch.E.J.* 1955 **1** 231.

[30] STIRBA C. and HURT D. M. *A.I.Ch.E.J.* 1955 **1** 178.

[31] DAVIDSON J. F. and CULLEN E. J. Paper read to Inst. Chem. Eng. (London) at Manchester, February 25, 1956.

Chemical Engineering Science, 1957, Vol. 6, pp. 188 to 189. Pergamon Press Ltd.

Temperature stability of fixed-bed catalytic converters

H. E. HOELSCHER

Department of Chemical Engineering, The Johns Hopkins University, Baltimore 18, Maryland

Abstract—The temperature stability of a fixed bed catalytic reactor is examined for several different kinds of operating conditions. The appropriate differential equation containing the generation function does not have a simple analytical solution for any but the most trivial cases. A generalized method of attack is shown permitting an analysis of the problem for any form of the generation function. The method is illustrated in detail for one form of a wall boundary condition. Solutions for another case are indicated.

Résumé—L'auteur exmine, pour différents modes opérationnels la stabilité de la température dans un réacteur catalytique à lit fixe. L'équation différentielle adéquate contenant la fonction de génération na pas de solution analytique sauf pour certains cas tout à fait simples. L'auteur préconise une méthode générale d'attaque, permettant l'analyse du problème pour une certaine forme de la fonction de génération.

La méthode est illustrée en détail pour un cas limité aux parois. Il indique d'autre part des solutions pour d'autres cas.

TEMPERATURE stability in a fixed bed catalytic reactor is a problem of obvious importance in the design of such pieces of equipment. The temperature distribution in a fixed bed catalytic reactor has been studied analytically by AMUNDSON [1]. These papers, although recent, are already classic in that they present a complete analytical description of the temperature distribution between fluid phase and solid surface in a packed bed catalytic reactor for the most general case. These solutions are necessarily complex and even machine computation is difficult. The following paper is an attempt to set up a generalized technique for estimating the axial temperature-length relationship in a fixed bed catalytic reactor for any form of the heat generation function. The axial temperature is always expected to be the extreme (either highest or lowest) value and, as such, constitutes an important design criterion. The method to be used, while general for any form of a generation function (to be defined later), is limited to the prediction of the *maximum* or *minimum* temperature at any axial position. It does not give a detailed temperature-position function throughout the bed. As such the resulting equations can only be considered to be design expedients. They are analytically simple for certain cases and capable of rapid and simple machine solution for most others.

The problem, then, is to determine that combination of variables (velocity, bed constants, and generation rate) such that a given reactor, with a known wall boundary condition, will operate at or less than a prescribed fixed maximum temperature throughout its length. A similar problem would be to determine at what reactor length the extreme (maximum or minimum) temperature – assumed to be at the axis of the bed – reaches a prescribed design value.

The applicable differential equation for this problem is as follows :

$$\frac{\partial T}{\partial \theta} + u\frac{\partial T}{\partial x} = K\nabla^2 T + \beta(T) \qquad (1)$$

This equation makes use of a generalized bed constant, K, which is the effective thermal diffusivity for the bed. The assumption is implicit herein that the gas phase temperature and the solid surface temperature are identical. If it is desirable to fasten one's attention on the fluid phase only, the constant K should be replaced by the eddy diffusivity. Similarly, if the solid surface temperature is most important, the thermal diffusivity for the solid must be used.

In the above equation it has been assumed that the radial velocity components are negligible. The function, $\beta(T)$, is the generation function and is a function of temperature. It is desirable to make two further assumptions as follows :

1. Longitudinal conduction is assumed negligible compared to lateral, or radial, conduction.
2. The length to diameter ratio is very much greater than one, and hence, the temperature profiles may be assumed similar (or affine) along the bed length.

The second statement implies that the temperature profile at any length may be superimposed upon the temperature profile at any other length by changing only a scale factor. It is not possible to validate this assumption from existing experimental data. However, the assumption seems wholly reasonable, in particular in the vicinity of the tube axis where (it will be shown) the method to be developed is most nearly correct.

It is convenient to introduce a dimensionless temperature and a dimensionless radial position. The dimensionless temperature, τ, will be defined most conveniently after consideration of the boundary conditions of interest to the problem. The dimensionless radial position, ρ, will be defined as follows :

$$\rho = \frac{r}{R} \tag{2}$$

and is zero along the axis of the cylindrical bed and unity at the wall.

Equation (1) then becomes :

$$\frac{\partial \tau}{\partial \theta} + u \frac{\partial \tau}{\partial x} = \frac{K}{R^2}\left(\frac{\partial^2 \tau}{\partial \rho^2} + \frac{1}{\rho}\frac{\partial \tau}{\partial \rho}\right) + \beta_1(\tau) \tag{3}$$

In eq. (3) the axial conduction term is assumed small – as previously stated – and dropped. The generation function $\beta_1(\tau)$ is related to $\beta(T)$ through a constant term only, depending specifically only on the form chosen for τ. Note, finally, that each term in eq. (3) has the dimensions of reciprocal time.

The complete solution of eq. (3), for $\beta_1(\tau)$ other than constant, is difficult and calculation for specific problems is frequently equally difficult even by machine methods. For the present problem, set

$$\tau = \tau_m(x, \theta) \cdot f(\rho) \tag{4}$$

where τ_m is the maximum (axial) τ and is a function only of x, and θ, and $f(\rho)$ is a suitable function of ρ, Note that

$$\frac{\int_A f(\rho)\, dA}{A} = \gamma \tag{5}$$

where γ is a constant.

Then, introduce eq. (4) into (3), multiply through by dA, divide through by A, and integrate term by term.

Proceeding, eq. (3) becomes :

$$\left.\begin{aligned} \frac{\int_A f(\rho)\, dA}{A} \cdot \frac{\partial \tau_m}{\partial \theta} + u \frac{\int_A f(\rho)\, dA}{A} \cdot \frac{\partial \tau_m}{\partial x} \\ = \frac{K \tau_m}{R^2} \frac{\int_A \left(\frac{\partial^2 f}{\partial \rho^2} + \frac{1}{\rho}\frac{\partial f}{\partial \rho}\right) dA}{A} \\ + \frac{\int_A \beta_1(\tau)\, dA}{A} \end{aligned}\right\} \tag{6}$$

Note that the coefficient of $\frac{\partial \tau_m}{\partial \theta}$ and $\frac{\partial \tau_m}{\partial x}$ are both constant. The coefficient of $\frac{K \tau_m}{R^2}$ is another constant, λ, which, like γ, depends on the form of the function $f(\rho)$. Thus :

$$\frac{\partial \tau_m}{\partial \theta} + u \frac{\partial \tau_m}{\partial x} = \frac{K \tau_m \lambda}{\gamma R^2} + \frac{\int_A \beta_1(\tau)\, dA}{A} \tag{7}$$

The integral term on the right hand side must be evaluated separately. It will be a new function $h(\tau_m)$, and will not be a function of ρ ; thus :

$$\frac{\partial \tau_m}{\partial \theta} + u \frac{\partial \tau_m}{\partial x} = \frac{K \lambda \tau_m}{\gamma R^2} + h(\tau_m) \tag{8}$$

Eq. (8) defines a $\tau_m - \theta - x$ surface in space. At any point on this surface, the normal will have

direction numbers $\frac{\partial \tau_m}{\partial \theta}, \frac{\partial \tau_m}{\partial x}, -1$, and, from an inspection of the differential equation (8), it appears that at this point there will be a tangent vector having components

$$1, u, \left[\left(\frac{K\lambda\,\tau_m}{\gamma\,R^2}\right) + h\,(\tau_m)\right] \qquad (9)$$

Further, all solution surfaces have a normal which is perpendicular to this vector. This normal will have direction numbers as just stated. Therefore, all solution surfaces are tangent to this vector. Thus to map the characteristics of the solution surfaces, the following system of *total* differential equations must be solved.

$$\frac{d\theta}{1} = \frac{dx}{u} = \frac{d\tau_m}{\frac{K\,\lambda\,\tau_m}{\gamma\,R^2} + h\,(\tau_m)} \qquad (10)$$

Using eq. (10), it is possible to map out the linear elements of which a particular solution surface (defined by specific values of the constants) is made. The $\tau_m - \theta$ characteristics defined by eq. (10), when projected on the $x - \theta$ surface, are straight lines with slope $= u$.

The following special cases will be considered as examples. They are intended only to illustrate the manner in which the resulting equation – eq. (10) – may be used. The first case to be examined will be for a particular wall boundary condition, namely the condition under which no heat is lost through the wall to the reactor. The boundary conditions are specified and lead to a particular form of the temperature profile. This case is probably not particularly realistic for a well-constructed homogeneous reactor but does serve to illustrate the application of the method to a practical problem. Case I-B provides the same boundary conditions but assumes that the generation function is more realistically defined in terms of an exponential in the reciprocal of temperature. Finally, the industrially realistic problem of a constant heat flux at the wall is set up and a solution indicated.

Case I – The "adiabatic" reactor

The dimensionless temperature, τ, will be defined as

$$\tau = \frac{T - T_w}{T_w} = \tau_m\,(x, \theta) f\,(\rho) \qquad (11)$$

There are four boundary conditions which may be written for the temperature – radial position (or $\tau - \rho$) relationship, these being the value of τ at $\rho = 0$ and $\rho = 1$ and the value of $\frac{\partial \tau}{\partial \rho}$ at $\rho = 0$ and $\rho = 1$. These four permit a third degree polynomial to be used to describe the temperature profile, viz.:

$$f\,(\rho) = A + B\rho + C\rho^2 + D\rho^3 \qquad (12)$$

The boundary conditions are :

$$\left.\begin{array}{lll} (1) & @\ \rho = 0 \text{ (centre)}, & T = T_m,\quad \tau = \tau_m \\ (2) & \rho = 0, & \frac{\partial T}{\partial r} = 0,\quad \frac{\partial \tau}{\partial \rho} = 0 \\ (3) & \rho = 1 \text{ (wall)}, & T = T_w,\quad \tau = 0 \\ (4) & \rho = 1, & \frac{\partial T}{\partial r} = 0,\quad \frac{\partial \tau}{\partial \rho} = 0 \end{array}\right\} \qquad (13)$$

Using these boundary conditions one obtains :

$$\tau = \tau_m\,(1 - 3\rho^2 + 2\rho^3) \qquad (14)$$

The form of the profile is shown in Fig. 1. The form of the equation for the temperature profiles

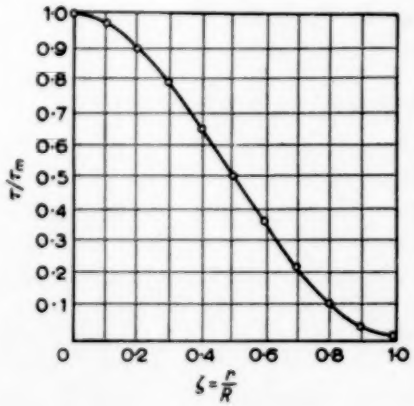

Fig. 1.

satisfies all boundary conditions. At this point – for the first time – it is necessary to decide on the cross section shape. For a circular cross

section, the constants γ and λ are found as follows :

$$\left.\begin{aligned}\gamma &\equiv \int_0^1 2\rho f(\rho)\, d\rho = 0.3 \\ \lambda &\equiv \int_0^1 2\rho\left(\frac{\partial^2 f}{\partial \rho^2} + \frac{1}{\rho}\frac{\partial f}{\partial \rho}\right) d\rho = 0\end{aligned}\right\} \quad (15)$$

Thus, the $\theta - \tau_m$ relationship defined by eq. (10) becomes :

$$\theta = \int_{\tau_{m0}}^{\tau_m} \frac{d\tau_m}{h(\tau_m)} \quad (16)$$

where $h(\tau_m)$, to be designated as the " instability integral," is given by :

$$h(\tau_m) = \frac{\int_A \beta_1(\tau)\, dA}{\gamma A} \quad (17)$$

A definite form for the generation function is now necessary.

Case I-A :

$$\left.\begin{aligned}&\text{Assume} \\ &\qquad \beta(T) = \alpha T \\ &\text{Then} \\ &\qquad \beta_1(\tau) = \alpha T_w(\tau + 1) \\ &\text{and} \\ &\qquad \beta_2(\tau) = \alpha(\tau + 1)\end{aligned}\right\} \quad (18)$$

The instability integral will then be

$$h(\tau_m) = \frac{\int_A \beta_2(\tau)\, dA}{\gamma A} = \frac{\alpha}{\gamma}\int_0^1 \rho(\tau + 1)\, d\rho \quad (19)$$

Using eqs. (14) and (15) it may be shown that

$$h(\tau_m) = \frac{\alpha}{2}\tau_m + \frac{\alpha}{0.6} \quad (20)$$

Eq. (16) then becomes :

$$\theta = \int_{\tau_{m0}}^{\tau_m} \frac{d\tau_m}{\frac{\alpha}{2}\tau_m + \frac{\alpha}{0.6}} = \frac{2}{\alpha}\ln\frac{\frac{\tau_m}{2} + \frac{10}{6}}{\frac{\tau_{m0}}{2} + \frac{10}{6}} \quad (21)$$

and

$$\tau_m = \left(\tau_{m0} + \frac{10}{3}\right)e^{-\frac{\alpha\theta}{2}} - \frac{10}{3} \quad (22)$$

Fig. 2 shows the $\tau_m - \theta$ relationship for the three possible types of thermodynamic situations. Furthermore, from eq. (10) it is also possible to compute the axial distance downstream at which any prescribed temperature is reached.

Case I-B :

Assume the generation function, $\beta(T)$, to be more realistically defined as follows :

$$\beta(T) = \alpha e^{-E/R'T} \quad (23)$$

Then

$$\beta_2(\tau) = \frac{\alpha}{T_w}\exp\left[-\frac{E}{R'T_w}\cdot\frac{1}{\tau + 1}\right.$$

The instability integral becomes

$$h(\tau_m) = \frac{\alpha}{T_w\gamma}\int_0^1 \rho\exp\left[-\frac{E}{R'T_w}\cdot\frac{1}{\tau + 1}\right]d\rho \quad (24)$$

Let $\epsilon = E/R'T_w$ and introduce the profile equation for τ :

$$\left.\begin{aligned}h(\tau_m) = &\\ &\frac{\alpha}{T_w\gamma}\int_0^1 \exp\frac{-\epsilon}{(\tau_m+1)-3\tau_m\rho^2+2\tau_m\rho^3}\rho d\rho \\ &= e^{\frac{-\epsilon}{1+\tau_m}}\cdot\frac{\alpha}{T_w\gamma} \\ &\int_0^1 \rho\exp\left[\frac{-3\tau_m\epsilon\rho^2\left(1-\frac{2}{3}\rho\right)}{(1+\tau_m)^2\left\{1-\frac{3\tau_m\rho^2}{1+\tau_m}\left(1-\frac{2}{3}\rho\right)\right\}}\right]d\rho\end{aligned}\right\} \quad (25)$$

Note that the group $\frac{3\tau_m\rho^2}{1+\tau_m}\left(1-\frac{2}{3}\rho\right)$ will always be less than unity. In particular, for the region near the tube axis, this group will be very small. As a first approximation, it will be assumed negligible in order to obtain some information concerning the identity of the instability integral.

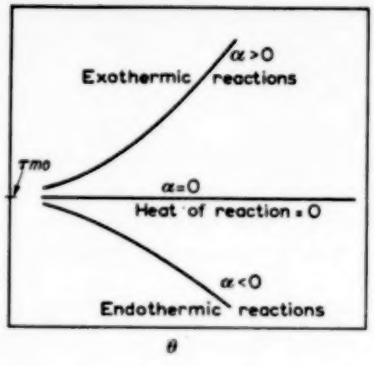

FIG. 2.

Thus :

$$h(\tau_m) = \frac{\alpha}{T_w \gamma} \cdot e^{\frac{-\epsilon}{1+\tau_m}} \int_0^1 \rho \exp\left[-\frac{3\tau_m \epsilon}{(1+\tau_m)^2}\rho^2 + \frac{2\tau_m \epsilon}{(1+\tau_m)^2}\rho^3\right] d\rho \qquad (26)$$

The positive exponential term may be expanded in a series, dropping terms in ρ^6 and higher with the following results :

$$h(\tau_m) = \frac{\alpha}{T_w \gamma} \cdot e^{-\frac{\epsilon}{1+\tau_m}} \left[\int_0^1 \rho\, e^{\frac{-3\tau_m \epsilon}{(1+\tau_m)^2}\cdot\rho^3} d\rho + \frac{2\epsilon\tau_m}{(1+\tau_m)^2}\int_0^1 \rho^4 e^{\frac{-3\epsilon\tau_m}{(1+\tau_m)^2}\cdot\rho^3} d\rho\right] \qquad (27)$$

Let $v = \dfrac{3\epsilon\tau_m}{(1+\tau_m)^2}$ with the following results :

$$\int_0^1 \rho\, e^{-v\rho^3} d\rho \cong \frac{1}{2v}$$
$$\frac{2}{3} v \int_0^1 \rho^4 e^{-v\rho^3} d\rho \cong \frac{\Gamma\left(\frac{5}{2}\right)}{3v^{3/2}} \qquad (28)$$

The last is the first correction term in the indicated series integration of eq. (26). For values of ϵ of the order of 10, which will be shown to be wholly reasonable, the correction term contributes less than 20 per cent to the value of $h(\tau_m)$ and the importance of the correction term diminishes with increasing ϵ. Thus :

$$h(\tau_m) \cong \frac{\alpha R'}{6E\gamma} e^{\frac{-\epsilon}{1+\tau_m}} \frac{(1+\tau_m)^2}{\tau_m} \qquad (29)$$

and the $\theta - \tau_m$ relationship is given as before :

$$\theta = \frac{6E\gamma}{\alpha R'} \int_{\tau_{m0}}^{\tau_m} \frac{\tau_m}{(1+\tau_m)^2} e^{\epsilon/1+\tau_m} d\tau_m \qquad (30)$$

The result of this integration is quite complex. The following three equations are quite close approximations. The equation for $\epsilon = 10$ was checked by graphical techniques and found to represent the true $\theta - \tau_m$ relationship within the permissible limits of the numerical integration.

$$\left.\begin{aligned} \tau_m &= \left(\frac{\theta}{7{\cdot}58\left(\frac{6E\gamma}{\alpha R'}\right)} + 1\right)^{2{\cdot}62} \quad \text{for } \epsilon = 5 \text{ and } \tau_m > 1 \\ \tau_m &= \left(3{\cdot}10 - \frac{\theta}{24\left(\frac{6E\gamma}{\alpha R'}\right)}\right)^{-{\cdot}616} \quad \epsilon = 10\ \tau_m > 0{\cdot}5 \\ \tau_m &= \left(330 - \frac{\theta}{183\left(\frac{6E\gamma}{\alpha R'}\right)}\right)^{-0{\cdot}40} \quad \epsilon = 15\ \tau_m > 0{\cdot}1 \end{aligned}\right\} \qquad (31)$$

Fig. 3 indicates the form of the $\tau_m - \dfrac{\theta}{\left(\frac{6E\gamma}{\alpha R'}\right)}$ relationship for $\epsilon = 5$, $\epsilon = 10$ and $\epsilon = 15$. Note that $\dfrac{\theta}{\left(\frac{6E\gamma}{\alpha R'}\right)} = \dfrac{\theta\alpha T_w}{6E\gamma}$. Thus, for a value of $\left[\theta/\left(\frac{6E\gamma}{\alpha R'}\right)\right] = 70$ and $\epsilon = 10$, $\theta = \dfrac{1260}{\alpha T_w}$. Thus, if α is large, the reactor is likely to be unstable, that is, the time required to reach an unstable operation will be small. Conversely, if α is small, the reactor is likely to be stable for large time ranges. If α is negative, it is evident from an inspection of equations (31) that τ_m will continually decrease with increasing times. Finally, if α is zero, τ_m will be constant. These possibilities correspond to the thermodynamic cases of a large exothermic heat of reaction, the unstable case only for long times, the endothermic reaction, and finally, the case of zero heat of reaction.

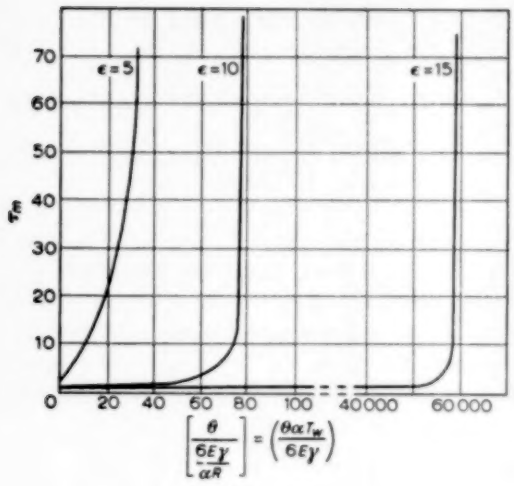

FIG. 3

Case II – The constant heat flux case

Assume that the rate of heat removal (or addition) through the walls of the reactor is constant at q BTU/hr ft^2 of surface area. The boundary conditions determining the equation for the temperature profile parallel those shown as eq. (16), viz.:

$$\left.\begin{aligned} &\text{(a) @ } \rho = 0 \quad , \quad T = T_m \quad , \quad \tau = \tau_m \\ &\qquad\qquad \frac{\partial T}{\partial r} = 0 \quad , \quad \frac{\partial \tau}{\partial \rho} = 0 \\ &\text{(a) @ } \rho = 1 \quad , \quad T = T_w \quad , \quad \tau = 0 \\ &\qquad\qquad \frac{\partial T}{\partial r} = -\frac{q}{k} \quad , \quad \frac{\partial \tau}{\partial \rho} = -\frac{qR}{kT_w} \end{aligned}\right\} \quad (32)$$

Evaluating the constants in eq. (15) one obtains

$$\tau = \tau_m\left[1 + \left(\frac{qR}{kT_w\tau_m} - 3\right)\rho^2 + \left(2 - \frac{qR}{kT_w\tau_m}\right)\rho^3\right] \quad (33)$$

Let

$$z = \frac{qR}{kT_w}$$

Then

$$\tau = \tau_m(1 - 3\rho^2 + 2\rho^3) + z(\rho^2 - \rho^3)$$

For this case,

$$\gamma = \frac{3\tau_m + z}{\tau_m}$$

$$\lambda = \frac{-20z}{8T_m + z}$$

The $\theta - \tau_m$ relationship is again available through eq. (10), viz.:

$$\theta = \int_{\tau_{m0}}^{\tau_m} \frac{d\tau_m}{\frac{-20Kz}{R^2}\frac{\tau_m^2}{(3\tau_m + z)^2} + h(\tau_m)} \quad (34)$$

This case may now be studied for various forms of the generation function as before.

SUMMARY AND CONCLUSIONS

A generalized approach to the problems of temperature stability of a fixed bed catalytic converter has been presented. The method permits examination of the conditions under which a converter of given length operating on an exothermic or endothermic reaction of known thermodynamics and kinetics will maintain an axial temperature within some arbitrary limits of a design optimum. The method appears to be applicable to a wide variety of problems in this area and to permit relatively easy exact solution for any given problem by analytical methods or by numerical or machine computations. The most difficult problem presented is the evaluation of a definite integral. The solution can often be approximated to an acceptable degree of accuracy by classical techniques. In addition, such problems are readily handled by modern computational methods. The method presented herein has been used on an industrial problem and found to yield meaningful information.

Acknowledgement—The author wishes to acknowledge the interest and suggestions of Dr. T. R. BERLIN and Dr. F. H. CLAUSER who contributed materially to this work.

NOTATION

A = cross sectional area
E = energy of activation
$h(\tau_m)$ = the instability integral defined by eqs. (7) and (8).
r = radial distance
R' = gas constant
R = tube radius
T = temperature
T_m = axial temperature, a function of x only.
T_w = wall temperature
u = linear velocity

v = a constant defined by eq. (28)
x = axial distance

Greek symbols :

α = a constant, defined by eq. (18)
$\beta(T)$ = the generation function defined by eq. (1)
$\beta_1(\tau)$, $\beta_2(\tau)$ = modified forms of the generation function defined by eqs. (3) and (18)
γ = a constant, defined by eq. (5)
ϵ = defined as E/RT_w.
K = thermal diffusivity
λ = a constant
θ = time
ρ = dimensionless radial position
τ = dimensionless temperature
τ_m = dimensionless maximum or axial temperature
τ_{m0} = dimensionless maximum or axial temperature at $x = 0$

References

[1] Amundson N. R. *Ind. Eng. Chem.* 1956 **48** 26-35, 1956 **48** 35-43.

Chemical Engineering Science, 1957, Vol. 6, pp. 190 to 203. Pergamon Press Ltd.

Studies in filtration

Blocking filtration

P. M. HEERTJES

Laboratory of Chemical Engineering of the Technical University, Delft

(*Received* 2 *October* 1956)

Abstract—A general equation of the form $R = R_f \left(\frac{OaN}{OaN - g} \right)^s$ in which the resistance R of the filter plus cake and the resistance R_f of the filter have been based on a simplified FANNING equation, has been derived for blocking filtrations of the type in which the filter is blocked strongly by the particles of the filtered suspension. Such a filtration will occur in many technical filtrations, preceding an actual cake filtration and also in the filtration of very dilute suspensions. Experimental proof of the validity of the equation is given for different and differing systems.

It has again been confirmed that for a certain system the type of filtration is governed by the concentration of the suspension. Starting from very dilute suspensions an increase in concentration shows a gradual change from a strong blocking filtration to a cake filtration. An indication has been obtained that a third type of filtration, the cake blocking filtration may exist.

Résumé—L'auteur donne à partir de l'équation simplifiée de FANNING une équation de la forme $R = R_f \frac{O_a N}{O_a N - g}$ dans laquelle R est la résistance globale filtre + gâteau et R_f la résistance du filtre seul. Cette équation a été calculée pour des filtrations à pré-filtre (blocking filtration) appartenant au type de celles où le filtre est bloqué fortement par les particules de la suspension filtrée. Une telle filtration est fréquente en pratique, et précède la filtration de suspensions trés diluées. La vérification expérimentale de cette équation est donnée pour des systèmes variés et susceptibles de modifications dans le temps.

Il est à nouveau démontré que pour certains systèmes le mode de fitration est imposé par la concentration de la suspension. En partant de suspensions trés diluées et eu faisant croître la concentration on peut observer une évolution progressive de la filtration à pré-filtre fortement bloqué jusqu'à la filtration avec gâteau. On met aussi en évidence un troisième type de filtration : la fitration à gâteau et pré-filtre (cake blocking filtration).

INTRODUCTION AND THEORY

IN previous work [1] the phenomena occurring during the filtration of very dilute suspensions of "puritine"* over nylon cloth have been described. It appeared that when suspensions containing about 1 mg of solid substance per litre were filtered a blocking of the filtercloth took place. The blocking decreased with an increase of the concentration, ranging from an almost absolute blocking to no blocking (cake filtration). For the blocking filtrations the "specific resistance" of the "cake" (so-called for convenience sake) increased with the amount of substance on the filter, the more so the nearer an absolute blocking was reached. For a cake filtration the specific resistance of the cake is independent of the amount filtered. A survey of the results obtained has been presented graphically in Fig. 12 of the paper cited.

An equation for an absolute blocking filtration has also been given. Expressed in the total resistance R† or in the differential specific

* An active carbon coal.

† For the significance of the symbols see the Nomenclature.

resistance r_d of the "cake," this equation could be given as :

$$R = R_f\left(\frac{aN}{aN-g}\right) \quad \text{or :} \quad r_d = \frac{R_f}{aN}\left(\frac{aN}{aN-g}\right)^2.$$

For the other types of blocking filtrations found, no mathematical expressions have been given. Partly because the physical phenomena were not clear to us, which was to some extent due to the fact that the amount of experiments on which the observations had been made were not sufficient and only based on one system. Therefore the work on the blocking filtration has been expanded, in particular to more defined systems. Some of the results obtained on blocking filtration will be given in this paper.

Before entering into the experimental details some considerations will be given, the choice and the treatment of which are determined by the systems investigated and by the present opinion obtained therewith.

Let us consider first an ideal system consisting of a horizontal filter with a large number N of circular pores per unit of surface by means of which a suspension of concentration c is filtered, which contains spherical particles of weight a and of a diameter larger than the diameter of the pores and smaller than the distance between the centres of two pores.

After a certain time θ a volume V has been filtered off. This amount V will be considered to have flown through in S steps, each step filtering an equal amount V'. Therefore :

$$V'S = V \tag{1}$$

If the filter has a surface A, after the first step the number of pores completely blocked will be $\frac{V'c}{a}$ and therefore the blocked surface will be : $\frac{V'c}{aN}$, if it is assumed that each particle reaching an open part of the filter blocks one pore completely.

The surface of the filter A' still open after filtering off V' therefore will be :

$$A' = A - \frac{V'c}{aN} \tag{2}$$

If the calculated amount of substance deposited per unit of filtering surface after filtering off a volume V is g :

$$g = \frac{Vc}{A} \tag{3}$$

Combination of the equations (2) and (3) gives :

$$A' = A\left(1 - \frac{g}{SaN}\right) \tag{4}$$

In the second step again a volume V' will be filtered. Because part of the pores are blocked, the phenomenon that the solid particles will not always follow exactly the streamlines of the fluid must be taken into account. Let us assume as a limiting case that the path of the particles over the whole length of the container over the filter does deviate less from the vertical than the distance between two pores, whereas the liquid can move freely. In that case the concentration c' of the second portion to be filtered will be less than c and is equal to :

$$c' = c\frac{A'}{A} \tag{5}$$

This phenomenon will be called the *dilution effect.** The still open surface A'' after the second portion has been filtered will be :

$$A'' = A' - \frac{V'c'}{aN} = A' - \frac{V'c}{aNA}A' = A'\left(1 - \frac{g}{SaN}\right) \tag{6}$$

Combination of (4) and (6) yields :

$$A'' = A\left(1 - \frac{g}{SaN}\right)^2$$

Using the same reasoning in the following steps, after S steps the free surface A^s can be expressed by :

$$A^s = A\left(1 - \frac{g}{SaN}\right)^S \tag{7}$$

From the filtration data, assuming laminar flow, the resistance of the filter R_f or of the filter with

* The phenomenon will also be encountered in the first step. Its magnitude will depend on the number of pores of the filter and the occurring deviation of the particles from the vertical. By the conditions chosen it has for convenience sake been eliminated in the first step.

cake R are defined by the special form of the FANNING equation :

$$\frac{1}{A}\frac{dV}{d\theta} = \frac{1}{\eta}\frac{\Delta P}{R(\text{or } R_f)} \tag{8}$$

For turbulent flow the form :

$$\frac{1}{A}\frac{dV}{d\theta} = \frac{1}{\eta^{0.5}\rho^{0.5}}\frac{(\Delta P)^{0.5}}{R(\text{or } R_f)} \tag{9}$$

has been used (see later).

(In both these equations R and R_f are independent of the "filtration pressure" ΔP and the viscosity η.

Considering that the open filter by definition has a resistance R_f :

$$\frac{A}{R} = \frac{A'}{R_f} \tag{10}$$

and therefore :

$$R = R_f\left(\frac{SaN}{SaN - g}\right)^S. \tag{11}$$

The differential specific resistance r_d per gram of solid substance defined by :

$$dR_b = r_d\, d\left(\frac{Vc}{A}\right)$$

in which $R_b = R - R_f$, is equal to :

$$\frac{dR_b}{dg} = \frac{dR}{dg}.$$

Thus :

$$r_d = \frac{R_f}{aN}\left(\frac{SaN}{SaN - g}\right)^{S+1} \tag{12}$$

For all values of S : $(r_d)_{g\to 0} = \frac{R_f}{aN}$.

The quantity of substance which actually blocks the pores g_b is smaller than the calculated quantity g. As :

$$A' = A\left(1 - \frac{g_b}{aN}\right) \tag{13}$$

it follows that :

$$g_b = aN\left\{1 - \left(1 - \frac{g}{SaN}\right)^S\right\} \tag{14}$$

A second case will now be considered in which more than one particle will finally block one pore.

Let us assume that all the pores participate at the same time to the same extent in the blocking operation. If laminar flow is present in the pores and if reduction of the surface of each pore is such that the diameter (or the equivalent) decreases from D_p to D after a volume V has been filtered off, then :

$$R_f = \frac{128L}{\pi D_p^4 N} \tag{15}$$

and

$$R = \frac{128L}{\pi D^4 N} \tag{16}$$

Now if it is assumed that each particle covers a surface equivalent to $\frac{1}{4}\pi D_s^2$, regardless of the actual diameter of the pore, so that :

$$\frac{1}{4}\pi D_p^2 - \frac{Vc}{ANa}\frac{1}{4}\pi D_s^2 = \frac{1}{4}\pi D^2$$

from which :

$$D^2 - D_p^2 = -\frac{Vc}{AaN}\cdot D_s^2 \tag{17}$$

combination of (15), (16) and (17) and introducing

$$n = \left(\frac{D_p}{D_s}\right)^2$$

gives :

$$R = R_f\left(\frac{naN}{naN - g}\right)^2 \tag{18}$$

If the flow in the pores is turbulent the same equation is valid. In that case however $n = \left(\frac{D_p}{D_s}\right)^{1.33}$.

The partially blocked filter with uniformly blocked pores can be visualized to consist of two parts, a completely blocked part and an open part of resistance R_f and of surface A_f.

From the considerations given, it is apparent that A_f can be expressed mathematically as :

$$A_f = A\left(1 - \frac{g}{naN}\right)^2 \tag{19}$$

The amount of substance filtered has covered a pore surface of $\frac{Vc}{a}\frac{1}{4}\pi D_s^2$. This is equivalent to a real blocked surface of

$$\frac{Vc}{a} \cdot \frac{1}{4}\pi D_s^2 \cdot \frac{1}{\frac{1}{4}\pi D_p^2 N}$$

The real open surface of flow A_r therefore is equal to :

$$A_r = A - \frac{Vc}{aN}\frac{D_s^2}{D_p^2} = A\left(1 - \frac{g}{naN}\right) \quad (20)$$

Its resistance is :

$$R_f = \left(1 - \frac{g}{naN}\right)^{-1}$$

If again the dilution principle is applied to the case under investigation and using the considerations given above we find that after the first volume V' has been filtered off the corresponding resistance R' is defined by :

$$\frac{R'}{R_f} = \left(\frac{naN}{naN - \frac{V'c}{A}}\right)^2 \quad (21a)$$

A second portion V' will give a filter with resistance R'' for which :

$$\frac{R''}{R'} = \left(\frac{n'aN}{n'aN - \frac{V'c'}{A}}\right)^2 \quad (21b)$$

In this equation $n' = \left(\frac{D'}{D_s}\right)^2$ in which D' is the diameter of the pores after filtering V'. Moreover :

$$c' = c\frac{A_r'}{A} = c\left(1 - \frac{g}{SnaN}\right) \quad (21c)$$

Because :

$$(D_p)^2 - (D')^2 = D_s^2 \frac{V'c}{AaN},$$

also :

$$n' = \left(n - \frac{g}{SaN}\right) \quad (21d)$$

Combination of the equations (21) gives :

$$\frac{R''}{R_f} = \left(\frac{SnaN}{SnaN - g}\right)^4 \quad (22)$$

Repeating this procedure S times yields for $R = R^s$:

$$R = R_f\left(\frac{SnaN}{SnaN - g}\right)^{2S} \quad (23)$$

The same equation holds for turbulent flow, in which again

$$n = \left(\frac{D_p}{D_s}\right)^{1.33}.$$

The cases described will not often be encountered. The form of the pores and of the particles will in general prevent complete blocking. In the next case it will be assumed that one pore will only be blocked partially by one particle and that the cake formed on the partially blocked pores will have negligible resistance compared with that of the blocked filter. The total volume of V will be filtered off in h portions of V'. After the first portion there will be an open filter of surface A' (resistance R_f) and a partially blocked filter of surface

$$A_b' = \frac{V'c}{aN} = A\frac{g}{haN}.$$

The resistance of this part R_f' can be found by applying the equations (15) and (16). One obtains that :

$$R_f' = R_f\left(\frac{D_p}{D}\right)^4$$

and because

$$D_p^2 - D_2 = D_s^2,\ R_f' = R_f\left(\frac{n}{n-1}\right)^2 = pR_f.$$

As far as flow is concerned the part of the filter of surface A_b' and resistance R_f' is equivalent with a filter of surface A_f', and resistance R_f in which

$$A_f' = \frac{1}{p}A_B'$$

Because :

$$\frac{A}{R'} = \frac{A' + A_f'}{R_f}$$

and

$$A' + A_f' = A - A\frac{g}{haN} + A\frac{g}{phaN},$$

it follows that :

$$\frac{R_f}{R'} = 1 - \frac{g}{haN} + \frac{g}{hpaN}$$

Upon filtering a second portion V', through the open filter (with surface A') will flow an amount of: $\frac{A'}{A' + A_f'}V'$. By this procedure a second portion

of the filter of surface $A_b'' = \frac{A'}{A' + A'} \cdot \frac{V'c}{aN}$ will be blocked. Again this is equivalent to a filter with resistance R_f of surface $A_f'' = A_b'' \frac{1}{p}$.

Therefore after the second portion has been filtered off, the surface of the free filter is A'', the blocked filter has a surface $A_b' + A_b''$, which is equivalent with a filter of resistance R_f of surface : $A_f' + A_f''$. Therefore :

$$\frac{R_f}{R''} = \frac{1}{A}(A'' + A_f' + A_f'')$$

After h portions have been filtered off therefore :

$$\frac{R_f}{R} = \frac{1}{A}(A^h + A_f' + A_f'' + \ldots A_f^h). \quad (24)$$

A solution of equation (24) can be approached in the following manner. We have seen that

$$\frac{R_f}{R'} = t_1 = 1 - \frac{g}{haN} - \frac{g}{phaN} = 1 - m + \frac{m}{p},$$

substituting $g/haN = m$. Also :

$$\frac{R_f}{R''} = t_2 = 1 - m + \frac{m}{p} - m + \frac{\frac{m}{p}}{1 - m + \frac{m}{p}} \cdot$$

Continuing, it can be derived that :

$$\frac{R_f}{R'''} = t_3 = 1 - m + \frac{m}{p} - m + \frac{\frac{m}{p}}{1 - m + \frac{m}{p}} - m + \frac{\frac{m}{p}}{1 - m + \frac{m}{p} - m + \frac{m/p}{1 - m + \frac{m}{p}}}$$

Therefore after the filtration of h portions :

$$t_h = t_{h-1} - m + \frac{\frac{m}{p}}{t_{h-1}} \text{ and } t_0 = \frac{R_f}{R_f} = 1 \cdot \quad (25)$$

A direct solution of this series has not yet been found by the present author.

An approximate solution takes the form :

$$t_h = 1 - m + \frac{m}{p} + \left(1 - \frac{m}{p}\right)(t_{h-1} - 1). \quad (26)$$

As :

$$t_h - t_1 = t_2 - t_1 + t_3 - t_2 + \ldots . t_h - t_{h-1}$$

and because :

$$t_2 - t_1 = \left(1 - \frac{m}{p}\right)\left(\frac{m}{p} - m\right),$$

$$t_3 - t_2 = \left(1 - \frac{m}{p}\right)^2\left(\frac{m}{p} - m\right), \text{ etc.}$$

it follows that :

$$t_h = 1 - (1 - p)\left\{\left(1 - \frac{m}{p}\right)^h - 1\right\}.$$

After substituting :

$$t_h = \frac{R_f}{R} \text{ and } m = \frac{g}{haN}$$

therefore

$$\frac{R_f}{R} = 1 - (1 - p)\left\{\left(1 - \frac{g}{hpaN}\right)^h - 1\right\} \quad (27)$$

If p is large compared with unity (for absolute blocking $p = \infty$) as in the cases investigated, the number h decreases to unity. For large values of p an approximative solution of (27) is :

$$\frac{R_f}{R} = 1 - \frac{q}{aN} + \frac{q}{paN}.$$

This equation can also be derived directly from (25). For large p :

$$t_h = t_1 = 1 - \frac{g}{aN} + \frac{g}{paN}$$

or :

$$\frac{R_f}{R} = 1 - \frac{g}{aN} + \frac{g}{paN} = 1 - \frac{g}{raN} \quad (28)$$

Along the same lines as given before it can be derived that if the dilution effect is applied to this case, that :

$$\frac{R_f}{R} = \left(1 - \frac{g}{SraN}\right)^s \quad (29)$$

The equations (11), (18), (23), (28) and (29) are valid for filtrations where the filter is blocked totally or partly but to a great extent. Moreover it has been assumed that if a cake is formed over the blocked pores its resistance compared with the resistance of the filter is negligible. For every

cake filtration it is possible and in most technical cases very likely that such a type of blocking filtration preceeds the cake filtration.

Taking into account that even in the case of complete blocking of the pores, the dilution effect needs not always to take place, due to the fact that the particles will always follow the streamlines of flow to a certain extent ; that unavoidable vibrations of the apparatus influence the movement of the particles and that the slurry will not always be homogeneous, the five cases mentioned can be represented by one general equation of the form :

$$\frac{R_f}{R} = \left(1 - \frac{g}{OaN}\right)^S$$

or

$$R = R_f \left(\frac{OaN}{OaN - g}\right)^S \qquad (30)$$

and the equation for r_d :

$$r_d = \frac{R_f}{aN} \cdot \frac{S}{O} \cdot \left(\frac{OaN}{OaN - g}\right)^{S+1} \qquad (31)$$

In these equations O and S can range from unity to any value greater than 1. In general, even with one particle blocking one pore $O \neq S$, the limiting case being that $O = S = 1$, absolute blocking of a pore by one particle without dilution effect. Another mathematical limiting case will be when S and therefore also O will reach infinity.

For $S = O = \infty$ the equations (30) and (31) transform to :

$$R = R_f e^{\frac{g}{aN}}$$

and

$$r_d = \frac{R_f}{aN} e^{\frac{g}{aN}}$$

It will appear later that before very large values of S and O are reached cake filtration occurs.

For one system, increasing S and O assuming the ratio $\frac{S}{O}$ to be constant, will result in smaller values for R and r_d at the same values of g, showing therefore an apparent decrease in blocking, although in effect the blocking of the pores is the same.

In order to check the two equations (30) and (31) it is necessary to know the values of OaN or O if aN is known and S. These values can be found from the R–V, R–g or r_d–g, data in principally the same manner. From the R–g (r_d–g) values, e.g. curves of $\log R$ versus $\log g$ are constructed. On this curve three points (1, 2, 3) are chosen such that $\log R_1 - \log R_2 = \log R_2 - \log R_3$.

For these points :

$$\log (OaN - g_1) - \log (OaN - g_2) = \log (OaN - g_2) - \log (OaN - g_3)$$

Therefore

$$OaN = \frac{g_2^2 - g_1 g_3}{2g_2 - (g_1 + g_3)}$$

From the values g_1, g_2 and g_3 therefore OaN can be calculated. Via this a plot of $\log R$ (or $\log r_d$) versus $\log (OaN - g)$ can be constructed, which ought to give a straight line with slope $-S$ (or $-(S+1)$).

For rather large values of S and O the $\log r_d$–$\log g$ line can appear to be almost straight, especially towards the higher values of $\log g$, having nevertheless a slope $\neq$ zero, therefore not representing a cake filtration. In such a case it is impossible by lack of accuracy to determine the value of OaN. It is therefore impossible to decide whether these filtrations belong to the filter-blocking type, or that they represent a third type, that of a cake-blocking type governed by a law of the form : $r_d = \text{const.}\,(g)^t$.

It seems worth while to try to indicate the factors governing the magnitude of the parameters S and O. Excluding the vibrations of the apparatus for which it is nigh to impossible to predict anything in this respect, there must amongst other things be an influence of the concentration of the slurry, of density differences between particle and liquid, of the size-spectrum of the particles and of the surface tension between particle and fluid. For the parameter O there is in general also an influence of the form of the pores and of the particles. As far as the concentration is concerned it may be realized that each particle will be surrounded by a volume of liquid of $\frac{a}{c}$. Therefore the distance between the particles will be directly proportional to $\left(\frac{a}{c}\right)^{1/3}$.

The slurry can be thought to be built up of layers containing $\left(\frac{c}{a}\right)^{2/3}$ particles on a distance of $\left(\frac{a}{c}\right)^{1/3}$. The path each particle has to travel from the layer nearest to the filter is : $\left(\frac{a}{c}\right)^{2/3}$. The larger the concentration, the smaller will be the length of this path. The smaller this length will be the less chance a particle will have to come into one of the streamlines directed towards the open pores and the bigger will be S and O. In connection with the foregoing the ratio between the amount of particles in one layer and the number of pores in the filter N will also be important. In the region smaller than unity, the larger this ratio the greater will be the chance that a particle will enter a pore, therefore the smaller will be S and O. An increase in concentration results in a shorter path, the particle has to travel therefore in a larger S and O.

It however also signifies a bigger number of particles per layer per pore which will tend to decrease S and O. Which of the two factors will prevail cannot be predicted, although because the number of particles per pore is very small in blocking filtration, the path influence seems to be the largest.

Increase of the density difference between pore and particle will tend to increase S and O.

A small number of pores will give rather curved streamlines near the pores which causes through the inertia that the path of the particles will show a greater tendency to deviate from the streamlines, increasing S and O. This will also depend on the size of the particles, on the density difference and on the filtration velocity. The whole situation seems rather complex.

EXPERIMENTAL

(With the collaboration of : J. P. BRANTS (Br.), H. S. JONGEPIER (J.), and H. J. M. VAN SOEST (v.S.).

Besides the experiments already published* several other types of filtration apparatus (with horizontal and vertical filters) and other systems have been investigated, to check the above considerations. Not every type of apparatus used will be described here. Only one set-up, as used by H. J. M. VAN SOEST (Fig. 1) will be discussed.

* Experiments by H. v. d. HAAS (v.d.H.).

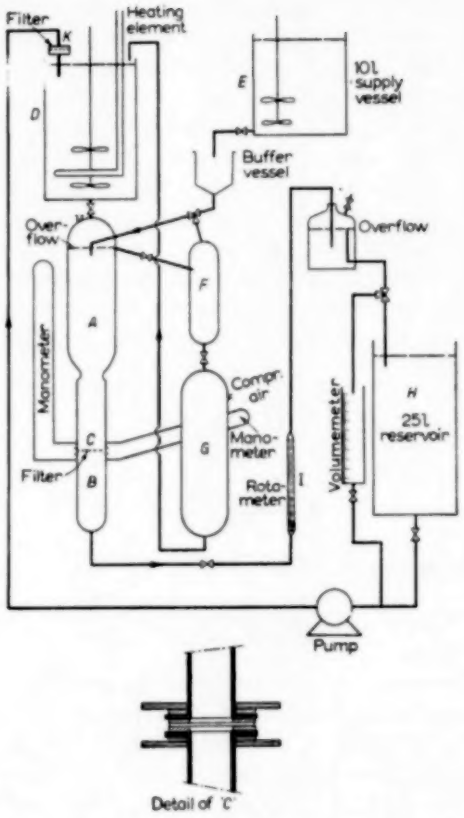

FIG. 1. Sketch of the filtration apparatus.

The horizontal filter (C) with the aid of two parted metal flanges (see detail) was mounted between two glass containers A and B provided with two ground glass flanges. Tubes 1 cm above and under the filter were connected with either a vertical or an inclining manometer. Two overflows of which one was adjustable enabled to establish the pressure difference over the filter. The resistance of the whole set-up could be changed by means of two stopcocks. The suspension to be filtered was prepared and stored in a container of 30 l. (D) made of stainless steel 316. One of the difficult problems was to prepare a homogeneous suspension. Therefore a smaller container of glass (E, 10 l.) was installed which could be stirred better with our equipment and which was filled by syphonic action from the large vessel. Overflowing suspension was assembled in the vessels (F) and (G) and returned periodically to the container (D) by means of compressed air. The filtrate was assembled in the reservoir (H) provided with a calibrated burette, which enabled the volume to be read. In some cases a rotameter (I) was used. By means of a small displacement pump the filtrate was pumped back via a filter (K) to the supply reservoir.

The filter proper was placed on a foam rubber cushion and the connections with the other parts of the apparatus were made of flexible tubing to reduce the influence of vibrations as far as possible. All the measurements were carried out at a constant temperature, maintained in the normal way in the supply-vessel.

Prefiltered and partly degassed water was always used in order to prevent a filter effect caused by impurities and (or) air bubbles.

Special precautions had to be taken with the horizontal filters to eliminate the air trapped under the filter. In most cases with the filtration of suspensions in water a small amount of wetting agent was added to promote the formation of a homogeneous suspension by breaking up particle-clusters.

Two liquids have been used: water ($\rho = 0{\cdot}998$, $\eta = 0{\cdot}915$ cp at 25°C), and a mixture of benzene and carbontetrachloride ($\rho = 1{\cdot}19$ and $\eta = 0{\cdot}803$ cp at 25°C).

Three different sorts of solid substances have been used:

(a) Two pearl polymers: methylmethacrylate ($\rho = 1{\cdot}19$ at 25°C); polystyrene ($\rho = 1{\cdot}045$ at 25°C).

These polymers were graded rather closely by careful sieving in the presence of a moist strip of filter paper followed by rolling the particles over an inclined glass-plate to obtain particles as spherical as possible. The mean diameter of the particles was determined by weighing about 3,000 particles and by calculating the diameter from the mean weight of one particle, assuming that it was a sphere.

(b) "Puritine" (as used before) as such or fractions obtained by sieving. The fractions are indicated by the measures of the two corresponding sieves.

Five different filters have been used. Two of these were nickel filters, made by electrolitical deposition, with a very regular pattern of circular pores. The three others were nylon filters with more or less rectangular pores. Some of the characteristics are given below.

	Indicated as	*Pore diameter in μ*	*Thickness in μ*	*N*
Nickelfilter I	1	260	appr. 100	400
Nickelfilter II	2	280	110	467
Nylonfilter I	3	80 × 65	–	1750
Nylonfilter II	4	50 × 40	–	2250
Nylonfilter III	5	15 × 25	–	4000

The pores of the nickel filter were not quite cylindrical, the opening at one side (the prefilt-side) being rounded, the other opening being rather sharp.

The surface of the filters used ranged from 0·8 — 15 cm².

The magnitudes measured were: V_θ, $\left(\frac{\Delta V}{\Delta\theta}\right)_\theta$ or $\left(\frac{dV}{d\theta}\right)_\theta$ and $(\Delta P)_\theta$, from which R, R_f and g could be calculated, because A, c and η were known.

Results and Discussion

For the nylon filters with their rather small pores it was not difficult to measure in the laminar region, without impairing the accuracy of ΔP too much. For the nickel filters this was not possible and the measurements had to be carried out in the turbulent region. To eliminate uncertainty for the very thin filters used, the transition region between laminar and turbulent flow has been determined. At the same time the powers of ΔP and η as used already in equation (9) for turbulent flow have been established. This has been carried out for the two nickel filters (1, 2) and one nylon filter (3) with both the liquids. The resistance of the filter R_f calculated from equation (8) and the Reynolds number Re calculated from:

$$(Re) = \frac{w\rho D_p}{\eta}$$

in which

$$w = \frac{4}{AN\pi D_p^2} \cdot \frac{dV}{d\theta}$$

have been determined at different ΔP and plotted in Fig. 2 as log R_f and log Re versus log ΔP. From the Fanning equation $\Delta P = 4f \frac{1}{2}\rho w^2 L/D$) it follows that for circular pores of diameter D_p:

For the laminar region:

$$f = \frac{16}{Re}: \quad R_f = \frac{128L}{\pi D_p^4 N} \tag{32}$$

$$Re = \frac{\rho D_p^3}{32L\eta^2}\,\Delta P. \tag{33}$$

For the turbulent region $\left(\text{assuming } f = \left(\frac{16}{Re^B}\right)\right)$:

$$R_f = \frac{4}{\pi N}\left(\frac{32\rho^{1-B}L}{D\rho^{5-B}\eta^{2-2B}}\right)^{\frac{1}{2-B}} \cdot \Delta P^{\frac{1-B}{2-B}} \tag{34}$$

$$Re = \left(\frac{\rho D_p^3}{32L\eta^2}\right)^{\frac{1}{2-B}} \cdot \Delta P^{\frac{1}{2-B}} \tag{35}$$

For rectangular openings analogous expressions have been used.

From Fig. 2, using the slopes of the lines as given there, based on equations (32), (33), (34) and (35), it can be calculated either based on the log Re lines or on the log R_f lines, that $B = 0{\cdot}20$ (as is often found) and that the transition region mentioned for the filters used lies between $Re = 3$ to 7.

All the measurements with the nylon filters have therefore been carried out in the region for which the Reynolds number was < 3, the resistances have been calculated with aid of the equation (8).

For the nickelfilters the measurements were carried out in the region for which the Reynolds number was > 7. The resistances have been calculated with the aid of equation (9).

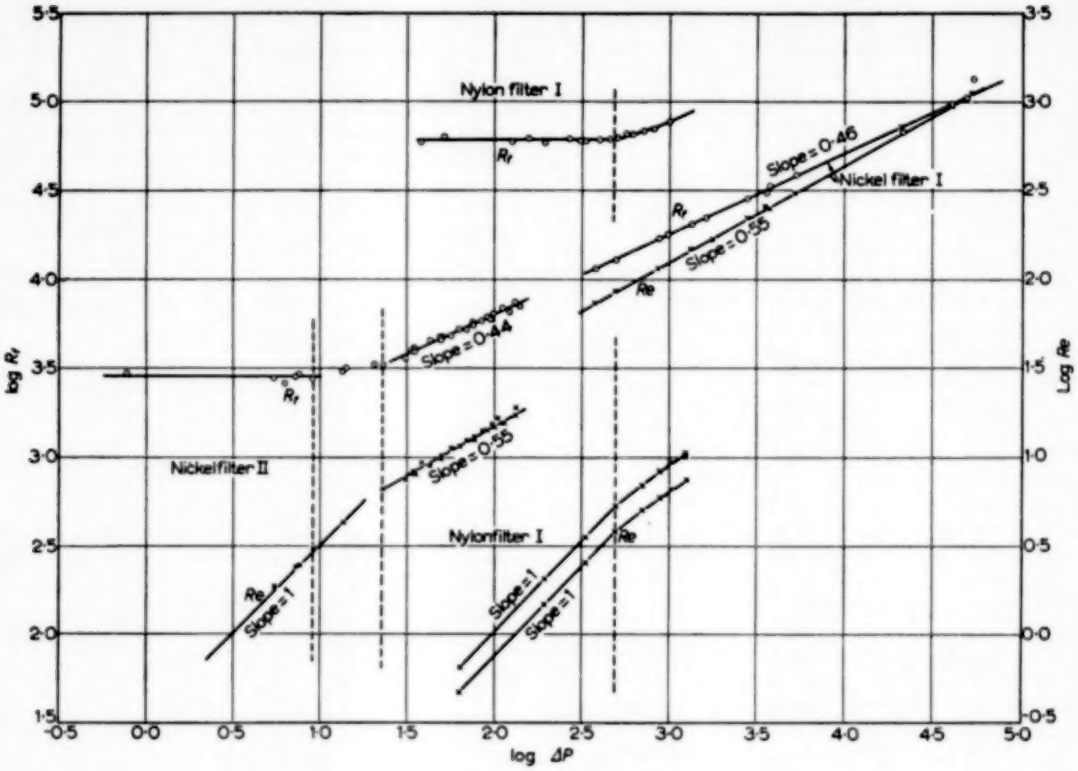

FIG. 2. Log R_f and log Re as a function of the filtration pressure ΔP.

The actual experiments can be compiled most conveniently in two series. The first series will contain the experiments carried out with the best defined systems, viz. the filtration of pearl polymers over nickel filters. The second series will contain the filtration of puritine over nylon filters.

In both series it has been found as before that an increase of the concentration caused the transition of a blocking filtration to a cake filtration. In the first series however this transition was far less reproducible than in the second series and more abrupt. In general the reproducibility in the first series, with the much larger particles was rather poor. It often happened that using one system with one concentration a blocking filtration was found in one experiment a pure cake filtration in another experiment. Two reasons mentioned before which are difficult to eliminate stand out: vibrations and lack of homogeneity. It must be kept in mind that the realization of a blocking filtration with rather large particles is a very delicate operation necessitating the use of a very dilute suspension. The lowest value used in this respect was a concentration of 1·8 particles per litre.

In the series to be presented here the cake-filtrations have not been incorporated. Moreover the few experiments in series two, where the $\log r_d - \log g$ lines appeared to be straight (see before) have been excluded. The experiments are presented in table form and characterized by the parameters S and O or OaN, which includes the first and almost most important conclusion that the initial stages of all the filtrations as carried out, giving a blocking filtration, *can* be represented in this way and therefore can be correlated by means of equation (30).

Deviations have been found but these are not incorporated. In most cases these deviations could be attributed to some disturbing influence, such as the filter effect, actual changes in concentration in the supply vessel, sudden observable extra vibrations in the building, formation of broken particles by the propellor or by the stirrer, small air bubbles in the water and leakage of the filter flanges.

Deviations also occurred near the moment the whole filter was blocked with particles.

In order to give an impression about the determinations a few worked out examples, taken from the two series will be given.

In Fig. 3 $\log r_d - \log g$ curves for puritine-nylon are presented and the corresponding $\log r_d - \log (OaN-g)$ lines in Fig. 4.

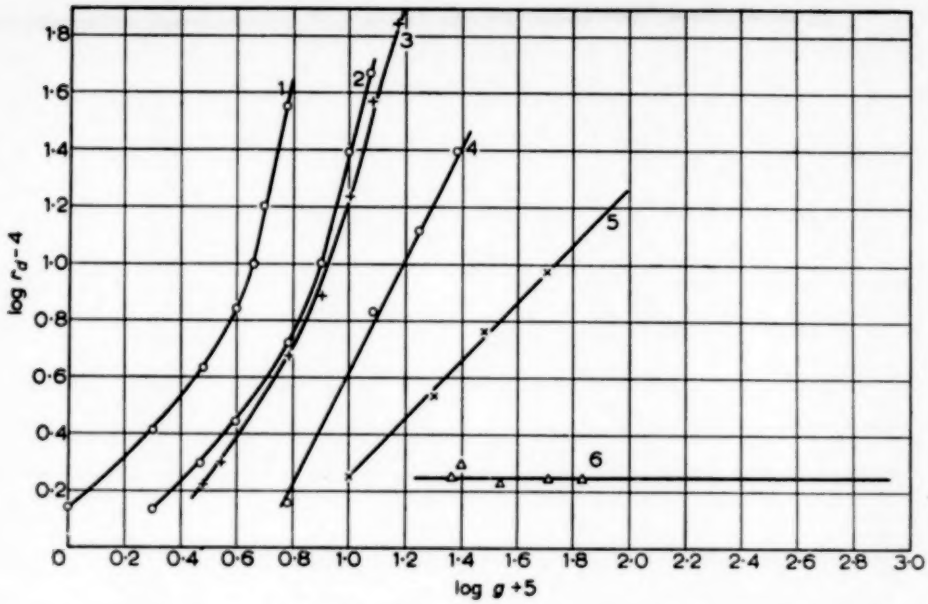

FIG. 3. The log r_d–log g curves for puritine-water filtered over nylon at different concentrations.
1 : $c = 1 \times 10^{-6}$ 2 : $c = 2 \times 10^{-6}$ 3 : $c = 3 \times 10^{-6}$ 4 : $c = 6 \times 10^{-6}$ 5 : $c = 10 \times 10^{-6}$ 6 : $c = 10 \times 10^{-6}$

In the Figs. 5 and 6 the log R – log g lines and their corresponding log R – log $(OaN - g)$ lines for polystyrene in water are given.

The data of the first series are compiled in Table 1, those of the second series in Table 2.

The dilution effect as introduced is clearly marked. In some cases it has been possible to give an additional confirmation in the following manner. After the filtration the container above the filter was drained quickly and the filter taken out carefully.

The number of pores blocked by one particle each was counted. For experiment v.S. 7 (Table 1) this appeared to be 4,400. From the volume filtered it was calculated

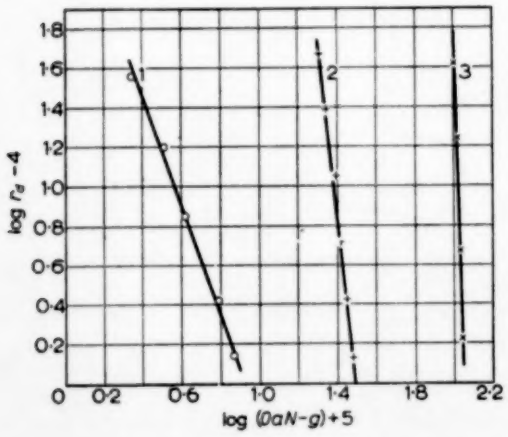

FIG. 4. The log r_d–log $(OaN–g)$ curves for the system puritine-water derived from the lines in Fig. 3.
1 : $c = 1 \times 10^{-6}$ 2 : $c = 2 \times 10^{-6}$ 3 : $c = 3 \times 10^{-6}$

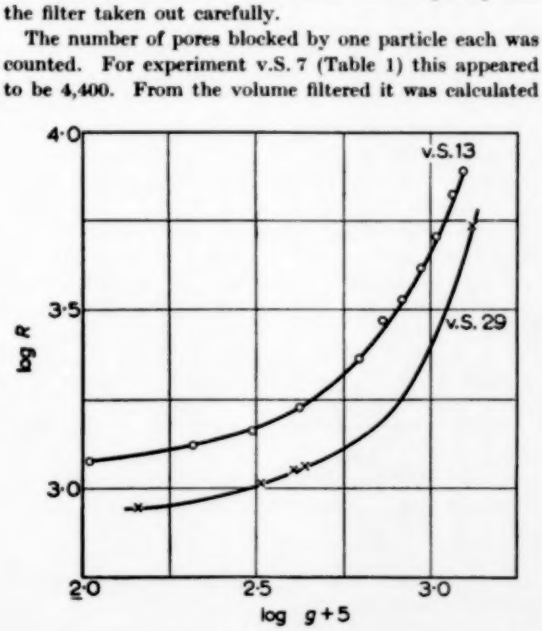

FIG. 5. Two log R–log g curves for polystyrene-water over a nickel filter.

Table 1. *Filtration of spherical particles through a filter with circular pores.*

System : Methylmethacrylate–benzene and carbontetrachloride ($\Delta\rho = 0$). Filter No. 1, $N = 400$, $D_p = 260\ \mu$, placed vertical.

Experiment	*Br* 4	*Br* 6	*Br* 12	*Br* 13	*Br* 15
c in 10^{-7} g/cm^3	1·2	1·5	3·1	3·4	4·7
a in 10^{-5} g	1·37	1·37	2·91	2·91	2·91
D particles in μ	280	280	360	360	360
Particles/litre	8·6	10·6	10·6	11·7	16·0
O	1·54	2·85	1·6	1·6	1·5
S	2·55	5·1	2·1	2·3	2·2
S/O	1·8	1·8	1·3	1·4	1·5

System : Polystyrene–water. Filter No. 1, $N = 400$, $D_p = 260\ \mu$, placed vertical.

Experiment	*Br* 47	*Br* 34	*Br* 35	*Br* 37	*Br* 38	*Br* 58
c in 10^{-7} g/cm^3	0·64	1·39	1·03	1·03	3·5	1·0
a in 10^{-5} g	1·49	2·58	2·58	2·58	2·58	5·7
D particles in μ	310	360	360	360	360	470
Particles/litre	4·3	5·4	4·0	4·0	13·4	1·8
O	1·55	7·4	1·2	1·6	1·4	1·6
S	3·3	10·3	5·7	3·6	2·8	5·5
S/O	2·1	1·4	4·7	2·2	2·0	3·4

System : Polystyrene–water. Filter No. 2, $N = 467$, $D_p = 289\ \mu$, placed horizontal.

Experiment	*v.S.* 7	*v.S.* 8	*v.S.* 9	*v.S.* 12	*v.S.* 13	*v.S.* 27	*v.S.* 29
c in 10^{-7} g cm^3	45	56	155	1,000	1,050	150	170
a in 10^{-5} g	3·0	3·0	3·0	3·0	3·0	3·1	3·1
D particles in μ	380	380	380	380	380	385	385
Particles/litre	150	187	517	3,330	3,500	484	548
O	4	1·2	1·8	4·0	1·8	1·2	1·0
S	6	1·3	1·8	7·0	3·0	1·9	1·0
S/O	1·5	1·1	1·0	1·8	1·7	1·6	1·0

that for this case $\frac{Vc}{a}$ was 4,680. If the mean real concentration as far as blocking is concerned is $\bar{c}$, for this experiment $\frac{\bar{c}}{c} = 0{\cdot}94$.

From equation (14) (using the different parameters O and S) it can be seen that :

$$\bar{c} = \frac{caN}{g}\left(1 - \left(1 - \frac{g}{OaN}\right)^S\right).$$

From this $\frac{\bar{c}}{c} = 0{\cdot}93$, which is in good agreement. By counting it was found that from the 280 particles retained in the apparatus 100 were already deposited on the filter. A photograph (Fig. 7) of this filter giving the underside and the top shows the phenomenon.

Inspection of the results given, especially of the parameters S and O (or OaN) shows that the conclusions to be drawn must be of a quantitative nature. In general it can be said that S and O increase with the concentration.

Table 2. Filtration of puritine in water over nylon-cloth with horizontal filter

Experiment	*v. d. H*	*v. d. H*	*v. d. H*	*v. S*	*v. S*	*v. S*	*v. S*
c in 10^{-6} g/cm³	1	2	3	1	2	3	5
Fraction in μ	total	total	total	60–90	60–90	60–90	60–90
N	4,000	4,000	4,000	2,250	2,250	2,250	2,250
OaN in 10^{-5} g	8	30	112	21	37	65	80
S	1·8	8	29	0·5	2·2	4·4	6·0
OaN/S in 10^{-5} g	4·4	3·8	3·9	42	17	15	13

Experiment	*v. S*	*v. S*	*v. S*	*v. S*	*v. S*	*v. S*
c in 10^{-6} g/cm³	1	2	5	1	2	5
Fraction in μ	90–150	90–150	90–150	150–220	150–220	150–220
N	2,250	2,250	2,250	2,250	2,250	2,250
OaN in 10^{-5} g	25	52	100	38	90	240
S	0·2	1·4	3·7	0·3	1·7	8·0
OaN/S in 10^{-5} g	125	37	27	125	53	30

Experiment	*v. S*	*v. S*	*v. S*	*v. S*	*v. S*	*v. S*
c in 10^{-6} g/cm³	1	2	5	1	2	5
Fraction in μ	½(60–90) ½(90–150)	½(60–90) ½(90–150)	½(60–90) ½(90–150)	½(60–90) ½(150–220)	½(60–90) ½(150–220)	½(60–90) ½(150–220)
N	22,50	2,250	2,250	2,250	2,250	2,250
OaN in 10^{-5} g	45	50	50	30	40	60
S	4·1	4·1	2·2	1·0	1·1	1·3
OaN/S in 10^{-5} g	11	12	23	30	36	46

Experiment	*v. S*	*v. S*	*v. S*	*v. S*	*v. S*	*v. S*	*v. S*	*v. S*	*v. S*	*v. S*	*v. S*	*v. S*
c in 10^{-6} g/cm³	1	10	2	5	10	1	2	3	10	½	1	5
Fraction in μ	0–50	0–50	0–50	0–50	0–50	0–50	0–50	0–50	0–50	0–60	0–60	0–60
N	1,750	1,750	1,750	1,750	1,750	1,750	1,750	1,750	1,750	4,000	4,000	4,000
OaN in 10^{-5} g	160	1,110	100	300	700	160	550	700	1,100	8	12	20
S	1·5	6·0	2	4	9	2	7	9	14	2·0	2·3	1·4
OaN/S in 10^{-5} g	107	185	50	75	77	80	79	77	78	4	5·2	14

For a polydispers system with irregular formed particles this effect was found to be more pronounced than for a monodispers system. Apparently in the last case by-effects have a great influence on the results. This also holds for the transition from blocking filtration to cake filtration. This transition, taking place upon increasing the concentration, in the systems investigated, always occurred before large values of S and O had been reached. Apparently at a certain concentration the distance of the particles is such that bridge formation over the pores overlaps the dilution phenomenon. Under optimum and carefully chosen conditions and with some luck with regard to the non-controllable influences an absolute blocking filtration for which $O = S = 1$, can be realised up to 90 per cent of the total blocking of the pores (Exp. v.S. 29).

There is an indication that for monodispers systems this optimum lies at a certain concentration, depending on N and particle size and $\Delta\rho$, below which S decreases, above which S increases with increase of the concentration. The possibility of such a behaviour has been indicated in the discussion and can be found by plotting S and versus $\frac{1}{3}\log\frac{c}{a}$.

In some cases with the puritine-water system for low concentrations S has been found to be < 1. This is an impossibility. The reason must be found in some

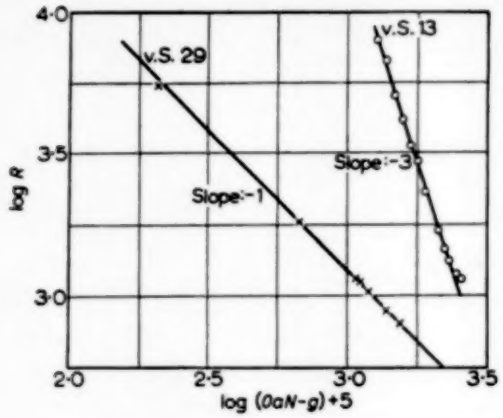

FIG. 6. The log R–log $(OaN–g)$ lines derived from Fig. 5.

uncertainty with regard to the zero point of the volume of the filtrate. A change in the zero point for V will change the S found. Although in this respect a correction is possible by displacement of the R–V lines such that $R_{V=0} = R_f$, for low concentrations with a relatively low value of $\frac{dR}{dV}$ at low values of V some uncertainty will remain. With the fractions containing small particles (the original puritine consisted for 85% of the 0-50 μ fraction) $\frac{OaN}{S}$ has been found to be constant. This signifies that $O = S$. In these cases $r_{d_{g=0}} = \frac{R_f}{aN}$, independent of the concentration. For the 0-50 μ puritine fraction with filter No. 3 (rather large openings) it could be observed that some substance passed the filter. This effect has the same influence as the dilution effect and will increase the magnitude of S and O.

A marked influence of the position of the filter, of N and of $\Delta\rho$ has not been found. Filtrations under still more idealized conditions, e.g. in a building without vibrations, must be carried out to find these influences. It is questionable whether such experiments are of importance for technical filtrations.

CONCLUSION

A blocking filtration in which the filter is blocked by the particles and in which a strong blocking occurs can be correlated by a general equation of the form $R = R_f \left(\frac{OaN}{OaN - g}\right)^S$ both for laminar and turbulent flow.

The parameters S and O in general increase with an increase of the concentration of the prefilt. After a certain concentration has been reached the filter-blocking filtration changes to a cake filtration. This change is gradual. There is an indication that a third type of filtration may exist, viz. the blocking of the cake. If this should be reality, this filtration stands in between the filter blocking filtration and the cake filtration.

A blocking filtration is defined as a filtration in which $r_d = \frac{dR}{dg} = f(g)$, whilst in a cake filtration $r_d \neq f(g)$. The occurring of a filter blocking filtration and a cake filtration coincides with the deposition of the cake in and over the pores of the filter. If the pores in a blocking filtration are not blocked strongly an analogous equation between R and R_f of a somewhat different type can be derived. This equation has not yet been checked experimentally nor the phenomenon been realized. It seems very likely that a moderate blocking will practically never occur.

Either the particles enter the pores of a filter and than almost always will give rise to a great increase of the resistance (a decrease in diameter of $\frac{1}{2}$ already signifies a 16 times larger resistance) or they form a cake over the pore. This seems the more true because particles, very small with respect to the diameter of the pores will pass the filter.

NOMENCLATURE

a	= weight of a particle	g
A	= surface of the filter	cm^2
B	= power of Reynolds number in friction factor	
c	= concentration of prefilt	$g\ cm^{-3}$
D_p	= diameter of pore	cm and μ
D_s	= equivalent diameter of surface covered by one particle	cm and μ
f	= friction factor	
g	= amount of solid substance per unit of filter area	$g\ cm^{-2}$
h	= parameter	
L	= length of a pore	cm and μ
m	= $\frac{g}{haN}$	
n	= factor	
N	= number of pores per unit of filter area	cm^{-2}
O	= parameter	
p	= factor	
ΔP	= pressure difference over the filter	$g\ cm^{-1}\ sec^{-2}$ (dyne cm^{-2})
r	= factor	
r_d	= differential specific resistance of one g of solid substance	$cm\ g^{-1}$ or $(cm\ g^{-1})^{0.56}$

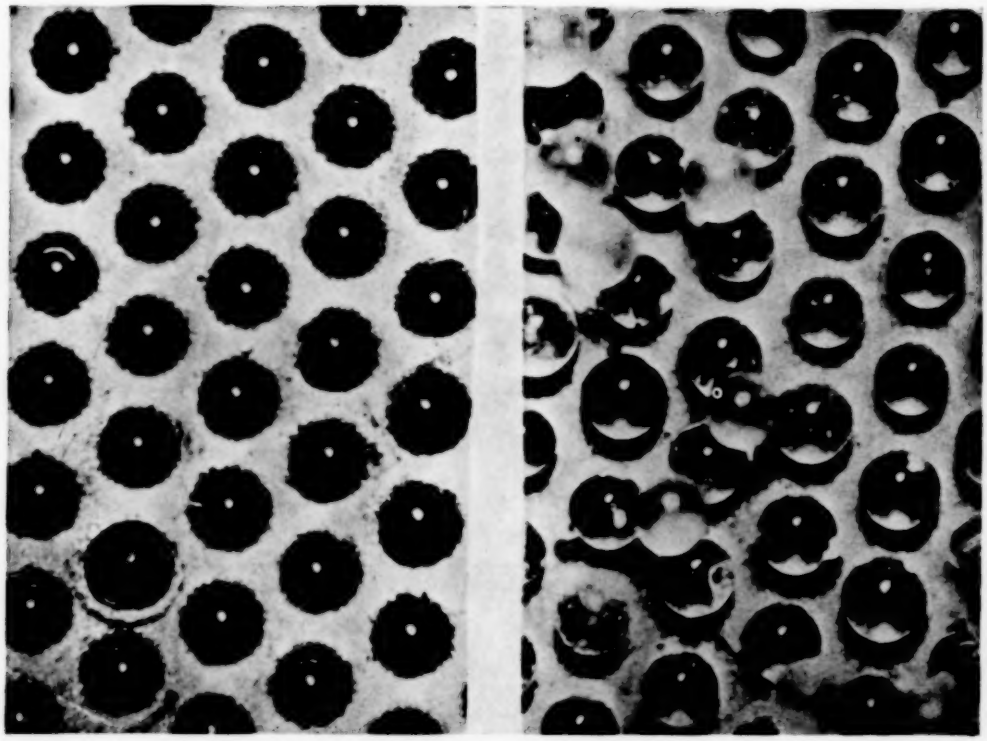

FIG. 7. The nickel filter with polystyrene particles, seen from the underside (left) and from above (right).

R = total resistance of filter and solid substance	cm^{-1} or $g^{0.44}\ cm^{-1.44}$	t = term of series	
		V = volume of filtrate	cm^3
R_K = resistance of cake	cm^{-1} or $g^{0.44}\ cm^{-1.44}$	w = velocity of fluid in a pore	$cm\ sec^{-1}$
R_f = resistance of filter	cm^{-1} or $g^{0.44}\ cm^{-1.44}$	ρ = density	$g\ cm^{-3}$
Re = Reynolds number		η = viscosity	$g\ cm^{-1}\ sec^{-1}$
S = parameter		θ = time of filtration	sec

If no indication is given the magnitudes are dimensionless.

Reference

[1] Heertjes P. M. and van de Haas H. *Rec. Trav. chim.* 1949 **68** 361.

Chemical Engineering Science, 1957, Vol. 6, pp. 204 to 214. Pergamon Press Ltd.

Mercury vapour transfer studies—I

R. W. Maxwell and J. Anderson Storrow*

Chemical Engineering Laboratory Applied Chemistry Department, College of Technology, Manchester, England

(*Received* 5 *February* 1956)

Abstract—Preliminary tests have demonstrated the valuable versatility of mercury evaporation as a technique for the study of mass transfer systems. The use of a sensitive ultra-violet absorptiometer for measuring the concentration of mercury vapour in gas streams enables studies to be made of systems with hydrodynamic control, the results agreeing with published correlations. The sensitivity of the detector allows measurements of transfer from very small surfaces, leading to surveys of positional effects. The choice of copper alloys as backgrounds for amalgamation gives great versatility in the study of transfer from any selected shape and also provides the possibility of introducing selected interfacial reaction kinetics into the process.

Résumé—Des essais préliminaires ont montré la souplesse qu'offre l'évaporation du mercure comme technique pour l'étude des phénomènes de transfert de masse. La mesure de la concentration du mercure dans la phase gazeuse par absorption dans l'ultra-violet permet l'étude des phénomènes contrôlés par l'écoulement gazeux : les résultats concordent avec les corrélations publiées. La sensibilité du détecteur permet des mesures de transfert à partir de surfaces extrêmement petites et donne une idée sur les effets de position. Le choix d'amalgames à base d'alliages de cuivre offre plus de possibilités dans l'étude des transferts à partir d'une forme géométrique choisie et permet ainsi d'introduire la cinétique des réactions interfaciales dans le phénomène d'échange.

The study of evaporation systems for the correlation of mass transfer coefficients is restricted when using liquids such as water by the difficulties of supplying liquid evenly to any specific shape of surface and supplying energy to maintain a system controlled by the resistances to the evaporation mechanism, and not by the energy transfer system from the fluid above or the material beneath the liquid. These restrictions can be avoided by the use of a liquid of low vapour pressure giving low evaporation rates requiring low energy transfer rates. Mercury surfaces appear to fulfil this requirement and to have the great advantage that the geometry of a desired system can be obtained readily in copper or brass and transformed to a mercury system by amalgamation. Once the clean mercury surface is formed it can be used for a short time without any significant change in the surface as evaporation proceeds. The work reported here consists of the initial tests to check the possible use of mercury transfer system and to assess their limitations. In using other low rate mass transfer systems, e.g. 2-naphthol into water, napthalene into air, the available shapes are limited and relatively fragile, but the main problem becomes the technique for measuring accurately very low concentrations of the transfer component in the moving fluid phase. With mercury in minute amounts in a gas stream the ultra-violet absorptiometer provides a powerful analytical tool. Instruments designed specially for the detection of mercury vapour in gas have hitherto been rare but the recent availability of the Hanovia apparatus has provided a ready and most sensitive method of analysis, which now makes it possible to use the mercury system to study many mass transfer problems and to exploit the ease of making an evaporative surface of any desired form. As the instrument is uncommon a brief comment on its operation and sensitivity has been included as an appendix.

*Present address : Levington Research Station, Levington, Nr. Ipwich, Suffolk.

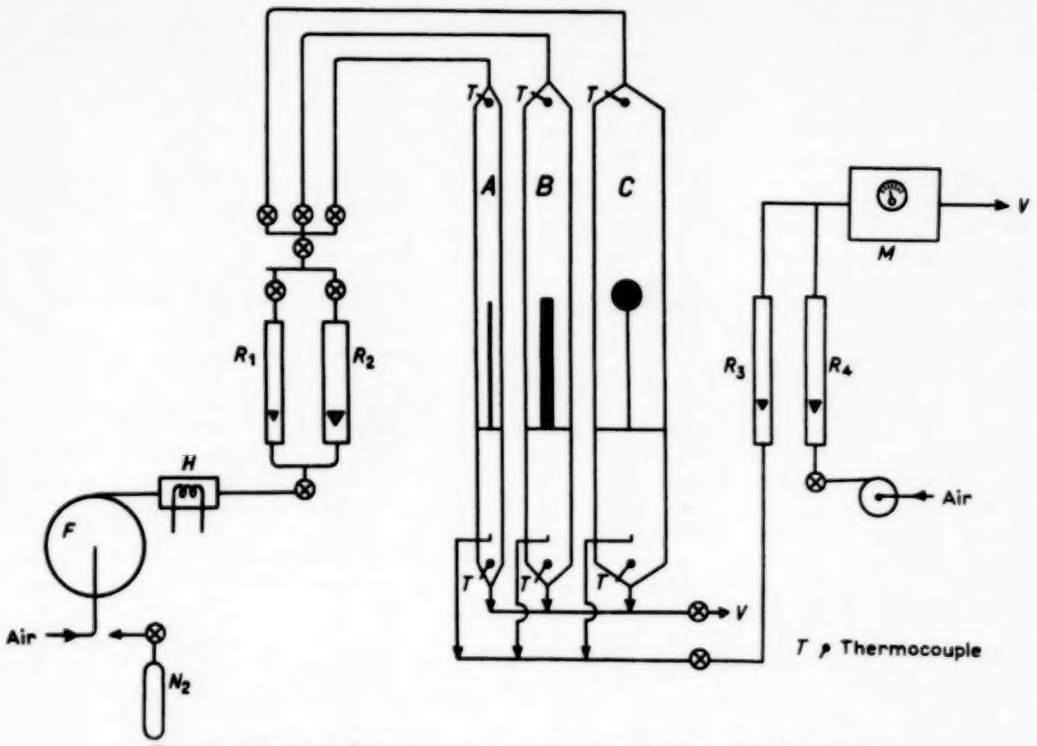

FIG. 1. Apparatus for mercury evaporation transfer from shaped surfaces.

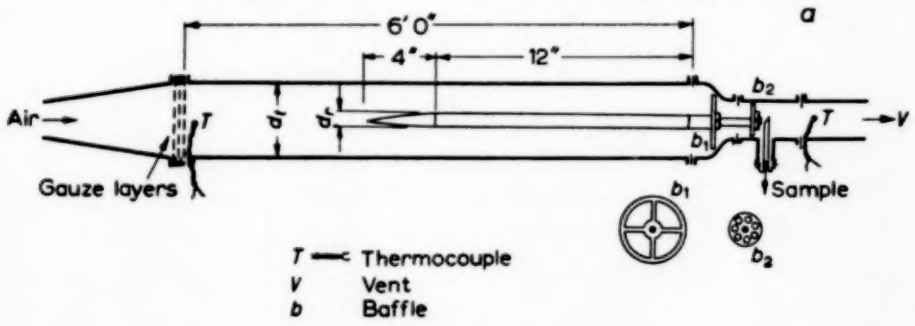

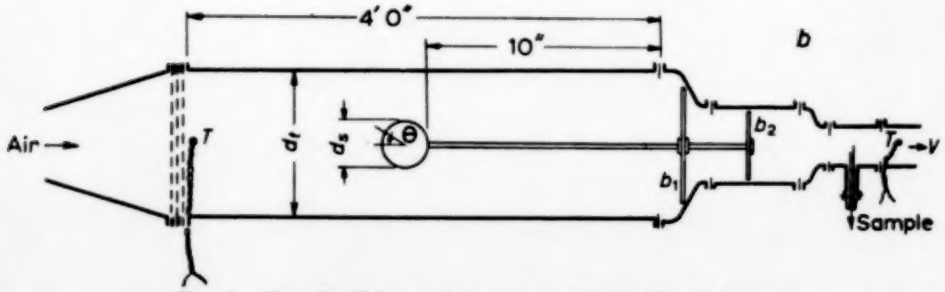

FIG. 2. Transfer Tubes and shapes. (a) Rods. (b) Spheres.

Apparatus

To enable tests to be made on transfer from rods and spheres a glass apparatus was constructed with the flow system shown in Fig. 1. Air or nitrogen was fed through a blower F, a Variac-controlled electric heater H, and a suitable rotameter R_1 or R_2 to one of the glass pipes of internal diameter A, 1 in.; B, 2 in.; C, 4 in. Mercury vapour evaporated from a surface within A, B, or C left the pipe with the gas stream. A continuous sample from this stream was passed through a rotameter R_3 and if necessary blended with fresh air from rotameter R_4 before flowing through the absorptiometer M for analysis. All exhaust gas containing mercury vapour from vents V was discharged outside the laboratory building. The major experimental adjustments consisted of controlling the input gas stream to pipe A, B, or C for both rate and temperature, and controlling the sample dilution ration with R_3 and R_4 when necessary to maintain the vapour concentration in the gas stream to the analyser within the desired range for accurate measurement. The sample rate through the analyser was always above the limit for avoiding oxidation of the mercury vapour in the analyser (see appendix).

Gas entering pipe A, B, or C passed through three screens of 30-mesh copper gauze to remove major swirls in the flow approaching the evaporative surface. With limited space available for the apparatus it was not possible to provide adequate calming sections. The major dimensions in Fig. 2 are given for the experiments discussed, as the disturbance in the fluid meeting the evaporative surfaces may have been significant. Brass rods were carried axially in the pipes by screwed extensions located by the perspex carrier baffles b_1 and b_2, the baffles being "sliding fits" in the appropriate glass pipe. The baffles were all perforated, b_1 cut away in quadrants to give the maximum opening and b_2 with holes near the axis to provide mixing of the outlet gas stream before it reached the sample withdrawal tube. By "painting" with mercury, any selected part of the rods or spheres could be tested for evaporation rate, allowing length effects and circumferential position effects to be studied, so long as the evaporative sections were kept a few diameters away from baffle b_1. Nonevaporative sections of the shapes were lacquered to prevent unwanted deposition of mercury during the preparation of the desired shape of surface and also during experiments from the gas stream on to copper surfaces downstream from the evaporative surface.

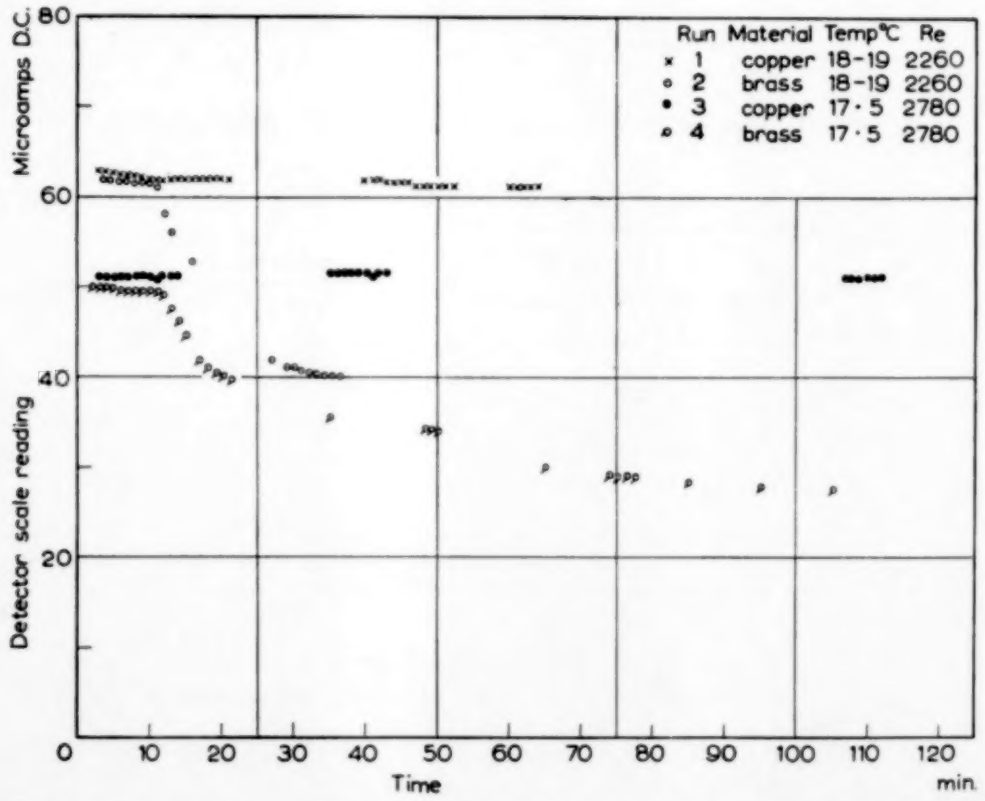

Fig. 3. Effect of time on mercury evaporation rate from copper and brass rods of 0·5 in. diameter in 1 in. diameter tube.

Experimental Results

The results were expressed in terms of mass transfer coefficients k based on the evaporative area and the logarithmic mean of the partial pressure difference $(p^* - p)$ along the axial length of the evaporative section. Correlations are given in terms of Sherwood numbers or Colburn j factors in conjunction with Reynolds and Schmidt numbers based on the physical properties of the carrier gas as the small mercury content of the stream had a negligible effect on these properties. The diffusion coefficient for mercury vapour into the gas stream was assumed to be the same as that for mercury into nitrogen [5]. The data were corrected for experimental conditions by the form

$$D = D_0 \left(\frac{T}{T_0}\right)^2 \frac{P_0}{P}.$$

The mercury surfaces were prepared on copper or brass backgrounds by rubbing mercury on to surfaces which had been cleaned in acid and allowed to stand in mercuric salt solution. The mercury surface was renewed for each short series of tests. The effect of time on the transfer rate is demonstrated by the variation of the outlet gas concentration in Fig. 3. The data for the copper base show a small fall in transfer rate with increasing time, the data being plotted as scale readings from the absorptiometer on the lower sensitivity range shown in the appendix. Only the copper shapes show this low rate of decrease over a period of hours. The data for brass bases of the same dimensions in Fig. 3 show a characteristic deviation from the ageing effect on copper. Brass bases show a slow initial fall, and agreement with the copper-base data,

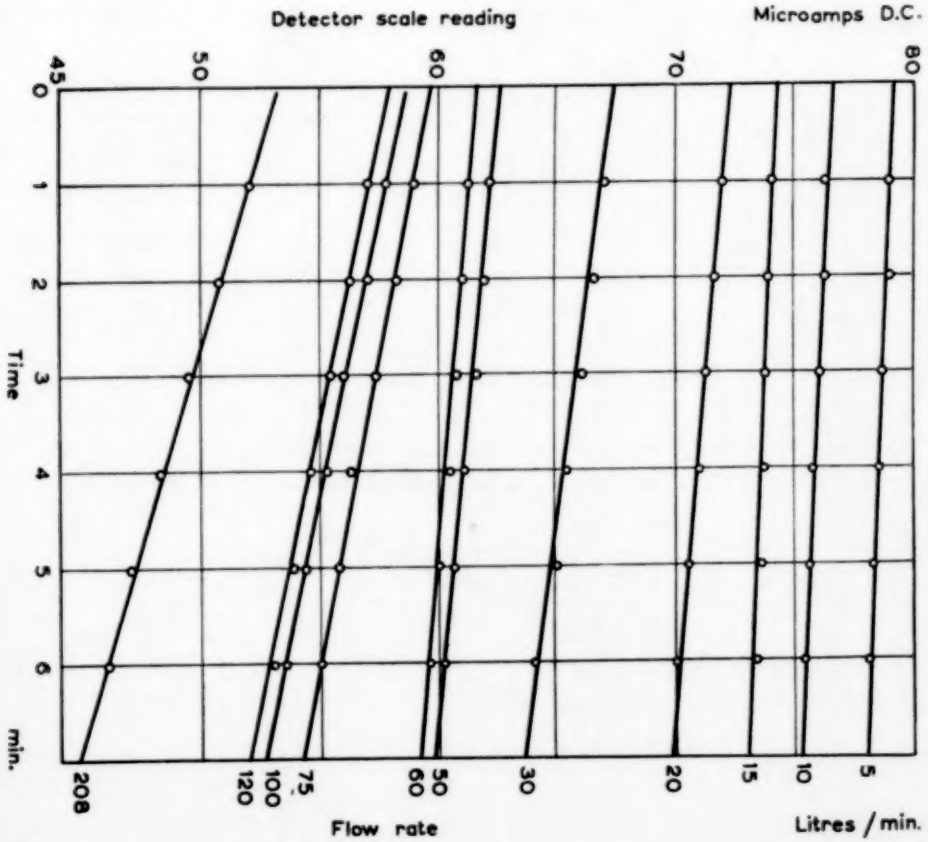

Fig. 4. Initial ageing lines for brass rods $\frac{1}{4}$ in. diameter in a tube 1 in. diameter with air between 14 and 17°C.

followed by an abrupt change to the exponentially decreasing form which appears to approach an asymptotic value after long evaporation periods.

From these initial studies, the evaporation process was clearly sensitive to flow, showed reproducibility between shapes of the same dimensions and also differences in ageing functions depending on the background metal. The last suggested that the mercury system could well provide a tool of wider scope than anticipated, with probably reaction kinetics systems available at the bounding surface. The sensitivity of the measuring apparatus and the consistency of measurement of small mercury concentrations also showed that the transfer system could be used on small transfer areas providing an unusual versatility for purposes of survey over surfaces. The tests now reported were undertaken primarily to check that the experimental apparatus could produce results comparable with accepted correlations from other systems and retain sensitivity to all major variables. Data from copper and brass surfaces were extrapolated to zero time from ageing plots, as in Fig. 4, comprising only the initial falling rate periods. They show below that as a good approximation the gas concentration at zero time may be taken as that corresponding to a nominal mercury surface, with the slow ageing effect to be considered as a minor modifying function.

Evaporation from spheres

With this assumption, that the zero time data were for a pure mercury surface, the mass transfer from spheres is exemplified by the data in Fig. 5 for the complete surface of a 1 in. diameter brass sphere in the pipe *C*. A satisfactory correlation is obtained using the physical characteristics of air, with reproducibility for two series of tests on separately prepared surfaces,

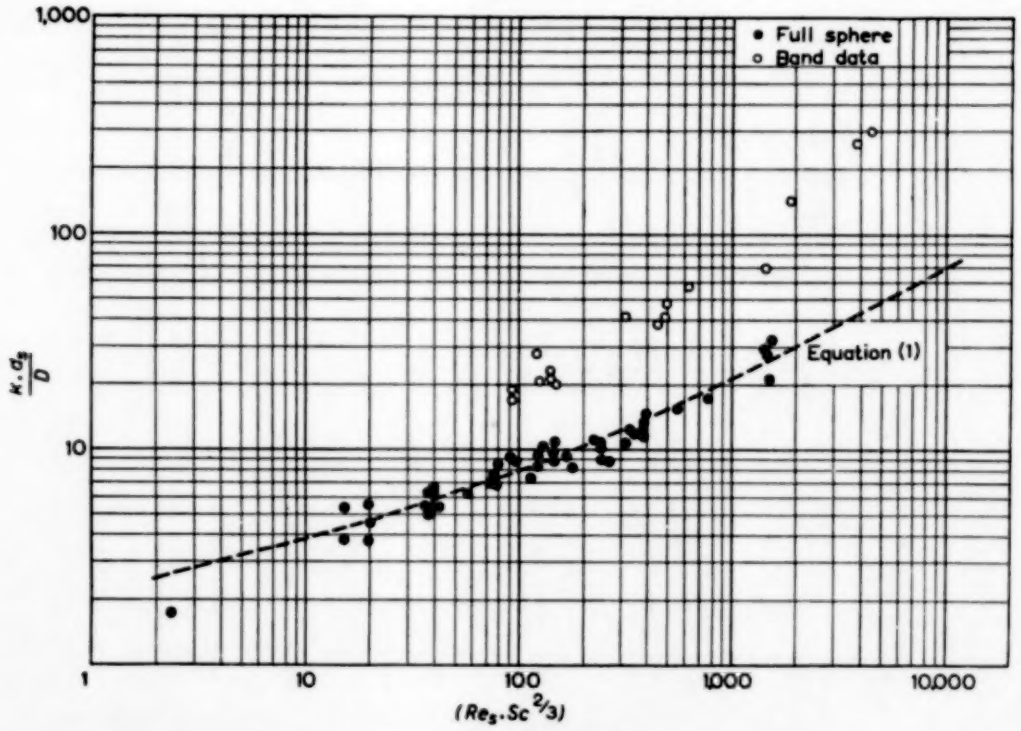

Fig. 5. Transfer from 1 in. diameter sphere in 4 in. diameter tube showing agreement with accepted correlations.

and agreeing with FROESSLING's equation for the evaporation of water, aniline, nitrobenzene, and naphthalene from spheres [6]:

$$\frac{k \cdot d_s}{D} = 2\left\{1 + 0{\cdot}276\left(\frac{V_a d_s \rho}{\mu}\right)^{\frac{1}{2}}\left(\frac{\mu}{\rho D}\right)^{\frac{1}{3}}\right\}. \quad (1)$$

This equation is confirmed by the data of other authors over the experimental range in the present work.

These data were for a spherical surface complete except for the relatively small disturbance caused by the holding rod behind the sphere. The influence of position on the sphere may be assessed by testing a band around the sphere at various positions along the tube axis. The data on Fig. 5 for a band from $\theta = 0$ to $\theta = 42°$ on the nose of the sphere (Fig. 2b) show that the apparatus is sensitive to the position effect despite the smallness of the transfer surface. The reproducibility with the small area is worse than with the complete sphere as must be expected, but the full sphere data compare very favourably with the bands of transfer data normally accepted as justifying correlations, such as the Froessling equation. The value of the technique is also shown in the large range of the abscissa, limited at the high rates by the blower used. The extreme sensitivity is exemplified by the point at the lowest abscissa included as a single test at the very low flow rate of 0·5 litre/min.

Evaporation from rods

The apparatus in Fig. 2a provided the j_m data in Fig. 6 showing agreement for different diameter ratios d_t/d_r with $j = f/2$ derived from the appropriate momentum transfer equation for laminar motion in an annulus [4]

$$f = 16\left(\frac{\mu}{V \cdot d_e \cdot \rho}\right) \cdot \phi\,(d_t/d_r), \quad (2)$$

$$\phi(d_t/d_r) = (d_t - d_r)^2 \Big/ \left[\frac{(d_t^2 - d_r^2)}{\log_e d_t/d_r} - (d_t^2 + d_r^2)\right],$$

and for turbulent flow in the annulus [1]

$$f = 0{\cdot}055\left(\frac{V \cdot d_e \cdot \rho}{\mu}\right)^{-0{\cdot}20}\left(\frac{d_t - d_r}{d_t}\right)^{0{\cdot}10}. \quad (3)$$

The equation (3) for j was found to require a modification in the diameter ratio parameter to correlate heat transfer data [8]

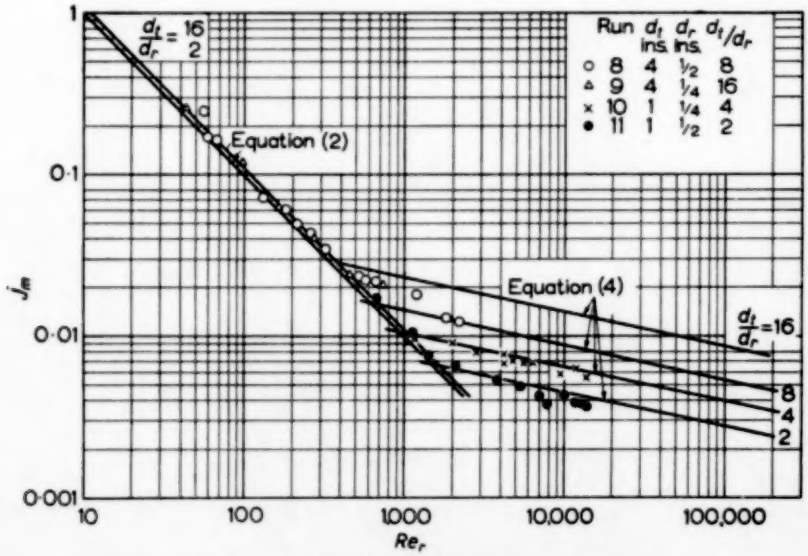

FIG. 6. Transfer to air flowing in annuli between rods and tubes of various diameters, showing effect of diameter ratio d_t/d_r.

$$j_h = 0{\cdot}20 \left(\frac{V \cdot d_e \cdot \rho}{\mu}\right)^{-0{\cdot}20} \cdot (d_t/d_r)^{0{\cdot}53} . \qquad (4)$$

The j lines for turbulent flow on Fig. 6 were based on equation (4). The difference between j values from equations (3) and (4) is significant for the diameter ratios in the present work. The data confirm the validity of equation (4) for relatively large d_t/d_r ratios. Fitting smoothing cones, of length equal to eight diameters of the rod, to the upstream face of the long cylinder (Fig. 2a) did not appear to affect the transfer coefficients significantly, though the flat end of the cylinders would be expected to show increased transfer by disturbing boundary layer formation, particularly in the laminar flow region. This effect is being studied further in tests on the distribution of local transfer coefficients along the length of the cylinders.

The j_m data agree very well with the narrow band of j for a wide range of d_t/d_r in laminar motion and also show the expected differences in the turbulent flow region, agreeing well with the appropriate equation (4).

Ageing effects on mercury surfaces

In Fig. 3 the outlet gas concentration at fixed flow rate show two periods of falling transfer rate. The first falling rate period appears with both copper and brass base surfaces and may reflect an oxidation reaction on the mercury surface giving progressive reduction in the

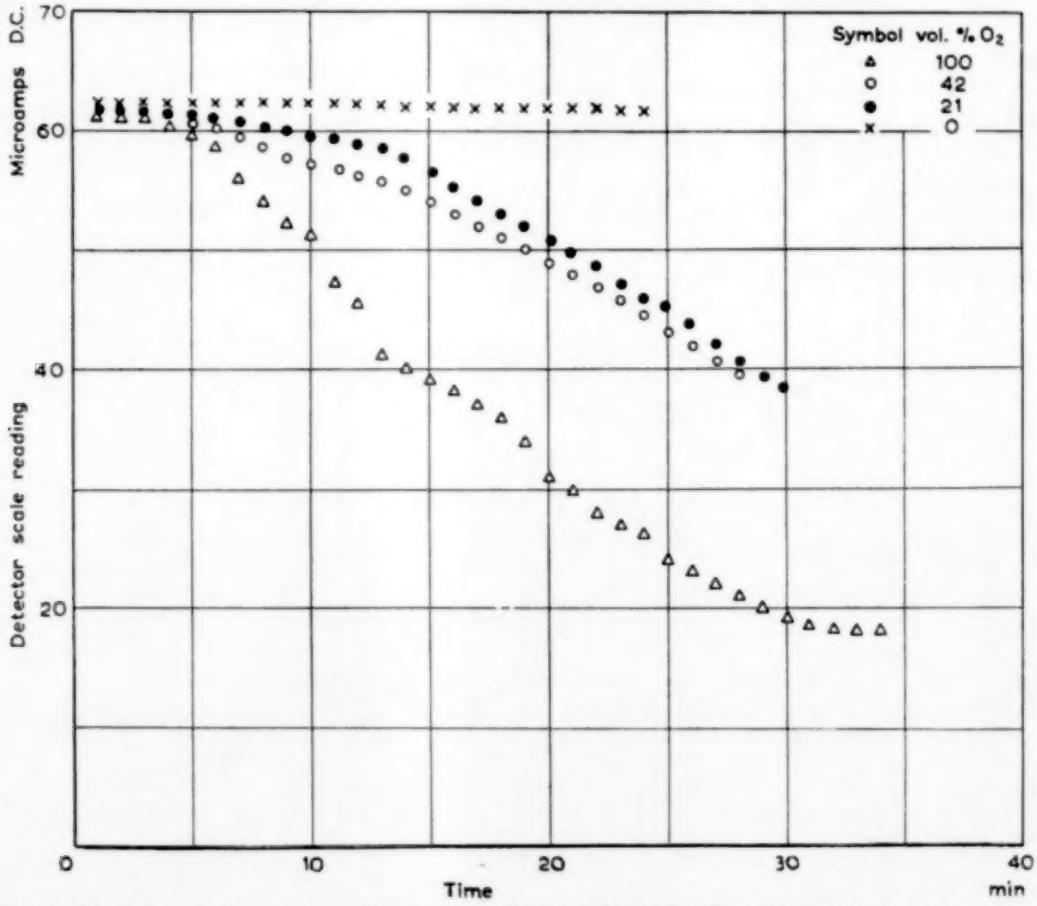

Fig. 7. The influence of oxygen concentration on ageing rates for an annulus of $d_t = 1$ in., $d_r = \frac{1}{4}$ in. with a constant gas rate of 50 litres/minute with $Re_r = 2220$.

evaporative surface. With a brass foundation this period is followed by a more rapid exponential function with an apparent asymptotic value for transfer rate after long periods which is only a small fraction of the initial rate. This period may be concerned with the diffusion of zinc from the brass base to the mercury-gas interface, there affecting the oxidation and transfer processes. It was observed that over the periods shown for the tests the mercury surfaces remained "mirror clean" and the apparatus is capable of sensing changes which are invisible. These processes are being studied in more detail but a preliminary comment is considered valuable in that the transfer system has obvious posibilities for studying overall transfer mechanisms involving moving phase dynamics and surface reactions, with modified surface reaction forms available by the choice of the amalgamation background. Should further studies of mercury condensation on metal collecting surfaces also prove successful, the mercury transfer system may provide an unusual versatility of great value.

The presence of oxidation reactions affecting

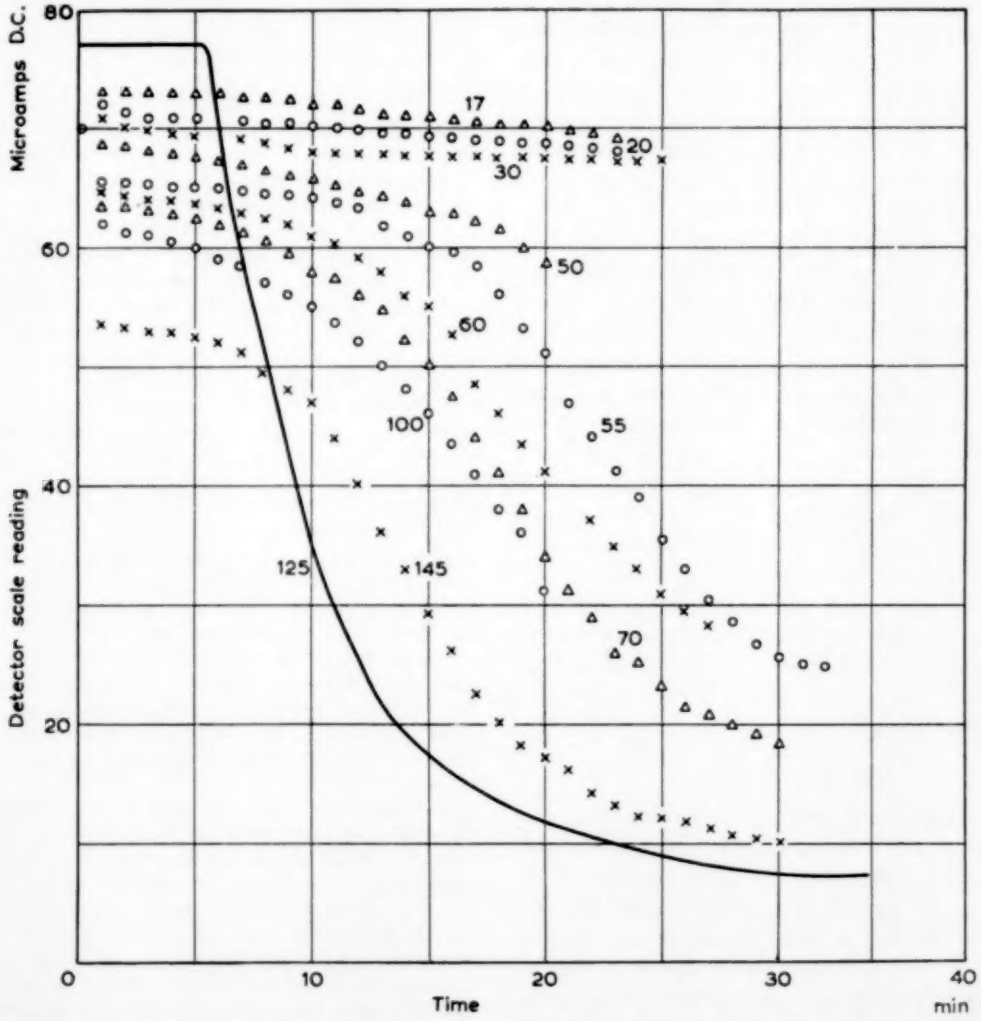

FIG. 8. Influence of air flow rate on ageing functions with annulus of $d_r = \frac{1}{4}$ in., $d_t = 1$ in., at 18°C with brass surface. Each curve is labelled with its constant flow rate in litres/min. the full line represents similar data at 36°C.

the ageing rate is demonstrated by the data on Fig. 7. For all gas mixtures at constant flow rate and temperature, the first falling rate period varies little though showing an ageing with oxygen which does not appear with cylinder nitrogen. The second period shows a much faster ageing which increases with increasing oxygen concentration. In these tests the enhanced oxygen concentrations were obtained from oxygen injection to the blower through a rotameter, the content being controlled by rates. For the pure oxygen and pure nitrogen data cylinder gases were fed directly to the heater *H*. The variation of apparent break-point with oxygen concentration may be merely fortuitous as the data have been pinned to an arbitrary zero of time for each test. The mercury film thickness may be a major variable controlling the incidence of the second falling rate period.

The dependence of the ageing functions on flow rate is shown in Fig. 8 which includes data for air flowing through an annulus at rates from 17 to 145 litre/min corresponding to Re_r from 760 to 6,450. The variable equivalent to transfer rate is given by the product of outlet concentration and flow rate, and further analyses of the effect are required, but the apparatus discriminates successfully. The curve for data at a higher temperature suggests the ability to provide analyses of the effect of this variable to assess its influence on the hydrodynamic and reaction mechanisms. The curves on Fig. 8 also show the need for a mechanism model which gives an inversion of curvature rather than an abrupt break-point separating the two falling rate periods. Further work on these problems is now proceeding.

Conclusions

The preliminary tests on the transfer of mercury vapour into gas streams have demonstrated that the system provides a valuable technique. By choosing the background metal for amalgamation and the gas for the fluid phase, it may provide a choice of control by hydrodynamic, surface reaction, or diffusion mechanisms. The hydrodynamic mechanism has been shown to agree closely with established correlations and the system can be used with ease to study the effect on local transfer coefficients of position on the selected surface shapes. The sensitivity of the detector apparatus is such that the survey of mass transfer on surfaces by amalgamation of a small test area appears more versatile than previous techniques and may provide a powerful tool for fundamental studies. The selective introduction of diffusion and surface reaction kinetics may extend the usefulness of the technique to reproduce a variety of processes occurring on any geometric form of surface, thus covering a very large number of problems.

Appendix

Calibration of mercury vapour detector

The study of the proposed transfer systems rests entirely on the use of an extremely sensitive detector for mercury vapour in a gas stream. The availability of a mercury vapour lamp as source of radiation of limited spectrum for the absorptiometer is a fortunate chance, and although the instrument can be used for measuring organic vapours in gas the high sensitivity to mercury is of major value. For stability the mercury vapour lamp must be supplied from a controlled stabilised voltage source and a balancing bridge circuit is required for measuring the output from the receiving photocell. The Hanovia instrument now incorporates both these features and although developed primarily for limit indication in toxicity surveys, its reproducibility, sensitivity and stability were exceptional for this type of absorptiometer. The instrument used in this work had two ranges of sensitivity. The calibration on the lower sensitivity range is shown in Fig. 9, the data showing the reproducibility after considerable use. Although the experiments discussed were concerned with evaporation from areas down to one square inch the lower sensitivity range was used throughout. The higher sensitivity would have given full scale deflection for a concentration of 100 microgram mercury per cubic metre of air, which could lead to more detailed surveys with either smaller areas or higher velocities than discussed above.

The use of such low vapour concentrations entails difficulty in calibration. The analysis of gas samples by chemical absorption methods was considered unsatisfactory and the calibration was based on the known function of vapour pressure of mercury with temperature [2]. It may be noted that the present calibration fell between two curves based on absorption of mercury in dithizone reagent which differed by a maximum of 30%. Air taken from outside the laboratory building passed through a saturating tube and was mixed with fresh air through calibrated rotameters before flowing through the absorptiometer. The calibration of the detector

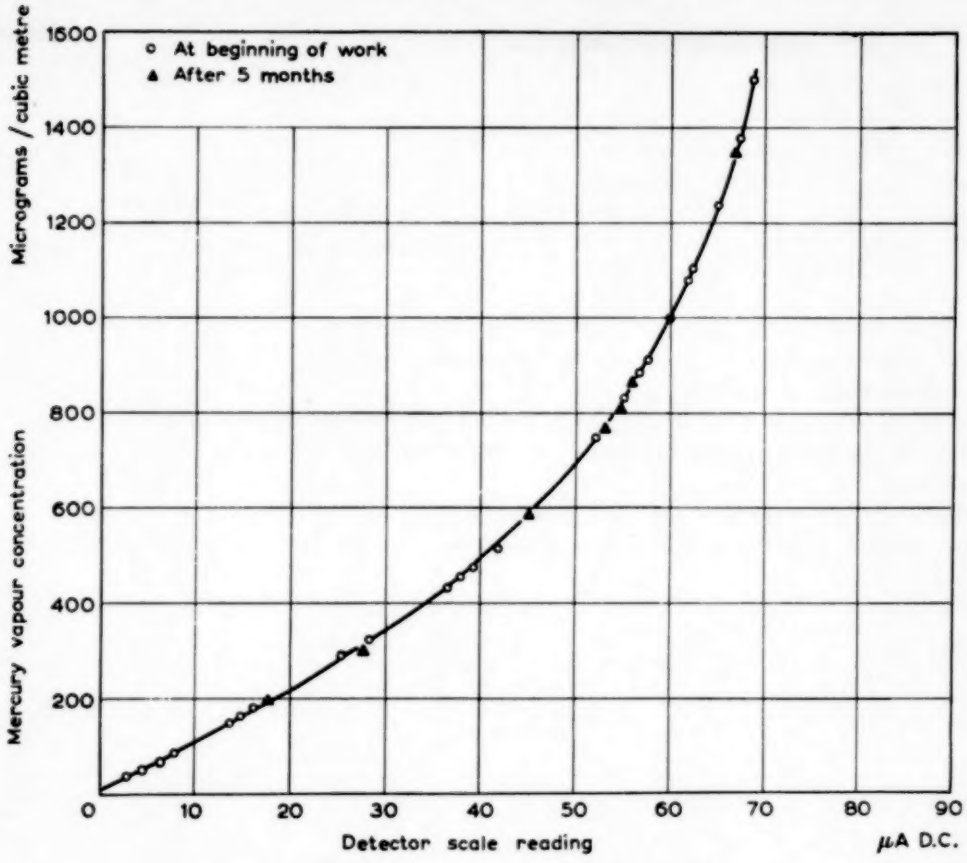

FIG. 9. Calibration curves for mercury vapour detector.

thus rested on the measured flow rates and presumed saturation of one stream. The saturation concentration was provided by using a glass column packed with rolled fine-mesh brass gauze with an amalgamated surface, an extra column being added occasionally to check that doubling or quadrupling the surface did not effect the concentration of the outlet gas within the sensitivity of the detector. A successful saturator for gas rates up to 2 litre/min comprised a column of 2 ft length and 3 in. diameter packed tightly with 30-mesh gauze, equivalent to about four times the minimum saturation column. The only limit on calibration and experimental flow rates through the absorptiometer is a minimum below which the mercury vapour is noticeably oxidized while within the ultra-violet absorption tube, the meter reading then depending on flow rate. In the present apparatus the limiting rate was 5 litre/min but an acceptable limit should be determined for any other detector as it clearly depends on residence time and hence on the geometry of the absorption tube.

Acknowledgements—The authors are indebted to Messrs. Hanovia Ltd., Slough, Bucks., England for assistance in the supply of the mercury vapour detector and also to Mr. G. S. OGDEN of the company's Manchester office for many useful discussions whilst assessing the potentialities of the instrument.

NOMENCLATURE

d = Diameter: sphere d_s; tube, internal d_i; rod, external d_r; annulus, effective $d_e = d_i - d_r$ (cm).

D = Diffusion coefficient: D_0 at standard pressure P_0 and temperature T_0 (cm^2/sec).

k = Evaporation transfer coefficient. [g/sec cm^2 (g/c.c.)].

p = Partial pressure of mercury vapour in gas; p^* in equilibrium with liquid mercury (atm.).

P = Total pressure (atm.).

T = Absolute temperature (°K).

V = Mean velocity in annulus (cm/sec).

V_a = Mean approach velocity for sphere (cm/sec).

ρ = Density of gas (g/c.c.).

μ = Viscosity of gas (g/cm sec).

Dimensionless groups

f = Friction factor.

j = Momentum transfer factor; $j = f/2$.

j_m = Mass transfer factor; $j_m = \frac{k}{V} \cdot (Sc)^{2/3}$.

Re = Reynolds number: sphere, $Re_s = \frac{V_a d_s \rho}{\mu}$; annulus, $Re_r = \frac{V d_e \rho}{\mu}$.

Sc = Schmidt number: $Sc = \mu\rho D$.

References

[1] Davis E. S. *Trans. Amer. Soc. Min. Met. Eng.* 1943 **65** 755.

[2] *International Critical Tables* 1928 **3** 206.

[3] Knudsen J. G. and Katz D. L. Fluid Dynamics and Heat Transfer. *Engineering Research Bulletin No.* 37. 1953 213. Engineering Research Institute, University of Mitchigan, U.S.A.

[4] *Ibid.* 132.

[5] Mullay J. M. and Jacques H. *Phil. Mag.* 1924 **48** 1105.

[6] Sherwood T. K. and Pigford J. L. *Absorption and Extraction*, p. 73. McGraw-Hill Co., New York, 1952.

Chemical Engineering Science, 1957, Vol. 6, pp. 215 to 226. Pergamon Press Ltd.

Diffusion in a ternary gas system with application to gas separation

J. J. KEYES, JR.* and R. L. PIGFORD
University of Delaware, Newark, Delaware, U.S.A.

Abstract—Measurements are reported of the separation effected by diffusion of a gaseous mixture of hydrogen and nitrogen through two organic vapours for the cases of (a) stagnant vapour and (b) countercurrent flow of the vapour relative to the hydrogen and nitrogen. Comparison of the data with classical diffusion theory is facilitated by the use of simple geometry in the diffusion zone, and by careful control of the experimental boundary conditions.

In general, the data agree well with theory based on a one-dimensional diffusion model, for both stagnant and flowing vapour. The role of countercurrent vapour flow in effecting large enrichments is particularly emphasized. For example, the measured separation factor for a hydrogen-nitrogen mixture was increased about thirty-fold when the mass flow of vapour was raised from zero to about three times the rate of feed flow.

The theoretical analysis is extended to determination of performance characteristics for a practical diffusion stage separating isotopes of low natural abundance of the light component.

Résumé—Il s'agit d'un compte-rendu de mesures de séparation effectuées par diffusion d'un mélange gazeux de H_2 et N_2 à travers deux vapeurs organiques dans deux cas :

(a) vapeur au repos.
(b) écoulement à contre-courant de la vapeur avec le mélange $N_2 - H_2$.

La comparaison des données avec la théorie classique de la diffusion et facilitée par l'usage de considérations géométriques simples dans la zone de diffusion et par un contrôle soigneux des conditions expérimentales aux limites.

En général, les données concordent bien avec la théorie basée sur le modèle unidimensionnel, à la fois pour la vapeur au repos et la vapeur en mouvement. Les auteurs ont particulièrement insisté sur le rôle de l'écoulement à contre-courant pour effectuer d'excellents enrichissements. Par exemple, le facteur de séparation mesuré pour un mélange H_2-N_2 est accru environ 30 fois pour une élévation du flux massique de la vapeur de 0 à 3 fois le taux d'alimentation.

L'analyse théorique est étendue à la détermination des caractéristiques de fonctionnement pour un étage pratique de diffusion comme de la séparation d'isotopes rares de composés légers.

INTRODUCTION

IT HAS been recognized [1, 2, 5, 8, 9] that partial separation of the components of a binary gas mixture can be effected by diffusion at constant total pressure through a third gas or vapour, provided there exists a difference in diffusivities of the components with respect to the vapour. The third component is commonly called the separating agent.

Past experimentation with this process, which has been referred to in the literature as " mass diffusion," " atmolysis," and " sweep diffusion," emphasized the performance characteristics of various practical stage configurations, in which the overall separation depended upon both the diffusive enrichment and concentration gradient effects normal to the direction of diffusion. This complicated comparison of the data with any theoretical treatment of multicomponent diffusion.

BENEDICT and BOAS [1] have published an excellent analysis of the mass diffusion process for two special cases :

(1) Isotopic mixtures for which the diffusivities with respect to separating agent of the components to be separated are nearly identical.
(2) Non-isotopic mixtures for which the mutual

* Present address : Union Carbide Nuclear Company, Oak Ridge, Tennessee, U.S.A.

diffusivitity of the components to be separated equals that of one of the components with respect to the separating agent.

Other methods for handling multicomponent diffusion calculations, such as those of COLBURN and DREW [3] and WILKE [12] are not sufficiently general to cover the important case of countercurrent flow of separating agent. Since the treatment of BENEDICT and BOAS is also somewhat limited in application, it was felt that, in addition to experimental measurements of the diffusive enrichment effect, a more general analysis of ternary diffusion would be useful. Comparison of experiment with theory for well defined diffuser geometry should, it was felt, provide a firmer basis for further application of mass diffusion.

Accordingly, experimental techniques and conditions were designed to reproduce as nearly as possible one-dimensional diffusion which occurs, for example, within a single " pore " of a mass diffusion partition, where the primary enrichment effect occurs. Two practical cases are treated :

(i) Diffusion of the binary mixture into a stagnant separating agent.

(ii) Diffusion of the mixture against the direction of flow of the separating agent. This situation, which might be termed " countercurrent gas extraction," results in greatly enhanced separation at the expense of throughput, a consequence of the effect of the counter-flow in selectively retarding diffusion of the heavy component, permitting the light one to progress against the flow. In previous work, this particular role of separating agent flow has not been adequately emphasized or evaluated.

The theoretical analysis with which the data are compared is derived from the classical theory of MAXWELL and STEFAN [10], as employed also by BENEDICT and BOAS. As will be evident, this simple approach is indeed adequate to describe one-dimensional diffusional separation.

The results will also have application to such problems as diffusion controlled catalytic reactions wherein one of the products must diffuse away from a surface in opposition to the inward diffusion of the reacting gases.

APPARATUS

Several requirements to be fulfilled by the apparatus were recognized :

(1) Steady flow of diffusing components had to be provided.

(2) Convective effects had to be minimized.

(3) Boundary conditions assumed in the mathematical derivations had to be accurately reproduced in the experimental procedure.

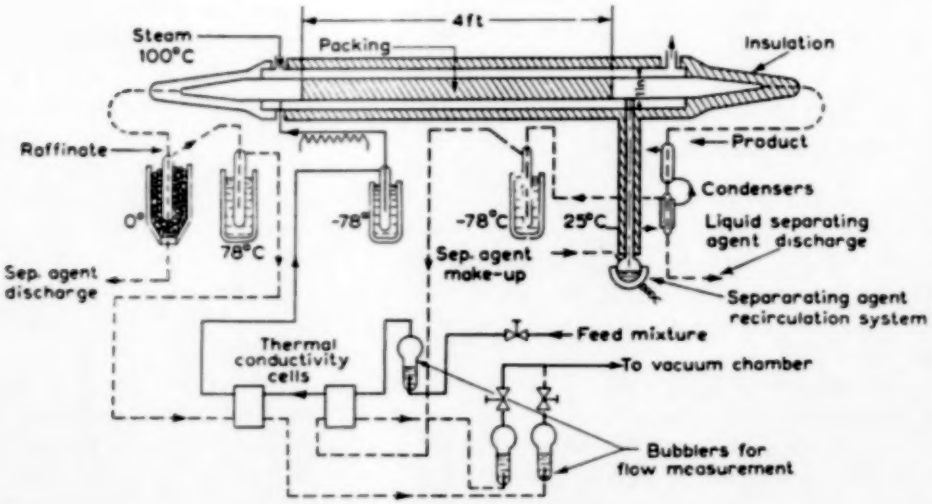

FIG. 1. Flow diagram.

Fig. 1 is the flow diagram. The diffuser consisted of a four-foot section of 1 in. copper tubing loosely packed with glass wool (97% free volume) this design having been found to minimize convection. The tube was jacketed for steam heating, and maintained at 100°C. Feed consisting of a binary gas mixture was admitted near one end of the diffuser at 100°C, 1 atm., where it was divided into two streams, the product diffusing toward the separating agent inlet, and the raffinate discharging close to the feed point. The separating agent, in this work a condensable vapour, was circulated at the product or discharge end of the diffuser by means of a reboiler-condenser combination indicated in Fig. 1. Because the rate of vapour circulation greatly exceeded the diffusion rate of the product stream, the concentration of the binary mixture at the point of product discharge was reduced essentially to zero. As will be seen, the assumption of negligible concentration of the diffusing mixture at the product end of the diffuser effects considerable simplification in the mathematical analysis, thus facilitating comparison with the data.

Product and raffinate streams were quantitatively freed of vapour by means of the condensers and cold traps indicated, and the residual binary mixtures were analysed by measuring their thermal conductivity relative to that of the feed mixture. Since the thermal conductivity cells gave vapour-free analyses, a method for determination of vapour concentration was developed. This involved sampling directly from the diffusion tube, condensing at constant volume, and applying the perfect gas law to compute the concentration of the third component from the changes in pressure and temperature.

Flows of all streams were controlled by means of micrometric needle valves operating as critical orifices. The extremely small gas rates involved in this work (about 100 std. cm^3 per hour) were measured by determining frequencies of bubble formation in a non-volatile oil.

All runs were made at essentially atmospheric pressure. Oil-pumped tank nitrogen and pure tank hydrogen gas were used as feed materials. The separating agents used were analytical reagent-grade organic vapours.

Experimental Procedure and Results

1. *Diffusion through stagnant separating agent* (*Table* 1, *Case I*)

No raffinate stream was removed; all of the feed gas diffused through the tube. This is equivalent to operation at total reflux, since no net material leaves the system. In addition, there is no net flow of separating agent. Of course continuous production of enriched mixtures is not possible, but there is a variation in composition of the feed mixture along the diffuser in order to maintain the proper diffusion rates of the two components. Fig. 2 illustrates this case. It is desired to compare measured and calculated compositions, utilizing the theory outlined in the Appendix and summarized in Table 1.

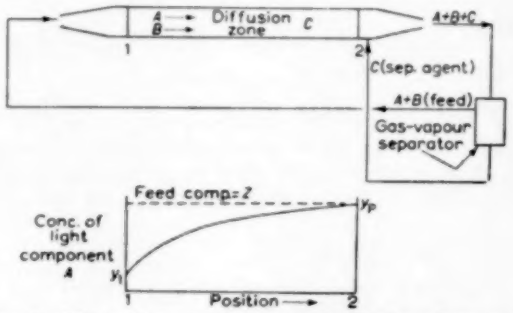

Fig. 2. Illustration of operation with diffusion of gases *A* and *B* through stagnant vapour *C*.

The composition ratio between the ends of the diffuser is conveniently expressed in terms of the separation factor.

$$\alpha = \frac{y_P\,(1 - y_1)}{y_1\,(1 - y_P)}$$

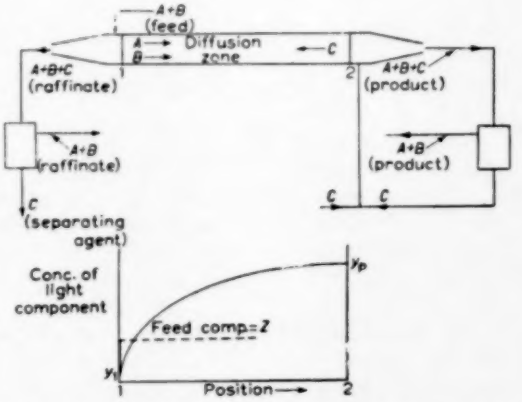

Fig. 3. Illustration of operation with countercurrent diffusion of gases *A* and *B* through vapour *C*.

where y_P is the vapour-free mole fraction of light component in the product stream (this is also equal to the feed composition, z, as is apparent from material balance considerations), and y_1 is its mole fraction at the inlet, just inside the feed point, on a vapour-free basis. Fig. 4 compares a few of the measured and calculated separation factors. The feed mixture was 45% hydrogen, 55% nitrogen ($z = 0{\cdot}45$). Measured and calculated vapour compositions are compared in Fig. 5.

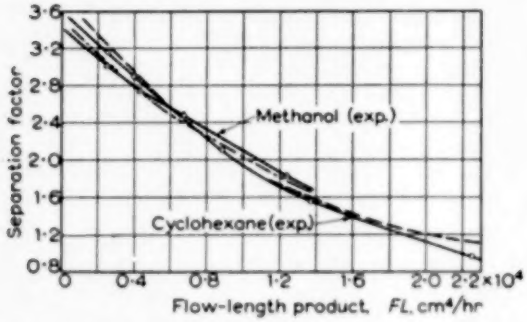

FIG. 4. Comparison of observed and calculated separation factors for diffusion of hydrogen-nitrogen mixture through stagnant vapours. $q = 0$ (stagnant separation agent); $z = 45\%$ H_2; ——— calculated for *cyclo*hexane; — — — calculated for methanol.

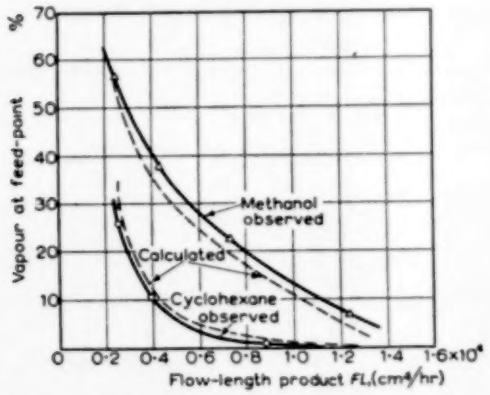

FIG. 5. Comparison of observed and calculated vapour compositions for diffusion of hydrogen-nitrogen mixture through stagnant vapours. $q = 0$ (stagnant separation agent); $z = 45\%$ H_2.

2. *Countercurrent flow of separating agent (Table 1, Case IIa, III and IV)*

If flow of separating agent is maintained opposite to the direction of diffusion of the feed mixture, the heavier component is selectively retarded, and the separation factor is increased above the value for stagnant separating agent (Case I). For this case, a fraction of the feed is discharged as raffinate stream, the remainder diffusing through the tube; see Fig. 3. The separation factor is:

$$\alpha = \frac{y_P\,(1 - y_1)}{y_1\,(1 - y_P)}$$

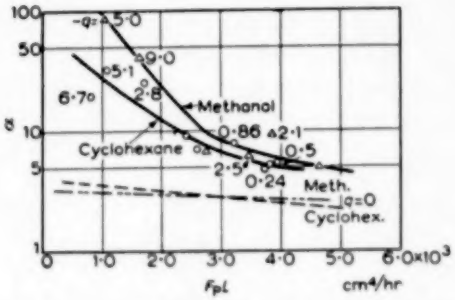

FIG. 6. Measured separation factors for diffusion of hydrogen-nitrogen mixture through flowing vapours (countercurrent). $q < 0$ (countercurrent flow); $z = 45\%$ H_2.

The data for 45% hydrogen, 55% nitrogen as feed mixture are summarized in Figs. 6 to 8. Theoretical points obtained from the parent relationship given in Table 1 are also plotted in Fig. 7. Runs were continued for a time (about 16 hours) sufficient to establish composition equilibrium in product and raffinate streams. Material balances closed to within 5-10%.

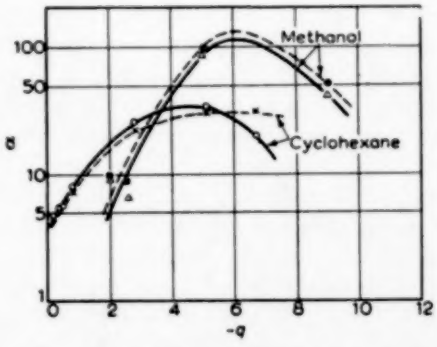

FIG. 7. Comparison of measured and calculated separation factors for diffusion of hydrogen-nitrogen mixture through flowing vapours (countercurrent). $q < 0$ (countercurrent flow), $z = 45\%$ H_2; ● calculated for methanol; × calculated for *cyclo*hexane; △ observed for methanol; ○ observed for *cyclo*hexane.

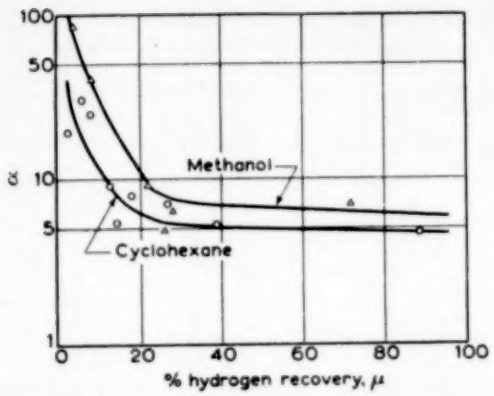

FIG. 8. Variation of separation factor with hydrogen recovery; countercurrent flow of separating agent. $q < 0$; $z = 45\%$.

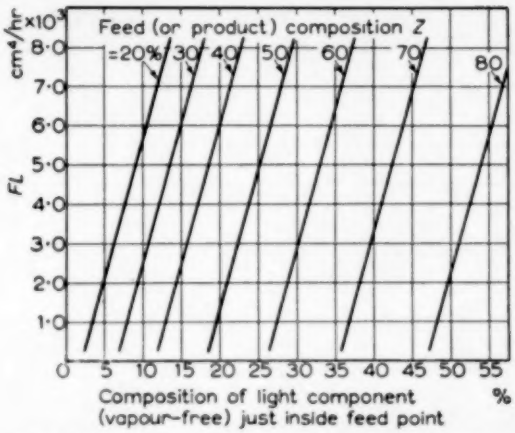

FIG. 9. Calculated product compositions for diffusion of hydrogen-nitrogen mixture through stagnant carbon-tetrachloride vapour.

SUMMARY OF THEORY

Solution of the MAXWELL-STEFAN [10] differential equations to obtain the steady-state composition variation along the diffuser is outlined in Appendix 1. Simplification of the general solution, equations (*d*), is effected by assuming negligible concentration of the components to be separated at the product end of the diffuser, a condition which was fulfilled also in the experimental work. Table 1 is a summary of solutions for the separation factor α including some detailed special cases of interest. The influence of the important parameter q, defined as the ratio of mass velocities of separating agent and of light component, N_C/N_A, will be emphasized in the discussion to follow.

Case I is applicable to the first phase of the experimental program, for which $q = 0$. α is seen to depend upon the binary feed composition, z, the three binary diffusivities, D_{AB} etc., the mass velocity of light component, N_A, the diffusion path length, L, total pressure p, and temperature, T. For the special case *I* (*a*), where components *A* and *B* approach infinite dilution in separating agent, *C*, the expression for α simplifies to a ratio of diffusivities, D_{AC}/D_{BC}. Fig. 9 illustrates the relationship between inlet and discharge concentration for the system hydrogen, nitrogen, carbontetrachloride.

The influence of separating agent flow, $q \neq 0$ is given by *Case II* when components *A* and *B* approach infinite dilution in the separating agent. Specifically, as countercurrent flow of the latter becomes very great, $q \gg 0$, the separation factor is seen to increase exponentially with the product $qN_AL = N_CL$, when $r_{BC} > r_{AC}$.

Cases III and *IV* are discussed under "Analytical Treatment for Special Cases," p. 222.

DISCUSSION OF EXPERIMENTAL RESULTS AND COMPARISON WITH THEORY

Phase A : $q = N_c = 0$

It is desired to compare the measured separation factors with values obtained from equation (2), Table 1. Observe that the tube length, L, and molar rate, N_A, appear together as a product. Converting molar rate to volumetric rate :

$$N_A L = 0{\cdot}232 \times 10^{-8}\, y_2\, FL$$

where F is the vapour-free flow rate in cm³/hr at 1 atm. and 20°C, y_2 is the vapour-free product composition. By retaining the flow-length product, extrapolation to other lengths and flow rates is facilitated.

The data for *cyclo*hexane and methanol as separating agents together with calculated curves equation (2), are plotted in Fig. 4. Note good agreement with theory over the range studied. Average deviation of the measured from the calculated separation factors is 3·2% for *cyclo*hexane and 1·5% for methanol.

Table 1. *Summary of theoretical relationships for the local separation factor,* α

Special cases of equations (d), APPENDIX 1, assuming negligible concentration of the components to be separated at the product end of the diffuser.

Note – *A*, *B* and *C* refer to light component, heavy component, and separating agent respectively.

PARENT RELATIONSHIP

$$\alpha = \frac{1}{n\phi}\left[\frac{\dfrac{(\theta - m_1 - n\phi)(\theta - m_2)}{\exp(m_2 N_A L)} - \dfrac{(\theta - m_2 - n\phi)(\theta - m_1)}{\exp(m_1 N_A L)} + n\phi\,\Delta m}{\dfrac{\theta - m_1 - n\phi}{\exp(m_2 N_A L)} - \dfrac{\theta - m_2 - n\phi}{\exp(m_1 N_A L)} + \Delta m}\right] \tag{1}$$

Case I. $q = N_C/N_A = 0$ (no net transport of separating agent).

$$\alpha = \frac{z}{1-z}\left\{\frac{\dfrac{z(z-1)(1-R_1)}{[z + r_1(1-z)]\exp(K_{AB}L)} + \dfrac{(z-1)R_1}{[z + R_1(1-z)]\exp(K_{ABC}L)} + \dfrac{z}{1+z}}{\dfrac{z(1-z)(1-R_1)}{[z + R_1(1-z)]\exp(K_{AB}L)} - \dfrac{z}{[z + R_1(1-z)]\exp(K_{ABC}L)} + z}\right\} \tag{2}$$

$$y_{C_1} = \exp(-K_{ABC}L) \tag{2a}$$

Note that implicit solutions for N_A and N_B in terms of compositions for the case $q = 0$ have been obtained by E. R. GILLILAND, as reported by SHERWOOD [10].

Case I (a). $y_{A_1}, y_{B_1} \to 0$ (Components *A* and *B* approach infinite dilution in separating agent).

$$\alpha_0 = \frac{D_{AC}}{D_{BC}} \tag{3}$$

Case II. $q = N_C/N_A \neq 0$; $y_{A_1}, y_{B_1} \to 0$ (Components *A* and *B* approach infinite dilution in separating agent).

$$\alpha = \frac{1 - \exp(-q\,r_{BC}N_A L)}{1 - \exp(-q\,r_{AC}N_A L)} \tag{4}$$

Case II (a). $q \to -\infty$ (Countercurrent flow of separating agent).

$$\alpha = \exp[-q(r_{BC} - r_{AC})N_A L] \tag{5}$$

Case II (b). $q \to \infty$ (Co-current flow of separating agent).

$$\alpha = 1 \tag{6}$$

Case III. $q = N_C/N_A < -1$; $n = N_B/N_A \ll 1$; $r_{AC} \neq r_{AB}$ (Dilute mixture of component *B* in component *A* on a separating agent-free basis).

$$\alpha = \frac{1 - \exp(-m_1 N_A L)}{1 - \exp(-m_2 N_A L)} \tag{7}$$

where $m_1 = r_{AB} + q\,r_{BC}$

$m_2 = r_{AC}(q+1)$

Case III (a). $m_1 N_A L$ and $m_2 N_A L$ are large quantities:

$$\alpha = \exp(\Delta m\, N_A L) \tag{8}$$

$$\Delta m = m_1 - m_2 > 0$$

Case IV. $q' = N_C/N_B < -1$; $n' = N_A/N_B \ll 1$. (Dilute mixture of component *A* in component *B* on a separating agent-free basis).

$$\alpha = \frac{1 - \exp(-m_2 N_B L)}{1 - \dfrac{1}{\phi + q'\Delta}\left[\dfrac{\phi}{\exp(m_2 N_B L)} + \dfrac{(q'+1)}{\exp(m_1 N_B L)}\right]} \tag{9}$$

$$y_{B_1} = \frac{1 - \exp(-m_2 N_B L)}{q' + 1} \tag{10}$$

Case IV (a). $m_1 N_B L$ and $m_2 N_B L$ are large quantities:

$$\alpha = \exp(\Delta m\, N_B L) \tag{11}$$

$$\Delta m = m_1 - m_2 > 0$$

The calculated values referred to are based upon three binary diffusion coefficients, D_{AB}, D_{AC}, and D_{BC}. From an average of values predicted by the semi-empirical method of GILLILAND [4], and that of HIRSCHFELDER *et al.* [6], together with some experimental data, a value of $D_{AB} = 1{\cdot}02\ \text{cm}^2/\text{sec}$ at 100°C, 1 atm. was chosen for the calculations :

$$r_{AB} = \frac{RT}{p\,D_{AB}} = 3{\cdot}0 \times 10^4\ (\text{cm})\ (\text{sec})/\text{g mole}$$

Diffusivities of hydrogen and of nitrogen through separating agent, D_{AC} and D_{BC} respectively, are calculated from the GILLILAND equation.

Calculated diffusivities and diffusional resistances of H_2 and N_2 in separating agents at 100°C, 1 atm.

*Cyclo*hexane	$D_{AC} = 0{\cdot}392$ cm²/sec $r_{AC} = 7{\cdot}82 \times 10^4$ (cm/sec)/g mole	$D_{BC} = 0{\cdot}100$ cm²/sec $r_{BC} = 30{\cdot}8 \times 10^4$
Methanol	$D_{AC} = 0{\cdot}681$ cm²/sec $r_{AC} = 4{\cdot}49 \times 10^4$	$D_{BC} = 0{\cdot}193$ cm²/sec $r_{BC} = 15{\cdot}9 \times 10^4$

Extrapolating the curves of Fig. 4 to $FL = 0$, the limiting separation factors at infinite dilution are :

Methanol : $\alpha_0 = 3{\cdot}45$
*Cyclo*hexane : $\alpha_0 = 3{\cdot}62$

From equation (3), Table 1, the calculated values are :

$$\text{Methanol} : \alpha_0 = \frac{D_{AC}}{D_{BC}} = 3{\cdot}53$$

$$\textit{Cyclo}\text{hexane} : \alpha_0 = \frac{D_{AC}}{D_{BC}} = 3{\cdot}92$$

A further test of the theory is a comparison of the observed vapour compositions at the inlet end of the diffuser with corresponding values predicted by equation 2 (a). Good agreement as shown in Fig. 5 is evidence of the effectiveness of the glass wool packing in eliminating mass convective mixing.

Phase B : Countercurrent flow of separating agent : $q < 0$.

For this case a fraction, h, of the feed gas is made to diffuse through the tube. In addition, the separating agent is made to flow counter to the direction of diffusion of the components of the feed mixture. It is the effect of this flow of separating agent that is to be emphasized in the following discussion.

Let the volumetric flow rates (20°C and 1 atm.) of the product, feed, and raffinate streams be designated by appropriate subscripts : F_P, F_F, F_R. For convenience, the flow-length product, F_PL, is retained. It is desired to investigate the effects of F_PL, of the separating agent/product ratio of q, and of the per cent recovery $\mu\ (= 100y_2\,h)/z$ on α.

The data for 45% H_2 – 55% N_2 feed mixture diffusing through methanol and *cyclo*hexane as separating agents are plotted in Figs. 6 to 8. From Fig. 6, it is evident that large enrichments can be attained by increasing the ratio of separating agent to product flow, $-q$. This increase is achieved at the expense of reduced throughput, however. The values of $-q$ that existed in the various experiments are listed beside the plotted points. For comparison, the lower, dashed, curves for $q = 0$ are replotted from Fig. 4.

The effect of countercurrent carrier flow is also demonstrated in Fig. 7, in which α is plotted against $-q$ directly, and the data compared with equation (1). The experimental points scatter, with maximum deviation of the measured from the calculated α of 25%. The averages are :

*Cyclo*hexane		Methanol
Average deviation of α :	1·0%	9·0%
Variance of α :	16·0%	15·0%

In view of the uncertainties in measurement, these deviations do not seem excessive, and point to a general corroboration of the theory.

At large values of $-q$, α is seen to fall off slightly. This is a consequence of the increase

in flow of the diffusing components which resulted from the experimental method of maintaining flow. The calculated curve takes this increase in rate into account.

Fig. 8 illustrates the rapid decrease in hydrogen recovery, μ, with increasing α, as is to be expected.

General conclusions :

(1) Large separation factors are associated with low product flow rate, small percentage recovery, and high separating agent-to-product flow ratio, although the correspondence is complicated by interdependence of the variables.

(2) Comparison of the data with theoretical calculations for countercurrent flow is within limits of experimental error. It is felt that this agreement, together with agreement for stagnant separating agent conditions constitute verification of the theoretical approach.

ANALYTICAL TREATMENT FOR SPECIAL CASES

Substantial simplification of the parent relationship is possible when one component of the feed mixture is present in small proportions. *Case III*, Table 1, is applicable when the heavy component, B, is dilute. To give some idea of the validity of this simplified relationship, a number of calculations of α was made for a range of values of n, q, and N_A, and the results compared with the accurate equation (1). It was concluded that a lower limit of $-q$ of 2 should not be exceeded for the error to be less than 30%, with n as great as 0·1 (10% of the heavy component).

Fig. 10, which is a graph of equation (7), illustrates the increase in α effected by (1) increasing the ratio, $-q$, of vapour to light component, at constant F_PL or (2) increasing F_PL at constant $-q$.

When the light component, A, is dilute, *Case IV*, Table 1, is applicable. Use is made of this relationship in Appendix 2 to derive an integrated expression for the performance of a large collection of parallel diffusion "pores," as would be employed, for example, in a mass diffusion stage of the type described by MAIER [8] and BENEDICT [1].

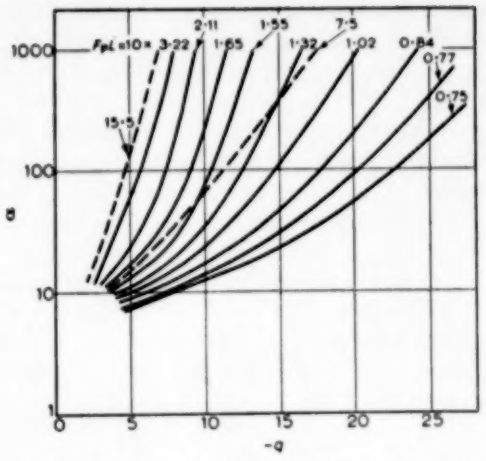

FIG. 10. Calculated separation factors for diffusion against methanol or *cyclo*hexane vapour-feed of a dilute mixture of nitrogen in hydrogen. ——— methanol ; — — — *cyclo*hexane ($n < 0·1$).

SUMMARY

Experimental measurements of diffusion rates and composition gradients in a long tube diffuser lend support to the three-component diffusion equations obtained here from the MAXWELL-STEFAN differential equations. Application to gas separation by extraction of the heavy component with counter flowing vapour emphasizes the role of the latter in effecting relatively large composition changes in a single pass.

APPENDIX 1

Theory of steady-state diffusion in a ternary gas mixture

The generalized MAXWELL-STEFAN equations (10) are assumed to apply :

$$-\frac{dp_i}{dx} = \frac{p_i}{p}\sum\frac{p_i}{D_{ij}}(u_j - u_i) \qquad \text{(a)}^*$$

where p_i and u_i are the partial pressure and diffusion velocity with respect to a space-fixed co-ordinate system of component i, x is the position coordinate in the direction of the u_i, D_{ij} the ordinary diffusion coefficient of i and j, and p the total pressure. It is to be noted that viscous effects and thermal diffusion are neglected, and that the

* It has been pointed out that equation (a) is a special case of a general relationship derived by CURTISS and HIRSCHFELDER [7] by assuming : 1 No thermal diffusion ; 2. No pressure diffusion ; 3. No forced diffusion ; 4. Constant temperature and pressure.

total pressure is constant. Furthermore, $D_{ij}\,(=D_{ji})$ is assumed constant, independent of concentration, and is further assumed to be equal to the value for binary diffusion, as a first approximation.

Following the nomenclature of SHERWOOD [10], let $N_i \frac{(\text{g}-\text{mole})}{(\text{sec})\,(\text{cm}^2)} = \frac{p_i u_i}{RT}$; $r_{ij} = \frac{RT}{p\,D_{ij}}$, a kind of diffusional resistance. Hence

$$-\frac{dpj}{dx} = r_{ij} \sum (N_j p_i - N_i p_j) \qquad \text{(b)}$$

Here the N_i are all constant for the steady state.

When equations (b) are solved simultaneously, the following pair of equations is obtained for the case of three components, A, B, and C:

$$\begin{aligned} d^2 p_A/dx^2 + K_1\, dp_A/dx + K_2\, p_A &= K_{3A} \\ d^2 p_B/dx^2 + K_1\, dp_B/dx + K_2\, p_A &= K_{3B} \end{aligned} \qquad \text{(c)}$$

where the K's are functions of the r_{ij}'s and N_i's and are independent of x.

Consider simultaneous diffusion of components A, B, and C in a tube of length L, the cross-section and mass fluid velocity being taken sufficiently small that composition differences perpendicular to the direction of diffusion are negligible. The solution for this case will be referred to as the point or local diffusion equations. Suppose as boundary conditions that known compositions of A and B (y_{A_1}, y_{B_1}) be maintained at the discharge end of the diffuser, $x = L$. It is convenient to introduce the flow ratios:

$$n = N_B/N_A, \quad q = N_A/N_C$$

Solving equations (c) by the usual method for differential equations with constant coefficients, noting that $y_A = y_{A_1}$, $y_B = y_{B_1}$ at $x = 0$:

$$\left.\begin{aligned} y_{A_1} &= \frac{y_{A_1}(\theta - m_2) - y_{B_1}\phi - \dfrac{(\theta - m_2 - n\phi)}{n+q+1}}{\Delta m \exp(m_1 N_A L)} \\ &\quad - \frac{y_{A_1}(\theta - m_1) - y_{B_1}\phi - \dfrac{(\theta - m_1 - n\phi)}{n+q+1}}{\Delta m \exp(m_2 N_A L)} \\ &\quad + \frac{1}{n+q+1} \\ y_{B_1} &= \frac{(\theta - m_1)\left[y_{A_1}(\theta - m_2) - y_{B_1}\phi - \dfrac{\theta - m_2 - n\phi}{n+q+1}\right]}{\phi\,\Delta m \exp(m_1 N_A L)} \\ &\quad - \frac{(\theta - m_2)\left[y_{A_1}(\theta - m_1) - y_{B_1}\phi - \dfrac{\theta - m_1 - n\phi}{n+q+1}\right]}{\phi\,\Delta m \exp(m_2 N_A L)} \\ &\quad + \frac{n}{n+q+1} \end{aligned}\right\} \qquad \text{(d)}$$

Where:

$$m_1, m_2 = (-K_1 \pm \sqrt{K_1^2 - 4K_2})/2N_A;\ \Delta m = m_1 - m_2$$

$$-K_1/N_A = (n+1)\,r_{AB} + (q+1)\,r_{AC} + (n+q)\,r_{BC}$$

$$K_2/N_A^2 = (n+q+1)\left[r_{AB}r_{BC} + n\,r_{AB}r_{BC} + q\,r_{AC}r_{BC}\right]$$

$$\theta = (q+1)\,r_{AC} + n\,r_{AB};\ \phi = r_{AB} - r_{AC}$$

Equations (d) are the steady-state solution of MAXWELL's ternary equations corresponding to the boundary conditions given, and solved for the upstream compositions.

Special Cases

In order to render the solution more workable, y_{A_1} and y_{B_1} will be set equal to zero, a case frequently encountered where two components are removed at a boundary by reaction, rapid dilution, etc. For this case,

$$\left.\begin{aligned} y_{A_1} &= \frac{1}{n+q+1}\left[\frac{\theta - m_1 - n\phi}{\Delta m \exp(m_2 N_A L)} - \frac{\theta - m_2 - n\phi}{\Delta m \exp(m_1 N_A L)} + 1\right] \\ y_{B_1} &= \frac{1}{n+q+1}\left\{\frac{1}{\phi\,\Delta m}\left[\frac{(\theta - m_1 - n\phi)(\theta - m_2)}{\exp(m_2 N_A L)} - \frac{(\theta - m_2 - n\phi)(\theta - m_1)}{\exp(m_1 N_A L)}\right] + n\right\} \end{aligned}\right\} \qquad \text{(e)}$$

Since, in most applications involving material transfer, it is desired to know the relative concentration change between two boundaries, the "separation factor," α, is introduced:

$$\alpha = \frac{y_{A_2}/y_{B_2}}{y_{A_1}/y_{B_1}} = \frac{1}{n}\frac{y_{B_1}}{y_{A_1}}.$$

Hence, from equations (e)

$$\alpha = \frac{1}{n\phi}\left[\frac{\dfrac{(\theta - m_1 - n\theta)(\theta - m_2)}{\exp(m_2 N_A L)} - \dfrac{(\theta - m_2 - n\phi)(\theta - m_1)}{\exp(m_1 N_A L)} + n\phi\,\Delta m}{\dfrac{\theta - m_1 - n\phi}{\exp(m_2 N_A L)} - \dfrac{\theta - m_2 - n\phi}{\exp(m_1 N_A L)} + \Delta m}\right] \qquad \text{(f)}$$

This is the parent relationship for α as given in Table 1 of the text, and from which the four detailed special cases are derived.

APPENDIX 2

Integration of the local diffusion equations for isotopic mixtures

For large scale separations, particularly separation of isotopes, economics dictate the use of multiple stages with large cross sectional area and short diffusion path. These requirements can be met by utilizing a porous partition to separate feed and separating agent streams, with diffusion occurring across this partition.

If the diffusion partition is visualized as consisting of a very large number of parallel pores, each of the type considered in this work, the local diffusion equations can be

integrated over the whole area to obtain the overall stage enrichment and capacity factors. BENEDICT and BOAS [1] have derived this integrated relationship for the case of isotopic mixtures where the diffusion coefficients D_{AC} and D_{BC} are nearly the same, with the added assumption of (a) balanced diffusion, wherein $N_A = -N_B$, or (b) $\phi = \tau_{AC} - \tau_{BC} \cong 0$. It is desired to outline a solution for isotopic mixtures which does not require either of assumptions (a) or (b), but which assumes negligible concentration of feed components on the back or separating agent side of the diffusion partition. For further simplification, let it be assumed also that the concentration of light component in the feed gas is small, as would be the case, for example, in the stripping section and adjacent to the feed point in a cascade used to separate isotopes having low natural abundance of the light component.

It is desired to relate the overall stage enrichment factor, ϵ, and the stage screen area, A, to the external flow conditions, namely the molal feed rate, F', and the molal raffinate rate, R.

The following assumptions will be made :

(1) Mole fraction of light component A on a separating-agent-free basis is small in comparison with unity, say $< 5\%$.

(2) Mole fractions of components A and B on the back side of the mass diffusion partition are negligible in comparison with unity.

(3) $q' = N_C/N_B < -1$, where N_C and N_B are the molal mass rates per unit area of separating agent and heavy component through the partition.

(4) $D_{AB} + D_{AC} \cong D_{BC}$.

(5) Feed gas to stage is free of separating agent.

(6) Countercurrent flow of feed and separating agent.

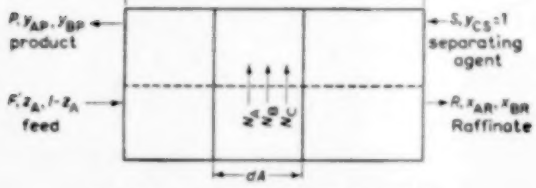

FIG. 11. Diffusion stage nomenclature.

Fig. 11 illustrates the main stage variables and nomenclature. The procedure for solution is as follows :

(1) The integrated ternary diffusion equations for the single pore, Table 1, *Case IV*, equations (9) and (10) are solved for the molal rates N_A and N_B as a function of diffusion coefficients and upstream point compositions.

(2) Light component composition is eliminated from differential material balances on A and B, and the resulting equations integrated over the diffuser area to give relationships between flow rates and compositions.

(3) Results obtained in (1) and (2) are combined with the definition of an enrichment factor, and with an overall material balance on component B.

Let the overall stage separation factor, based on product and feed compositions be defined as

$$f = \frac{y_{Ap}}{y_{Bp}} \Big/ \frac{z_A}{1 - z_A} \simeq \frac{y_{Ap}}{y_{Bp}} \Big/ z_A$$

For an even split of feed flow between product and raffinate streams, the usual cascade arrangement, it can be shown that $\ln (2 - f) \cong -\epsilon$, since, for the case under consideration, $\epsilon \ll 1$.

In BENEDICT's notation, with $\gamma = \frac{D_{AC}}{D_{BC}} - 1$ (the separability), the desired solution for the overall stage enrichment becomes :

$$\frac{\epsilon}{\gamma} = \ln 2 \, \frac{(\ln 2R/F')}{(\ln R/F')} \ln \left(\frac{2R/F'}{\ln 2} \right)$$

The expression for the total stage area, A is :

$$\frac{A}{F' L \tau_{BC}} = \frac{(1 - R/F')}{\ln \left(\frac{\ln 2}{\ln 2R/F'} \right)}$$

where L is the total diffusion path length, including screen and boundary layer thicknesses.

For the separating agent which diffuses across the boundary into the raffinate stream, there is obtained,

$$\frac{S_0}{F'} = P_{\min.} = \frac{R}{F'} - \frac{1}{2}$$

Note that the dimensoinless stage parameters ϵ/γ,

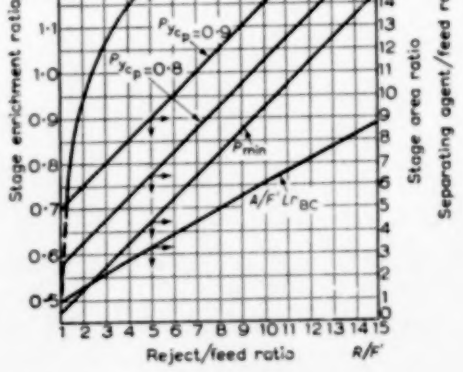

FIG. 12. Calculated performance of an extractive diffusion stage for isotopes.

$A/F'\,L\,r_{BC}$, and P_{min} are expressed as functions of the raffinate/feed ratio, R/F', alone. Fig. 12 illustrates the relationship graphically.

P_{min} corresponds to the amount of separating agent which actually diffuses into the reject stream. The total carrier required to reduce the back pressure of A and B to zero is, of course, infinite. However, it is reasonable to expect only a small change in ϵ if the concentration of agent in the product, y_{C_P}, is reduced to 0·8 or 0·9 mole fraction. Accordingly, lines are drawn representing these conditions and can be used as a first approximation to the relative amounts, P of separating agent required. The levelling off of ϵ/γ at large values of R/F' contrasted with the nearly linear rise of the area function would seem to indicate that the optimum R/F' will not be very large, possibly $2 < R/F' < 5$.

Acknowledgement—This research was conducted under an Atomic Energy Commission Pre-Doctoral Fellowship grant. The authors wish to express appreciation also to the *Union Carbide Nuclear Company* for permission to publish Appendix II.

Notation

A = total stage area, cm^2

D_{AB}, etc. = mutual diffusion coefficient for pair A-B, etc., $\frac{cm^2}{sec}$

F = volumetric flow rate (1 atm., 20°C) of diffusing components, cm^3/hr

F' = stage feed flow rate, g mole/sec

h = fraction of feed gas diffusing

$-K_1/N_A = (n+1)\,r_{AB} + (q+1)\,r_{AC} + (n+q)\,r_{BC}$, $\frac{(cm)\,(sec)}{g\ mole}$

$+K_2/N_A^2 = (n+q+1)\,[r_{AB}\,r_{AC} + n\,r_{AC}\,r_{BC} + q\,r_{AC}\,r_{BC}]$, $\frac{(cm^2)\,(sec)^2}{(g\ mole)^2}$

$K_{AB} = r_{AB}\,N_A/z$, cm^{-1}

$K_{ABC} = [z\,r_{AC} + (1-z)\,r_{BC}]\,N_A/z$, cm^{-1}

L = diffusion path length, cm

$m_1, m_2 = (-K_1 \pm \sqrt{K_1^2 - 4K_2})\,/2N_A$, $\frac{(cm)\,(sec)}{g\ mole}$

N_A, etc. = molar mass velocity of component, A, etc. $\frac{g\ mole}{(sec)\,(cm^2)}$

$n = N_B/N_A$

$n' = N_A/N_B$

p = pressure, atmosphere

$P = S/F$; $P' = S_0/F$

$q = N_C/N_A$

$q' = N_C/N_B$

r_{AB}, etc. = $RT/p\,D_{AB}$, etc.

R = gas constant = $82{\cdot}1\ \frac{(cm^3)(atm.)}{(g\ mole)\,(°K)}$

R = stage raffinate flow rate, g mole/sec

$R_1 = \frac{D_{AC}\,(D_{BC} - D_{AB})}{D_{BC}\,(D_{AC} - D_{AB})}$

S = stage separating agent flow rate, g mole/sec

S_0 = flow rate of separating agent across diffusion boundary, g mole/sec

T = absolute temperature, °K

u = diffusion velocity, cm/sec

x = distance coordinate, cm

y = mole-fraction of component A on a separating agent-free basis

y_{A_1}, etc. = mole fraction of component A, etc.

z = feed composition, mole fraction

$\alpha = \text{local separation factor} = \frac{y_1}{y_P}\frac{(1-y_1)}{(1-y_P)}$

α_0 = local separation factor at infinite dilution

$\gamma = \text{separability} = \frac{D_{AC}}{D_{BC}} - 1$

$\Delta = r_{AC} - r_{BC}$

$\Delta m = m_1 - m_2$

ϵ = stage enrichment factor

$\theta = (q+1)\,r_{AC} + n\,r_{AB}$

$\phi = r_{AB} - r_{AC}$

$\psi = r_{AB} - r_{BC}$

Subscripts

A = light component

B = heavy component

C = separating agent

F = feed stream

P = product stream

R = raffinate stream

1 = inlet end of diffuser

2 = discharge end of diffuser

References

[1] Benedict M. and Boas A. *Chem. Eng. Prog.* 1951 **47** 51, 111.

[2] Cichelli Mario T., Weatherford Jr. W. D. and Bowman J. R. *Chem. Eng. Prog.* 1951 **47** 63, 123.

[3] Colburn A. P. and Drew T. B. *Trans. Amer. Inst. Chem. Engrs.* 1937 **33** 197.

[4] Gilliland E. R. *Ind. Eng. Chem.* 1934 **26** 681.

[5] Hertz G. *Physikal. Zeit.* 1922 **23** 433; *Z. Physik* 1923 **19** 35.

[6] Hirschfelder J. O., Bird R. B. and Spotz E. L. *Chem. Revs.* 1949 **44** 205.

[7] HIRSCHFELDER J. O. and CURTISS C. F. *J. Chem. Phys.* 1949 **17** 550.

[8] MAIER G. G. Mechanical Concentration of Gases. *U.S. Bureau of Mines Bull.* 1940, 431.

[9] SCHWERTZ F. A. *Amer. J. Phys.* 1947 **15-1** 31-36.

[10] SHERWOOD T. K. *Absorption and Extraction* p. 3. McGraw-Hill, New York (1937).

[11] *Op. Cit.* p. 10.

[12] WILKE C. R. *Chem. Eng. Prog.* 1950 **46** 95.

Chemical Engineering Science, 1957, Vol. 6, pp. 227 to 233. Pergamon Press Ltd.

Notes on the diffusion-type model for the longitudinal mixing of fluids in flow

OCTAVE LEVENSPIEL and W. K. SMITH
Bucknell University, Lewisburg, Penn., U.S.A.

(*Received* 3 *July* 1956 ; *revised version* 18 *January* 1957)

Abstract—The longitudinal mixing of fluids in flow can sometimes be characterized by a single parameter D, the " longitudinal dispersion coefficient." which is analogous to and has the same units as the coefficient of molecular diffusion. The results of a study of this model show that a dimensionless parameter, the Peclet number can be used as the similarity criterion for longitudinal mixing. Also, it is pointed out that the obvious and direct method of calculating the mean velocity of flow, by injecting a tracer into the fluid stream at one point and measuring its maximum concentration at a given point downstream, may in some cases lead to an appreciable error, even in situations where the diffusion-type model is applicable. Methods are shown for evaluating D from experimental measurements, examples are worked out and conditions for applicability of the model are discussed.

Résumé—En écoulement des fluides, le mélange dans le sens longitudinal peut être caractérisé par un paramètre unique D : " coefficient de dispersion longitudinal " analogue au coefficient de diffusion moléculaire et exprimé avec les mêmes unités. Les résultats d'une étude de ce type montre que le nombre sans dimension de Perclet peut être utilisé comme critère de similitude pour les mélanges " longitudinaux." De même les auteurs signalent que la méthode classique et directe pour la mesure de la vitesse d'écoulement d'un fluide par introduction d'un traceur et mesure de sa concentration maximum en un point donné, peut en certain cas donner des erreurs appréciables, même dans les cas où le type de diffusion modèle peut être appliqué. Ils indiquent des méthodes pour calculer D à partir de mesures expérimentales, donnent des exemples avec les conditions d'utilisation.

LONGITUDINAL self-mixing is of interest in the study of fluids in flow and it is only in the last few years that significant progress has been made in the analysis and understanding of this phenomenon. With respect to an analysis of fluid self-mixing the various physical situations may be placed in two broad categories depending on whether there is or whether there is not macroscopic variation in flow conditions at different locations along the flow path. We may consider that no such variations occur in flow through long pipes and long packed beds which may be characterized as infinite in length. On the other hand significant variations may be expected to occur in flow through tanks, short pipes, fluidized beds, filter cakes as well as through and around obstructions. This paper is primarily concerned with the case characterized by the infinite pipe.

In an attempt to provide an analytical solution to the problem of fluid mixing in pipes, packed beds, etc., an obvious first approach is to consider the analogy between mixing and molecular diffusion. However, to do this we must have a counterpart to the molecular diffusion coefficient which we shall call the " longitudinal dispersion coefficient." The model we propose to explore assumes that the longitudinal dispersion coefficient, D, as defined in equation (1), is independent of position and provides a measure of the degree of mixing occurring during flow. We use the word " longitudinal " above because we wish to distinguish mixing in this direction from mixing in the lateral direction which may be quite different in magnitude. For example, in streamline flow of fluids through pipes the longitudinal mixing is due mainly to the fluid velocity gradients while lateral mixing is a result of molecular diffusion. Numerous authors

[2, 3, 6, 7, 8, 9, 13, 14, 15, 16] have pointed out that longitudinal mixing can be treated like diffusion and much has been done to develop the consequences of such a treatment.

THEORY

Consider a fluid flowing v ft³/sec through a pipe which stretches to infinity in either direction. Let the fluid enter an experimental section of this pipe at $x = 0$ and leave at $x = L$, the volume of this section being V ft³.

Now at about time $\theta = 0$ rapidly inject into the entering fluid a quantity of tracer which at unit concentration would have a volume Q ft³. If the flow rate and degree of mixing are independent of radial position, the slug of tracer will move downstream at an average velocity $u = vL/V$ ft/sec and its location at time θ will be $x = u\theta$. With these conditions the mixing of tracer with the surrounding fluid is given by

$$\frac{\partial C}{\partial \theta} = D\frac{\partial^2 C}{\partial x^2} \tag{1}$$

where D, the longitudinal dispersion coefficient, macroscopically determines the mixing process.

If the tracer is injected essentially instantaneously into fluid at rest at $x = 0$, the solution to equation (1) which gives the tracer distribution as a function of θ and x is, from CARSLAW [1],

$$C = \frac{QL}{2V\sqrt{\pi D\theta}}\, e^{-\frac{x^2}{4D\theta}}, \tag{2}$$

a family of normal or Gaussian error curves symmetric about the origin, with θ as parameter. However, in our case the fluid is not at rest but is moving down the pipe; thus equation (2) is modified to yield

$$C = \frac{QL}{2V\sqrt{\pi D\theta}}\, e^{-\frac{(x-u\theta)^2}{4D\theta}}. \tag{3}$$

At position $x = L$ the concentration of tracer as a function of time is given by replacing x by L in equation (3), which on rearranging becomes

$$\frac{CV}{Q} = \frac{1}{2\sqrt{\pi\left(\frac{v\theta}{V}\right)\left(\frac{D}{uL}\right)}}\, e^{-\frac{\left(1-\frac{v\theta}{V}\right)^2}{4\left(\frac{v\theta}{V}\right)\left(\frac{D}{uL}\right)}}. \tag{4}$$

Equation (4), when plotted on CV/Q vs. $v\theta/V$ co-ordinates, results in a family of curves with D/uL as parameter. This is the C-curve [2] and it represents the concentration of tracer as it passes the downstream recording point.

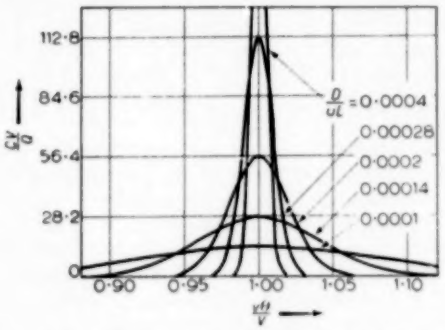

FIG. 1. C-curves for small values of the longitudinal dispersion number D/uL (equation (5)).

Figs. 1 and 2 show the C-curves for various values of the parameter D/uL, which is the reciprocal of the Peclet number. Note that the skewness increases with D/uL; also for very small values of D/uL equation (4) approaches the normal

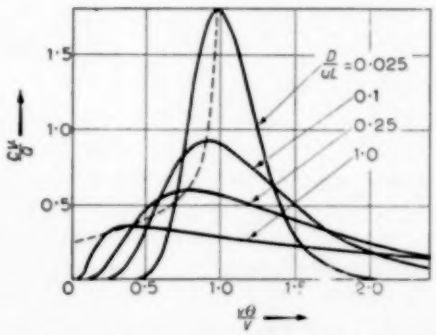

FIG. 2. C-curves for large values of the longitudinal number $\frac{D}{uL}$ (equations (4) and (8)).

error curve. This can be shown as follows: when D/uL is very small the values of $v\theta/V$ must be taken close to 1 (otherwise the values of CV/Q are essentially zero); and for $v\theta/V$ close to 1 equation (4) is approximately

$$\frac{CV}{Q} = \frac{1}{2\sqrt{\pi\left(\frac{D}{uL}\right)}}\, e^{-\frac{\left(1-\frac{v\theta}{V}\right)^2}{4\left(\frac{D}{uL}\right)}}, \qquad (5)$$

which is normal.

Physically this means that when D/uL is very small the concentration curve, which is normal in shape at any instant, does not change appreciably in the time interval required for the fluid to pass by the recording point. However, when D/uL is of the order of 0·01 or greater the concentration curve flattens out rapidly and its shape changes significantly during the time required for the tracer to pass the recording point; this is the cause of the skewness.

It is often sufficiently accurate to assume (e.g. Danckwerts [2] and Taylor [13, 14]) that the maximum value of VC/Q occurs for $v\theta/V = 1$. This is, in fact, not quite the case, as will now be shown. If equation (4) is differentiated with respect to $v\theta/V$ and the derivative equated to zero the solution, which represents the time at which the maximum concentration occurs, is

$$\frac{v\theta}{V} = \sqrt{\left(\frac{D}{uL}\right)^2 + 1} - \left(\frac{D}{uL}\right) \qquad (6)$$

which can also be written as

$$\frac{v\theta}{V} = \frac{1}{\sqrt{\left(\frac{D}{uL}\right)^2 + 1} + \frac{D}{uL}} \qquad (7)$$

It is evident from this latter form that the maximum concentration always occurs for values of $v\theta/V$ between 0 and 1 and that for very small values of D/uL the maximum value of CV/Q is achieved when $v\theta/V$ is very close to, but less than 1. However, if D/uL is of appreciable size the value of $v\theta/V$ given by equation (7) is approximately $\frac{1}{2\,(D/uL)}$ and thus may depart measurably from 1.

When the value of $v\theta/V$ from equation (6) is substituted in equation (4) the result is

$$\left(\frac{CV}{Q}\right)_{max} = \frac{1}{2\sqrt{\pi\left(\frac{D}{uL}\right)}\sqrt{\sqrt{\left(\frac{D}{uL}\right)^2+1}-\frac{D}{uL}}}\, e^{-\frac{\sqrt{\left(\frac{D}{uL}\right)^2+1}-1}{2\left(\frac{D}{uL}\right)}} \qquad (8)$$

The dotted line in Fig. 2 shows the locus of $\left(\frac{CV}{Q}\right)_{max}$. Fig. 3 gives the plot of $\left(\frac{CV}{Q}\right)_{max}$ versus D/uL and also $\left(\frac{CV}{Q}\right)_{\frac{v\theta}{V}=1}$ versus D/uL, which from equation (4) is

$$\left(\frac{CV}{Q}\right)_{\frac{v\theta}{V}=1} = \frac{1}{2\sqrt{\pi}}\left(\frac{D}{uL}\right)^{-\frac{1}{2}} \qquad (9)$$

Examination of Fig. 3 shows that the two CV/Q values are practically identical for all but large values of D/uL.

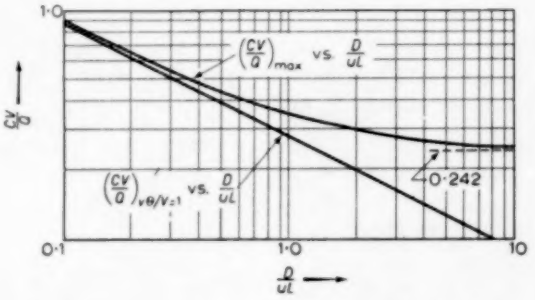

Fig. 3. Output values of $\left(\frac{CV}{Q}\right)_{max}$ and $\left(\frac{CV}{Q}\right)_{\frac{v\theta}{V}=1}$ as functions of the longitudinal dispersion number $\frac{D}{uL}$ (equations (8) and (9)).

Finally, for use in the next section, we develop the variance σ^2 of the function in equation (4). This is found, using the formula

$$\sigma^2 = \int_a^b x^2 f(x)\,dx - \left[\int_a^b x f(x)\,dx\right]^2 \qquad (10)$$

[17], where x corresponds to $v\theta/V$, $f(x)$ is the function governing its variation – equation (4) in the present case – and the interval from a to b is the domain of the variable x, namely,

o to ∞ for $v\theta/V$. Thus, the equation for the variance becomes

$$\sigma^2 = \int_0^\infty \left(\frac{v\theta}{V}\right)^2 \cdot \frac{1}{2\sqrt{\pi\left(\frac{D}{uL}\right)\left(\frac{v\theta}{V}\right)}} e^{-\frac{\left(1-\frac{v\theta}{V}\right)^2}{4\left(\frac{D}{uL}\right)\left(\frac{v\theta}{V}\right)}} d\left(\frac{v\theta}{V}\right) - \left[\int_0^\infty \left(\frac{v\theta}{V}\right) \frac{1}{2\sqrt{\pi\left(\frac{D}{uL}\right)\left(\frac{v\theta}{V}\right)}} e^{-\frac{\left(1-\frac{v\theta}{V}\right)^2}{4\left(\frac{D}{uL}\right)\left(\frac{v\theta}{V}\right)}} d\left(\frac{v\theta}{V}\right)\right]^2. \quad (11)$$

This expression can be evaluated by first letting

$$\frac{v\theta}{V} = \frac{x + \sqrt{x^2+4}}{2},$$

then later substituting

$$\frac{x^2}{4\left(\frac{D}{uL}\right)} = y.$$

This enables one to convert the integrals in equation (11) to gamma functions whence it is a simple matter to find

$$\sigma^2 = 8\left(\frac{D}{uL}\right)^2 + 2\frac{D}{uL}), \quad (12)$$

or, solving for D/uL,

$$\frac{D}{uL} = \frac{1}{8}(\sqrt{8\sigma^2+1} - 1). \quad (13)$$

If D/uL is small enough so that $(D/uL)^2$ can be neglected, the solution of equation (12) is

$$\frac{D}{uL} = \frac{1}{2}\sigma^2. \quad (14)$$

EXPERIMENTAL DETERMINATION OF THE DISPERSION COEFFICIENT

In this section methods will be suggested for determining the value of D from experimental results, following which examples will be worked out as illustrations of the methods. These may be broadly classified as methods requiring only one tracer concentration reading and methods involving a series of tracer concentration readings.

If only one reading is to be taken it may be either the maximum concentration or that at $v\theta/V = 1$, whichever is more convenient to obtain. It uses the fact that either of these values is a function of D/uL; thus, knowing Q, u, L and the concentration value, it is possible to find D. More data are required if a series of readings is to be taken; however, it probably is worthwhile, for the results will be more informative (e.g., as a check on the suitability of the model) and the estimated D will be more reliable. Also, one may use either the C- or F-curves (2) directly, the F-curve being the output for a step function input. If the C-curve is used, the method exploits the relation between its variance, σ^2, and D/uL; again, knowing u, L, and the computed variance but this time not requiring Q it is possible to solve for D. If the F-curve is used one may either reduce it by differentiation to the corresponding C-curve, or else if D/uL is small one may plot the F-curve on probability graph paper from which the variance is found directly.

Example 1 : *use of one concentration reading of the C-curve*

Consider water flowing at 1·17 ft/sec through a 1·124" diameter pyrex tube. A volume of 1% $KMnO_4$ solution, which would fill one inch of tube, is rapidly injected into the flowing water and 9 feet downstrean from this point of injection the concentration of $KMnO_4$ in the water is measured by an emission type photoelectric cell hooked up to a milliammeter. A camera photographs the milliammeter dial 7·7 seconds after introduction of $KMnO_4$. This corresponds to the time for one test section – volume of fluid to pass through the test section. The photograph shows that a 0·00555% $KMnO_4$ solution passes the recording point.

From the above data :

$L = 9$ ft.
$u = 1{\cdot}17$ ft/sec.
$v = 1{\cdot}17$ A ft^3/sec.
$V = 9$ A ft^3.
$\theta = 7{\cdot}7$ sec.
$C = 0{\cdot}00555\%$.
$Q = \frac{A}{12}$ ft^3 of 1% $KMnO_4$ solution, considered of unit concentration ;

therefore $v\theta/V = 1$
and $CV/Q = 0{\cdot}6$
From Fig. 3 $D/uL = 0{\cdot}217$
hence $D = 2{\cdot}28\ \text{ft}^2/\text{sec}$.

Note that from figure 4 $CV/Q_{max} = 0{\cdot}64$, a value which is only slightly higher than that found at $v\theta/V = 1$. However, from Fig. 2 or equation (6) we find that C_{max} occurs at $v\theta/V = 0{\cdot}8$, so if this method is used to find the flow rate of fluids and it is assumed that one volume of tracer has passed through the test section when C_{max} occurs a 20% error will result. The flow condition and D value for this example approximate Run 194 of FOWLER and BROWN [4].

Example 2: *use of a series of readings of the C-curve*

Consider the experimental set-up of example 1 but with one modification, readings of the milliammeter dial are taken at 2 second intervals. The results for the flow conditions of example 1 are shown in Table 1.

Table 1.

Time (sec)	$KMnO_4$ *Concentration* (*arbitrary units*)
0	0
2	11
4	33
6	64
8	58
10	48
12	39
14	29
16	22
18	16
20	11
22	9
24	7
26	5
28	4
30	2
32	2
34	2
36	1
38	1
40	1
42	1

To estimate the variance of the time-concentration curve formula (10) is modified, essentially by replacing the integrals by finite sums and by replacing the theoretical function of equation (4) by the observed concentration readings. Thus, the modified formula is

$$\sigma_\theta^2 = \frac{\Sigma x^2 f}{\Sigma f} - \left(\frac{\Sigma xf}{\Sigma f}\right)^2, \qquad (15)$$

where x corresponds to θ, f corresponds to or is proportional to CV/Q and the summation is taken over all the uniformly spaced readings. Evaluating the individual terms of equation (15),

$\Sigma f = 386$
$\Sigma xf = 4252\ \text{sec}$
$\Sigma x^2 f = 65392\ \text{sec}^2$.

Hence, from equation (15)

$$\sigma_\theta^2 = 48\ \text{sec}^2,$$

or in terms of reduced time units $v\theta/V$,

$$\sigma^2 = 0{\cdot}81$$

From equation (13)

$$\left(\frac{D}{uL}\right) = 0{\cdot}217$$

hence

$$D = 2{\cdot}28\ \text{ft}^2/\text{sec}.$$

Note that neither the quantity of injected tracer nor the actual outlet concentration need be known. Also, it may be seen from the data in Table 1 that the time-concentration curve has a long 'tail'. This is in accord with the theory which indicates that such a situation should occur for the D/uL value of this example. Skewness of this sort has been found experimentally [13, 14] and various explanations have been proposed to account for it.

Example 3: *use of a series of readings of the F-curve*

To illustrate the use of the F-curve in finding the dispersion coefficient consider the data of VON ROSENBERG [11] for the displacement of benzene by n-butyrate in a $1\frac{1}{2}''$ diameter packed column. Take the run at the lowest flow rate, $2{\cdot}19 \times 10^{-5}$ ft/sec, which is about 2 feet/day.

Concentrations were determined by refractive index measurements and when plotted, the time-concentration curve was found to be *S*-shaped. However, when plotted on probability paper the raw data [12] for this run fall approximately on a straight line as shown in Fig. 4.

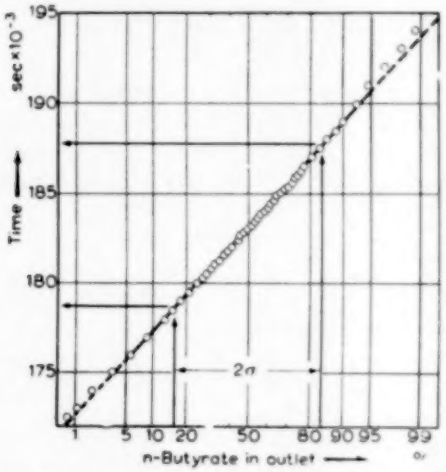

FIG. 4. Data of VON ROSENBERG plotted on probability (or normal curve) paper (example 3).

The standard deviation, σ, of a normal distribution which plots as a straight line on probability paper is found by using the following property of a normal distribution : namely, that the interval between the 16th and 84th percentile points is two standard deviations [17]. The 84th percentile line intersects the straight line at 187750 secs and the 16th percentile line intersects it at 178550 secs, so the difference, 9200 seconds, is taken as the value of 2σ. Therefore

$$\sigma_\theta = 4600 \text{ sec}$$

But the time necessary for one pore-volume of fluid to pass through the packed bed is 183,000 secs. Therefore, in terms of $v\theta/V$

$$\sigma = 0{\cdot}0252.$$

From equation (14)

$$D/uL = 0{\cdot}00032$$

But $u = 2{\cdot}19 \times 10^{-5}$ ft/sec
and $L = 4$ ft,
so $D = 2{\cdot}8 \times 10^{-6}$ ft^2/sec

which is in the order of magnitude of the molecular diffusion coefficient.

This method should only be used when the *F*-curve plots as a straight line on probability paper, or equivalently, when D/uL is small so that the *C*-curve is approximately normal. As $D/uL < 0{\cdot}01$ in this example, we are justified in using this method.

DISCUSSION

In this treatment, D has been considered to be independent of position. This holds for either of two conditions, the first being that in which fluid velocity and mixing are uniform. In flow through a bare pipe this condition certainly does not hold at low Reynolds numbers but is more closely approached at high Reynolds numbers. In packed beds of solids it may be expected that these conditions hold fairly closely, although recent experiments [5, 10] show that there is an appreciable variation in flow velocity with lateral position.

There is another condition for which we may apply this model even if the velocity is far from uniform, namely, when the lateral dispersion of material (for instance, by molecular diffusion or turbulence) is great enough to ensure a uniform tracer concentration at any given cross section. In determining when this condition holds, the diameter and length of the experimental section must be considered as well as the mixing of material. For example, for given flow conditions the longer the experimental section the smaller the longitudinal mixing effect will be relative to the total amount of fluid. However, the lateral mixing is unaffected by such changes in length of experimental section. As a result, the longer the tube the greater is the lateral mixing with respect to the longitudinal mixing and the more reliable is the model [13, 14].

As D is independent of position when either of the above two conditions is approximated we may expect this model to be fruitful in studying conversions in homogeneous flow reactors (high flow rate, hence condition 1 holds), in calculating the degree of contamination in the successive flow of fluids in pipe lines (large length to

diameter ratio, hence condition 2 holes) and finally in estimating the depth of the frontal mixing zone between fluids when an oil reservoir is being invaded (turbulences restricted to the size of the pores, large length to pore diameter ratio, hence both conditions hold).

If varying flow conditions exist in different parts of the experimental section, an average D value will result. For example, consider flow through a reaction vessel in which the tracer is introduced at the inlet and the C-curve is obtained from the outlet stream. In this situation, end effects may be appreciable since flow conditions close to the injection and recording points may differ widely from those found in the rest of the equipment. The magnitude of these effects would depend on both the actual hydrodynamic situation and D/uL for the vessel. For small D/uL end effects can be ignored but for large D/uL these effects should be considered, due to their distortion of the expected C- and F-curve. As yet no treatment of end effects is available and, until such time that their magnitude is known, they will have to be ignored.

It should be noted that the longitudinal and lateral dispersion of material are intimately related and for flow through a tube this relationship forms the basis for a theoretical prediction by TAYLOR [13, 14] of the longitudinal dispersion coefficient. Considerable data appear in the literature which if reanalysed should yield useful correlations relating the longitudinal dispersion coefficient to the properties of the system. Such experimental results should also be compared with TAYLOR's theoretical predictions. A study of this kind is being made and will soon be reported.

NOTATION

A = cross sectional area of tube (L^2)
C = concentration of tracer in the fluid (dimensionless]
C_0 = initial concentration of tracer in fluid (dimensionless)
D = the longitudinal dispersion coefficient, defined in equation (1) (L^2/T)
$\frac{D}{uL}$ = the reciprocal of the Peclet number (dimensionless)
L = length of experimental section of tube (L)
Q = volume of tracer of unit concentration which would correspond to the actual amount of tracer introduced into the fluid (L^3)
$u = vL/V$, the average flow velocity (L/T)
v = volumetric fluid flow rate (L^3/T)
V = volume of tube (L^3)
$\frac{v\theta}{V}$ = reduced time (dimensionless)
x = distance from entrance of the experimental section of tube (L)
θ = time, measured from time of injection of tracer into the flowing fluid (T)
σ^2 = the variance of the C-curve (dimensionless)
$\sigma_\theta^2 = \left(\frac{V}{v}\right)^2 \sigma^2$, the variance of the time-concentration curve (T^2).

REFERENCES

[1] CARSLAW H. S. *Introduction to the Mathematical Theory of the Conduction of Heat in Solids* (2nd Ed.) p. 153 Dover Publications, N.Y. 1945.
[2] DANCKWERTS P. V. *Chem. Engng. Sci.* 1953 **2** 1.
[3] DEISLER Jr. P. F. and WILHELM R. H. *Industr. Engng. Chem.* 1953 **6** 1219.
[4] FOWLER F. C. and BROWN G. G. *Trans. Amer. Inst. Chem. Engrs.* 1943 **39** 491.
[5] HARAI E. *Chem. Eng.* (Japan) 1954 **18** 328.
[6] HULL D. E. and KENT J. W. *Industr. Engng. Chem.* 1952 **44** 2745.
[7] KLINKENBERG A. and SJENITZER F. *Chem. Engng. Sci.* 1956 **5** 258.
[8] KRAMERS H. and ALBERDA G. *Chem. Engng. Sci.* 1953 **2** 173.
[9] LAPIDUS L. and AMUNDSON N. R. *J. Phys. Chem.* 1952 **56** 984.
[10] SCHWARTZ C. E. and SMITH J. M. *Industr. Engng. Chem.* 1953 **45** 1209.
[11] VON ROSENBERG D. U. *AIChE Journal* 1956 **2** 55.
[12] VON ROSENBERG D. U. personal communication.
[13] TAYLOR G. I. *Proc. Roy. Soc.* 1953 **A219** 186.
[14] TAYLOR G. I. *Proc. Roy. Soc.* 1954 **A223** 446.
[15] WEHNER J. F. and WILHELM R. H. *Chem. Engng. Sci.* 1956 **6** 89.
[16] WILHELM R. H. *Chem. Engng. Progr.* 1953 **49** 150.
[17] WILKS S. S. *Elementary Statistical Analysis* p. 117, p. 145. Princeton University Press 1948.

Book reviews

O. KUBASCHEWSKI and E. LL. EVANS : **Metallurgical Thermochemistry.** (Second Edition), Pergamon Press, 1955, xiv + 410 pp. 35s.

THE appearance of a second edition of "Metallurgical Thermochemistry" is an indication of both the well-deserved success of its predecessor and the continued interest in the practical applications of thermodynamics, especially in the field of process metallurgy. The basic arrangement of the book has not been altered, but it has been significantly revised and extended. The theoretical treatment in Chapter 1 (which still assumes a familiarity with the elements of the subject) now includes a consideration of recent work on non-regular solutions and a section on slag-metal equilibria. The two following chapters, on experimental methods (with emphasis on calorimetry) and the estimation of thermodynamic data, have also been slightly enlarged. The main contribution to the new edition's extra 42 pages however, is the revision of the tabulated data which form Chapter 4. Together with the earlier one on experimental methods, this chapter is a forceful reminder that although the science of thermodynamics is exact, a precise measurement of the thermodynamic properties of a system is often a matter of considerable difficulty. Thus, as the authors observe, a revised value does not always fall within the limits of accuracy assigned to the original one ; continued caution in the setting of accuracy limits is therefore wise, especially since a value can often be useful despite a fairly large probable error.

This compilation of data is compact and well-presented, and its revision will serve to retain for the volume a leading position among works of reference in this field. It is not, however, the book's only asset, as those actually engaged in the improvement and extension of the data of chemical thermodynamics will discover. The chapter on experimental techniques for example, should do much to eliminate inconsistencies of the type that the authors have had to face in preparing Chapter 4.

The printing and binding are adequate, and the price is modest.

H. C. COWEN

O. KUBASCHEWSKI and J. A. CATTERALL : **Thermochemical Data of Alloys.** Pergamon Press, 1956. vi + 198 pp. 45s.

THIS book is a critical compilation of data for a total of about 230 binary and ternary systems. It includes in addition to purely metallic systems the binaries formed by the transition metals with carbon, phosphorus, nitrogen, sulphur and oxygen. Some of the data are included in "Metallurgical Thermochemistry," but in the present volume each system is dealt with in a separate section which contains, as far as possible, the partial and integral values of the enthalpy, entropy and free energy changes occurring throughout the system together with volume changes and latent heats of fusion and transformation. The data have been gathered from over 500 sources, and include values reported up to 1955. There is undoubtedly a real need for such a volume, especially in view of the rate at which information in this field is now accumulating. Despite this activity however, the authors reveal many gaps and uncertainties in our present knowledge. The book will be of value mainly to research workers, who will be grateful that so much experience in the handling and assessment of such data lies behind this compilation.

The book is satisfactorily printed and bound, and reasonably priced.

H. C. COWEN

Combustion Processes. Edited by B. LEWIS, R. N. PEASE and H. S. TAYLOR. Volume 2 of the series of 12 volumes on **High Speed Aerodynamics and Jet Propulsion,** Princeton University Press, London : Cumberlege. 1956. pp. xv + 662, with 16 plates. 84s.

SINCE the end of the war a vast amount of work, experimental and theoretical, has been done in the field of combustion. Outside the universities the chief stimulus has been the tremendous technical developments of new engines for aircraft and rockets. The series which includes this volume has been prepared in order to " bring together in convenient, accurate and organized form the basic information that has evolved in the last decade in the related fields of gas dynamics, aerodynamics, combustion and jet propulsion."

This volume sets out to treat aspects of combustion processes other than physical measurements in combustion (to which volume 9 of the series is devoted). There are 15 chapters grouped into six principal sections : 1. Thermodynamics of Combustion, 2. Chemical Kinetics of Combustion, 3. Flame Propagation in Gases, 4. Combustion of Liquids and Solids, 5. Detonation Processes in Gases, Liquids and Solids, 6. Energy Production by Nuclear Reactions. Although the standards of the various sections differ, the wide scope attempted gives this book a superficial attraction and libraries already embarked on purchasing this series may not wish to omit one volume. But it is a book with serious weaknesses.

Firstly, much of the work described in it is already out-of-date. The preface states that the first draft was

completed in 1951 and this impression is confirmed by the duplication of material here in a text written independently by two of the authors and published in 1952.

Secondly, the value and usefulness of the various sections is markedly uneven. Who in 1957 would consult this work for information on energy production by nuclear reactions? Who would use in combustion the tensor formulation of the so-called "thermodynamics" of irreversible processes? Certainly the other authors of the volume themselves do not.

Thirdly, and most seriously, there are too many authors. There are eighteen: their separate contributions have not been successfully unified. Editors and authors, of whom we read in the general preface as "sacrificing their spare time" to write the book, must share the blame. There is still need for a book on combustion whether by one man or a few which is conceived as a whole and written as a whole-time task.

PETER GRAY

WALTER L. BADGER and JULIUS T. BANCHERO: **Introduction To Chemical Engineering.** McGraw-Hill Book Co. Inc., New York, 1953. ix + 753 pp. £3 11s. 6d.

OVER a quarter of a century ago Professor W. L. BADGER produced a book entitled *Elements of Chemical Engineering* in association with Dr. W. L. MCCABE. It had an immediate success not only because of the shortage of books on this new subject but also because infinite pains had been taken with the drawings and presentation of facts to make the subject attractive to the young engineer. Since then Professor BADGER has become a consulting engineer and has brought the practical assessment to the academic approach. In this new book with Professor BANCHERO of the University of Michigan he maintains this outlook. As the book jacket notes "there is much we do not yet know about all the unit operations and there is a difference between what is postulated in theory and what may actually be encountered in practice." Items not covered before are "dimensional analysis, orifices, rotameters, modern evaporators and Ponchon diagrams."

In dimensional analysis the treatment consists of selecting a number of properties and arranging these in certain dimensionless groups. This gives the beginner the wrong idea. Most of the groups used today have been derived from the standard mathematical equations for hydrodynamics, heat and mass transfer, etc. This line of thought leads for example to persistence in using the Dittus and Boelter equation (which is only a slight modification of the original Nusselt equation of 1910), instead of realizing that, with a slight transposition, an equation can be produced which is exactly analogous with the empirical equation relating the friction factor with the Reynolds number. The difficulty of revising a book on a quickly expanding subject is that, sooner or later, the time comes when the whole concept has to be altered and perhaps, when this time does arrive, it is better to start from scratch and write a new book.

M. B. DONALD